MAPPING THE TAU PROTEIN INTERACTOME USING THE BIOID2 *IN SITU* LABELLING APPROACH

Ву

Ahmed Atwa

A THESIS

Submitted to
Michigan State University
in partial fulfillment of the requirements
for the degree of

Neuroscience—Master of Science

2022

ABSTRACT

MAPPING THE TAU PROTEIN INTERACTOME USING THE BIOID2 IN SITU LABELLING APPROACH

By

Ahmed Atwa

Pathological inclusions composed of tau protein are hallmarks of neurodegenerative diseases collectively known as tauopathies, of which the most common is Alzheimer's Disease (AD). Tau is most well-known as a microtubule-associated protein involved in regulating microtubule dynamics, but accumulating evidence suggests tau is involved in many biological functions. Deciphering the tau protein interactome is critical for better understating the physiological and pathological roles of tau. This work aimed to identify tau interacting partners using the *in situ* protein labelling BioID2 method by creating fusion proteins between full-length human tau and either BioID2 on the N-terminus (BioID2-Tau) or C-terminus (Tau-BioID2). A total of 372 proteins were identified, of which 269 interacted with Tau-BioID2, 169 with BioID2-Tau, and 66 proteins overlapped between both tau proteins. Gene Ontology (GO) cellular component analysis mapped protein interactions in the mitochondria, cytoskeleton, dendrites, nucleus, synaptic vesicles, and the ribonucleoprotein complex. While GO molecular function pathways identified proteins involved in RNA binding, translation regulation, ubiquitin ligase activity, kinase binding, mitochondrial oxidoreductase, and peroxidase activity. KEGG pathway analysis identified proteins associated with neurodegenerative diseases, including AD, Parkinson's disease, Huntington's disease, and Amyotrophic lateral sclerosis. Thus, this approach can identify members of the tau interactome via in situ labeling, that may help shed light on tau's functional roles and provide novel therapeutic strategies for neurodegenerative diseases.

This thesis is dedicated to Mom, Da	ad, my Wife, and my Ba believing in me.	by Boy. Thank you for always

ACKNOWLEDGEMENTS

I would like to start this by expressing my utmost gratitude to my mentor, Dr. Nicholas Kanaan. Since day one, Dr. Kanaan has been extremely supportive on both the academic and the personal levels. Dr. Kanaan introduced me to this project and guided me through the experimental planning, he always excelled at putting me on the right track. Dr. Kanaan encouraged me to present my work at conferences and supported my application to receive a travel fellowship award. I am extremely grateful for the opportunities he gave me; he is a true mentor and I am very much looking forward to my next years in his lab working on my PhD.

I would like to thank all members of the Kanaan lab. Tessa is a great lab manager, she always made my life a lot easier. Dr. Benjamin Combs, Dr. Mattew Benskey, Mohammed, and Rebecca helped me a lot with the experiments. All members of the lab are extremely supportive, friendly, and this work couldn't have been finished on time without their contribution.

I would like to thank my committee members Dr. Irving Vega, Dr.Scott Counts, Dr. Min-Hao Kuo, and Dr. Nicholas Kanaan. They guided me during this thesis work. Our discussions always challenged me and certainly made me a better critical thinker.

Finally, I would like to thank my family and friends. They showed all kinds of emotional support during those past two years of a pandemic. My wife Shahd and my baby Jayd are my greatest support in life, I was very lucky to have such a wonderful supportive wife. This couldn't have been done without you. Thank you for everything.

TABLE OF CONTENTS

LIST OF TABLES	viii
LIST OF FIGURES	ix
KEY TO ABBREVIATIONS	x
INTRODUCTION	1
Tau protein expression and structure	
Physiological functions of the tau protein	
Tau protein pathology in neurodegenerative diseases	
Tau protein-protein interactions	10
Enzyme-mediated proximity labeling: A novel approach to study protein-prof	.ein
interactions	14
THESIS OBJECTIVE	
Aim Statement	
Hypothesis	19
MATERIALS AND METHODS	20
Creating Tau-BioID2 expression plasmids using Restriction Cloning	
Site-directed mutagenesis	
Preparation of LB/agar plates and LB broth medium	
Transformation of XL10-Gold ultracompetent cells	
Transformation of Stbl3 competent <i>E.coli</i>	
Plasmid DNA Miniprep	
Plasmid DNA Maxiprep	
Restriction Digestion	
DNA Gel Electrophoresis.	
Gel purification and DNA ligation	
Human embryonic kidney (HEK293T) cell culture	
Transfection of HEK293T cells	
HEK293T protein lysate collection	
SDS-PAGE and Western blotting	
Generation of Lentiviruses that express the BioID2 proteins	
Lentiviruses production in HEK293T cells	
Immunocytochemistry (ICC)	29
Lentiviral functional titer determination using ICC	30
Embryonic day 18 mouse primary cortical neuron culture preparation	
Immunocytofluorescence (ICF)	
Lentivirus transduction efficiency	32
Lentiviral transduction in neurons	33
Endogenous tau vs lentiviral tau expression levels	33

Mass Spectrometry identification of biotinylated proteins	34
Optimization of Biotin dose and incubation time	34
Primary neurons protein lysate collection	35
Biotin-streptavidin affinity pulldown	35
Liquid Chromatography-MS/MS	36
Mass spectrometry protein identification	38
Label-free quantification of identified proteins	
Functional protein association networks	
Gene Ontology enrichment analysis	
Validation of tau protein interacting partners	
Antibodies	
Data representation and statistical analysis	
RESULTS	43
Generation and validation of Tau-BioID2 expression plasmids and lentivirus	
Mutagenesis of the BioID2 expression plasmids and creating the Tau-BioID2	
fusion proteins	44
Creating BioID2 lentiviral transfer plasmids	
Lentiviruses generation and determination of the functional titer	52
Optimizing lentiviral transduction of primary cortical neurons	55
Determining optimal titer for primary neuron transduction	55
Lentiviruses express the Tau-BioID2 proteins at near physiological levels	59
Optimization of biotin dose and incubation time	61
Affinity pulldown and mass spectrometry identification of biotinylated tau	
interacting proteinsinteracting proteins	64
Optimization of the biotin-streptavidin affinity pulldown using HEK293T cell	
lysates	
Optimization of the biotin-streptavidin affinity pulldown using primary cortical	
neurons lysates	
Identification of the tau protein interactome using mass spectrometry	
Gene ontology enrichment analysis of tau interactome	
GO enrichment analysis reveals distinct cellular components for Tau-BioID2	
BioID2-Tau interacting partners	
Validation of the identified tau interacting partners	
DISCUSSION	82
Tau interactome mapping	
Distinct and overlapping interactions between BioID2-Tau and Tau-BioID2	
Tau protein interactions in various cellular localizations	
Technical development of the approach	
Cloning of BioID2 and Tau fusion proteins	
Lentiviruses production	
Lentiviruses production Lentiviral-mediated transduction of primary cortical mouse neurons	
· · · · · · · · · · · · · · · · · · ·	
Mass spectrometry identification of tau interacting proteins Validation of identified tau interacting partners	
vanganon or igentifica taa jineraomia Dalliicia	

	Limitations of the approach	95
	Future directions	
APPE	NDICES	
	APPENDIX A: Table 3: List of the identified tau protein interacting partners APPENDIX B: Table 4: List of tau interacting partners identified in ClueGo	
	cellular components	116
	molecular function pathways	125
REFE	RENCES	130

LIST OF TABLES

Table 1: Cycling parameters for mutagenesis reactions	22
Table 2: KEGG pathway analysis associated proteins with neurological disorders	. 76
Table 3: List of the identified tau protein interacting partners	100
Table 4: List of tau interacting partners identified in ClueGo cellular components	116
Table 5: List of tau interacting partners identified in ClueGo molecular function pathways	125

LIST OF FIGURES

Figure 1: Design of the BioID2 constructs4	13
Figure 2: Restriction cloning of the BioID2 fusion proteins4	l 6
Figure 3: Validation the lentiviral transfer plasmids expressing the BioID2 constructs5	50
Figure 4: Lentiviruses functional titer and validation5	53
Figure 5: Expression of the BioID2 proteins in primary cortical neurons5	57
Figure 6: Lentiviral expression of Tau-BioID2 compared to WT Tau expression6	30
Figure 7: Optimization of biotin dose and incubation time6	32
Figure 8: Schematic representation of the experimental paradigm selected for primary neurons affinity purification and mass spectrometry experiments6	
Figure 9: Affinity capture of biotinylated proteins using streptavidin Dynabeads6	34
Figure 10: Optimization of affinity pulldown in HEK293T cell lysates6	6
Figure 11: Optimization of affinity pulldown in primary neurons lysates6	39
Figure 12: Venn diagrams of the identified preferential interacting proteins7	'2
Figure 13: STRING analysis for the identified total tau interactome	'3
Figure 14: ClueGo gene ontology enrichment analysis for the total tau interactome7	'5
Figure 15: GO enrichment cellular component analysis	'8
Figure 16: Validation of Tau interacting partners by western blotting	31

KEY TO ABBREVIATIONS

ACN acetonitrile

AD Alzheimer's disease

ALS amyotrophic lateral sclerosis

CBD corticobasal degeneration

CMF calcium-and magnesium-free

Co-IP co-immunoprecipitation

CTE chronic traumatic encephalopathy

ddH₂O double-distilled water

DIV day in vitro

DMEM Dulbecco's Modified Eagle Medium

DPBS Dulbecco's phosphate-buffered saline

E.coli Escherichia coli

FBS fetal bovine serum

FTDP frontotemporal dementia with parkinsonism

GO gene ontology

GS goat serum

HD Huntington's disease

HEK human embryonic kidney

ICC immunocytochemistry

ICF immunocytofluorescence

MAP microtubule-associated protein

MCL Markov clustering

MOI multiplicity of infection

MS mass spectrometry

MTBR microtubule binding region

NBM neurobasal medium

NFTs neurofibrillary tangles

PART primary age-related tauopathy

PD Parkinson's disease

PL proximity labeling

PPI protein-protein interactions

PSP progressive supranuclear palsy

PTMs post-translational modifications

SDS sodium dodecyl sulfate

STRING search tool for the retrieval of interacting genes/proteins

TKO tau knockout

WT wild type

INTRODUCTION

Tau protein expression and structure

The human tau protein is encoded by the microtubule-associated protein tau (MAPT) gene on chromosome 17q21 which contains 16 exons (Neve et al., 1986). Exons E4A, E6, and E8 are transcribed preferentially in the peripheral tissue (Caillet-Boudin et al., 2015). In the human brain, the 5'- untranslated region is encoded by exons E0 and E1. while the 3'- untranslated region is encoded by exon 14. Constitutive exons in the MAPT gene are E1, E4, E5, E7, E9, E11, E12, and E13 while exons E2, E3, and E10 are subject to alternative splicing in the adult brain (Himmlert, 1989). Exon E3 expression is dependent on the presence of exon E2 while exon E2 can be expressed independently of exon E3 (Andreadis et al., 1992). Thus, alternative splicing of exons E2, E3, and E10 yields the six MAPT mRNAs found in the adult human brain (Goedert et al., 1989). Splicing of exons E2 and E3 give rise to tau transcripts that are different in the aminoterminus (N-terminus) by the absence or presence of one or two N-terminus inserts (0N, 1N or 2N). Exon 10 encodes for the repeat domain R2, alternative splicing of exon E10 yields transcripts that either have three or four repeat domains (3R or 4R). Accordingly, the six tau isoforms found in the human brain are 0N3R, 1N3R, 2N3R, 0N4R, 1N4R, and 2N4R ranging from 352 to 441 amino acids (Goedert & Jakes, 1990).

The expression of the human tau protein isoforms is developmentally regulated. In the fetal brain, only the shortest tau isoform which lacks exons E2, E3, and E10 is present (0N3R, 352 amino acids)(Lee et al., 2001b). In the adult brain, equal levels of the 3R and 4R isoforms are expressed while the expression levels of the 0N, 1N, and 2N isoforms are ~37%, ~54%, and ~9% respectively (Y. Wang & Mandelkow, 2016). In the adult

mouse brain, only the 4R tau isoforms are present. In addition, the longest isoform of the human tau protein contains an N-terminus segment (amino acids 17-28) that is not found in the murine tau protein which might play a role in tau protein-protein interactions (PPIs) (Hernández et al., 2020a).

The tau protein has four major domains: the N-terminus projection domain, the proline rich region, the microtubule binding region (MTBR), and the C-terminus domain. The longest isoform of the human tau protein (2N4R, hTau40) contains the two highly acidic 29-amino-acid inserts (exons E2-E3) followed by the basic proline rich region (amino acids Isoleucine 151- glutamine 244). The N-terminus domain (amino acids methionine 1 – tyrosine 197) does not bind to the microtubules and is followed by the MTBR which contains the four repeat domains encoded by exons E9-E12 (R1-R4; amino acids Glutamine 244 – Asparagine 368). The C-terminus domain contains amino acids Lysine 369 – Leucine 441 (Mandelkow et al., 1995; Sergeant et al., 2005; Y. Wang & Mandelkow, 2016).

Under physiological condition, tau is a highly soluble protein that is structurally dynamic and lacks a stable globular conformation as is characteristic of members of the so-called intrinsically disordered protein family. Tau has an asymmetric distribution of charges due to the presence of 56 negative aspartic acid/glutamic acid residues and 58 positive lysine/arginine residues. The electrostatic interaction between the opposite charges is consistent with the proposed paperclip-like confirmation in which the C-terminus domain folds over the MTBR and the N-terminus projection domain folds back and on the C-terminus (Jeganathan et al., 2006). The high degree of flexibility tau displays

is thought to play a role in its folding as well as its functional interactions with other proteins.

Physiological functions of the tau protein

Tau protein was first isolated in 1975 from porcine brain as a heat-stable protein that associates with tubulin and is required for the assembly and stabilization of the cerebral microtubules (Weingarten et al., 1975). However, accumulating evidence suggests that tau exhibits several biological functions in various neuronal subcellular compartments including axons, dendrites, and the nucleus. Tau is a microtubule-associated protein (MAP) that stabilizes and promotes the assembly of microtubules in vitro by binding to the interface between α- and β- tubulin heterodimers at its MTBR evolutionary conserved residues 224-237, 245-253, 275-284, and 300-317, while the intervening unbound residues are flexible supporting the dynamic nature of the tau protein binding to microtubules within the context of in vitro assays (Kadavath et al., 2015). In another study using neurons, tau was instead shown to regulate the dynamics of the microtubules rather than stabilizing them (Qiang et al., 2018). Tau was more abundant on the labile region of the microtubules rather than the stable region. Depletion of tau in cultured rat neurons reduced the labile domain of the microtubules (marked by the presence of tyrosinated tubulin) and increased the mass of the stable regions of the microtubules (an observation attributed to the increased expression of MAP6 upon tau depletion). Thus, tau can be considered as a multi-functional MAP that might have functional connections with other MAPs (e.g. MAP6) and is likely to play a role regulating the dynamics of the microtubules rather than their stability in neurons.

Within the axon, several studies have identified roles for tau in regulating both anterograde and retrograde axonal transport. Early studies suggested tau might compete with kinesin and dynein motor proteins for binding to microtubules affecting both types of active axonal transport of cytoplasmic organelles (Dixit et al., 2008). In the same study, the authors reported that kinesin motors tended to detach from the microtubules in regions of bound tau (shortest and longest tau isoforms) while the dynein motors did not detach from the microtubules but rather tended to reverse direction. However, other studies have challenged the notion that tau physically interferes with motor proteins (Morfini et al., 2007) by showing that exogenous perfused tau in isolated squid axoplasm had no effect on axonal transport. Tau can also regulate kinesin-mediated anterograde axonal transport via its phosphatase-activating domain (Kanaan et al., 2011a). The phosphatase activating domain is an N-terminus region comprised of amino acids 2-18 that was found to activate PP1 which in turn dephosphorylates and activates GSK3ß leading to phosphorylation of kinesin motors causing cargo release. Thus, tau has important functions in regulating kinesin- and dynein- mediated axonal transport within the neurons which might be modulated by its protein-protein interactions.

Tau also localizes to the somatodendritic compartment (Papasozomenos & Binder, 1987) and the nucleus (Loomis et al., 1990). However, the physiological functions in these compartments are not well characterized. Tau was required for the dendritic and synaptic maturation of new-born hippocampal granule neurons as well as the formation of dendritic spines and postsynaptic densities (Pallas-Bazarra et al., 2016). *In vitro* and *in vivo* studies showed that physiological tau localizes to the nucleus and binds double-stranded and single-stranded DNA as well as the histone-DNA complex. Tau binding

maintains the integrity of genomic DNA (Camero et al., 2014) and protects DNA against reactive oxygen species-induced heat stress (Sultan et al., 2011). Moreover, tau deficient mice showed altered integrity of genomic DNA, cytoplasmic, and nuclear RNA suggesting a role for physiological tau in maintaining the integrity of the nucleic acids (Violet et al., 2014). Studies in tau knockout (TKO) mice suggested a function of physiological tau in neurogenesis and synaptic plasticity. TKO mice showed impaired hippocampal neurogenesis (Hong et al., 2010) as well as selective deficit in hippocampal long-term depression but not long-term potentiation (Kimura et al., 2014). In contrast, Ahmed and colleagues reported that tau deletion impaired long-term potentiation but not long-term depression (Ahmed et al., 2014). Tau was also found to interact with neural plasma membrane through its N-terminus projection domain (Brandt et al., 1995), mediated by Annexins A2 and A6 (Gauthier-Kemper et al., 2018a). Several of the interacting partners and functional roles of tau are currently being elucidated and likely will contribute to tau's participation in the pathogenesis of human neurodegenerative diseases.

Tau protein pathology in neurodegenerative diseases

Intracellular tau accumulation is a hallmark of a heterogenous group of neurodegenerative disorders collectively known as tauopathies, of which the most common form is Alzheimer's disease (AD). Mutations in the *MAPT* gene as well as post-translational modifications (PTMs) of the tau protein might reduce the affinity of tau binding to microtubules and mediate the tendency for intracellular aggregation of abnormal tau species (reviewed in (Alquezar et al., 2021; Pîrşcoveanu et al., 2017).To date, 112 *MAPT* mutations were identified in both the intronic and exonic sequences. Several of the mutations were experimentally linked to tau neuropathological alterations,

while the functions of other mutations remain understudied (ALZFORUM, 2022). Tau PTMs and the mutations of the *MAPT* gene might alter the protein interactome of tau which in turn may impact its functional role in disease pathogenesis.

The switch from soluble physiological -to- insoluble aggregated tau is suggested to follow a sequence of events that is not entirely understood. Insoluble filamentous tau aggregates including straight filaments (SF) and paired helical filaments (PHF) are predominant in tauopathies and comprise the various hallmark inclusions of each tauopathy. This includes neurofibrillary tangles (NFTs), globose tangles, neuropil threads, neuritic plaques, Pick bodies, astrocytic plaques, tufted astrocytes, and coiled bodies (Chung et al., 2021). Aggregation is thought to evolve from the successive multimerization of soluble tau species. Tau monomers self-associate into dimers which contribute to the formation of smaller order soluble tau oligomers that can either be on-pathway or off-pathway for filament formation. On-pathway oligomeric tau can then form filamentous aggregates that coalesce into the inclusions described above. Many lines of current research are focused on understanding the mechanistic regulators involved in tau seeding and aggregation under pathological conditions (reviewed in (Cowan & Mudher, 2013; Mamun et al., 2020)).

Tauopathies can be classified into a) 3R-tauopathies such as Pick's disease (PiD) (Pickering-Brown et al., 2004), b) 4R-tauopathies such as corticobasal degeneration (CBD), progressive supranuclear palsy (PSP), Huntington's disease (HD) (Baba et al., 2007), c) tauopathies involving both 3R and 4R Tau isoforms including AD, Lewy body dementia, chronic traumatic encephalopathy (CTE), primary age-related tauopathy (PART), and tangle-only dementia; and d) inherited frontotemporal dementia with

parkinsonism linked to chromosome 17 (FTDP-17) characterized by autosomal dominant mutations of the *MAPT* gene on chromosome 17q21 that can present with 3R, 4R or mixed isoform pathologies (Goedert & Jakes, 2005; Wszolek et al., 2006). Tauopathies also are categorized as primary or secondary tauopathies depending upon whether tau is the primary defining pathology or another form of pathology is present as a defining feature, respectively.

Alzheimer's disease is a secondary tauopathy first described in 1906 by Alois Alzheimer (Alzheimer, 1911). The neuropathological hallmarks of AD as described by the National Institute on Aging – Alzheimer's Association (NIA-AA) include the deposition of the extracellular amyloid-β plagues, intracellular aggregation of the tau protein, and neurodegeneration (Jack et al., 2018). Tau pathology progresses from the entorhinal and transentorhinal cortices (Braak stages I and II), to the hippocampal formation (stages III and IV) and later spreads to the cerebral cortices (stages V and VI) (Braak et al., 1995, 2006; Braak & Braak, 1991). Abnormal phosphorylation of all six isoforms of tau was reported in AD suggesting that some forms of phosphorylated tau may play a role in the development of tau pathologies (Goedert et al., 1992; Grundke-Igbal et al., 1987; IHARA et al., 1986). The longest tau isoform (2N4R) has 85 potential phosphorylation sites (serine, threonine, and tyrosine residues) making phosphorylation the most prominent PTM of the tau protein. Phosphorylation at some sites within tau can reduce microtubule binding and may increase the aggregation propensity of tau (Alonso et al., 2001; Bramblett et al., 1993; Lindwall & Cole, 1984). More recent work, also suggest specific tau modifications may precipitate pathogenic changes in tau (e.g. exposure of the Nterminal phosphatase activating domain) that facilitate mechanisms of tau-mediated

toxicity (Combs et al., 2019; Mueller et al., 2021). Other tau PTMs reported in AD include acetylation, methylation, ubiquitination, SUMOylation, O-GlcNAcylation, N-glycosylation, and truncation (reviewed in (Alquezar et al., 2021; Carroll et al., 2021)). Further studies are required to better understand the crosstalk between the various roles tau PTMs play in regulating tau pathological progression in AD.

Other secondary tauopathies include HD, synucleinopathies, and CTE, among several others. HD is an autosomal dominant disorder characterized by the aggregation of huntingtin protein (Labbadia & Morimoto, 2013). Increased levels of rod-like tau deposits of the 4R isoform, tau oligomers as well as abnormally phosphorylated tau (colocalized with mutant huntingtin) were reported in post-mortem HD brains (Fernández-Nogales et al., 2014; Vuono et al., 2015). Synucleinopathies are neurodegenerative disorders characterized by the presence of α -synuclein aggregates (Lewy bodies). Both NFTs and increased levels of phosphorylated tau were reported in Lewy body dementia, suggesting a synergistic interaction between tau and α -synuclein in synucleinopathies (Chin et al., 2020; Irwin et al., 2013; Joachim et al., 1987). CTE is another secondary tauopathy involving both 3R and 4R tau isoforms. The main driver of CTE is believed to be various forms of brain injury (e.g. concussive and/or repetitive subconcussive injuries) and is characterized by elevated levels of phosphorylated tau in neuronal and glial inclusions, axonal injury, and progressive neurodegeneration (Katsumoto et al., 2019).

To date, more than 13 neurological disorders have been identified as primary tauopathies in which tau is considered the major contributor of the pathological processes. Those include FTDP-17, PiD, PSP, CBD, and PART, among others (Josephs, 2017). FTDP-17 is characterized by several mutations of the *MAPT* gene (Strang et al.,

2019a). FTDP-17 mutations were suggested to alter tau polymerization kinetics, morphology of tau aggregates, propensity to aggregate, and microtubule binding (Combs & Gamblin, 2012). The P301L and the P301S missense mutations in exon E10 induced tau phosphorylation and aggregation (4R isoforms), NFT formation, synaptic dysfunction, and neuronal loss in several brain regions of transgenic mutant tau mouse models (Götz & Ittner, 2008; Lewis et al., 2000; Sperfeld et al., 1999). Accordingly, tau transgenic mouse models expressing P301L and P301S mutations are extensively used to study tau aggregation, axonal degeneration, and impaired memory function. Other FTDP-17 mutations (K257T, G272V, AK280, V337M, G389R, and R406W) were reported to reduce tau binding to microtubules, induce microtubule instability, and promote abnormal tau phosphorylation (reviewed in (Lee et al., 2001a; Strang et al., 2019b)). Moreover, FTDP-17 tau mutant carriers present the diverse clinical and neuropathological presentations that resemble other primary sporadic tauopathies such as PiD, PSP, and CBD.

PiD is characterized by severe atrophy in the hippocampus, frontal cortex and temporal cortex with neuronal tau inclusions of the 3R isoforms known as Pick bodies. Pathological phosphorylated tau was reported in the cortical and subcortical regions of post-mortem brains of subjects with PiD (Delacourte et al., 1996). PSP is characterized by tau inclusions composed primarily of the 4R isoform (Richter-Landsberg, 2016). NFTs, tau-positive tufted astrocytes and oligodendroglia coiled bodies were reported in PSP patients (Dickson et al., 2007). CBD is another 4R tauopathy characterized by astrocytic plaques, coiled bodies, and dense glial threads (Komori, 1999; Komori et al., 1998). The term PART was first proposed in 2014 to describe the progression of NFTs in cognitively normal aged individuals as well as in demented patients previously referred to as tangle-

only dementia, tangle-predominant senile dementia, and preferential development of NFT without senile plaques. PART is characterized by the presence of NFT with spatiotemporal progression similar to that seen in AD and without or with few amyloid- β plaques (NFT+/ amyloid- β –) (Crary et al., 2014). Taken together, there is a heterogeneity in the pathognomonic tau inclusions in both primary and secondary tauopathies that could be regulated in part by tau PTMs, *MAPT* mutations, as well as differences in tau protein-protein interactions.

Tau protein-protein interactions

Tau participates in various microtubule-dependent and -independent processes at the physiological and pathological level (reviewed in (Guo et al., 2017; Y. Wang & Mandelkow, 2016)). Although pathological tau dysfunction is the hallmark of the heterogenous group of neurodegenerative tauopathies, the varying disease-related mechanisms involving tau mutations, PTMs, and aggregation await further elucidation (Arendt et al., 2016; M. Morris et al., 2011). One way to better understand the various biological roles of tau in health and disease is by studying the tau protein interactome. The physiological and pathological functions of tau in the various cellular compartments are regulated by its multifaceted direct and indirect protein-protein interactions (Limorenko & Lashuel, 2022; Stancu et al., 2019). For example, tau not only acts as a substrate for other proteins such as kinases and phosphatases (reviewed in (Mietelska-Porowska et al., 2014)), but also act as a scaffolding protein that may regulate several kinase and phosphatase-mediated signaling pathways (Mueller et al., 2021).

Several studies have utilized crosslinking, co-immunoprecipitation (Co-IP) and mass spectrometry (MS) to identify tau protein interacting partners. In a human

neuroblastoma SH-SY5Y cell model, the authors transfected SH-SY5Y cells with enhanced green fluorescent proteins fused to the C-terminus of a) Full-length tau (amino acids 1-441), b) tau (amino acids 1-255), c) tau (amino acids 256-441), and d) tau amino acids 1-441 with the FTDP P301L mutation (Geeth Gunawardana et al., 2015). Transfected cells were crosslinked, lysed and the tau proteins interactors were affinity captured using GFP-trap beads, and then quantified by MS analysis. Proteins were identified as interacting partners based on an enrichment ratio >1.2 compared to the enhanced green fluorescent proteins-only transfected cell lysates. Utilizing this approach, the authors identified 190 tau interacting proteins which included RNA binding proteins, translation initiation and elongation factors, ribosomal proteins, histones, cytoskeletal, and proteasomal proteins. Histones, RNA binding, ribosomal, and translation proteins were preferentially interacting with the N-terminus of tau (amino acids 1-255), while members of the 14-3-3 protein family, actin binding, heat shock, and proteasomal proteins were preferentially interacting with the C-terminus of tau (amino acids 256-441). Moreover, the P301L mutation impaired tau binding to heat shock proteins, and proteasomal proteins, while it enhanced binding to ribosomal proteins.

In another study, *in vivo* crosslinking was used in 7-month-old wild type (WT) and transgenic rats expressing tau amino acids 151-391 of the 4R isoform (Sinsky et al., 2020). The protein lysates were extracted from the brain stem, separated by affinity chromatography using tau antibodies DC18 (amino acids 168 -181), DC25 (amino acids 347 -353), and DC190 (amino acids 368 - 376). Tau cross-linked proteins were then identified by mass spectrometry. Utilizing this approach, the authors identified 175

proteins as tau interactors, of which 39 were associated with AD, 10 with Parkinson's disease, and 22 with both.

Alternative splicing of the *MAPT* gene at exons E2 and E3 generates the 0N,1N, and 2N tau isoforms that are different by the expressing either 0,1, or 2 N-terminal inserts. The mouse *MAPT* gene generates only the 4R tau isoforms 0N4R, 1N4R, and 2N4R (Hernández et al., 2020b). To identify the interacting partners with each of the three isoforms of mouse tau, whole brain lysates from WT mouse were co-immunoprecipitated by antibodies specific to either 0N, 1N, or 2N isoforms (C. Liu et al., 2016). MS analysis identified a total of 101 proteins in all three tau isoforms lysates that were at least 10% enriched compared to lysates from TKO mice. The identified proteins were localized to the cytoplasm, cytoskeleton, and membrane-bound organelles including mitochondria, plasma membrane, and vesicles. Moreover, the authors reported preferential interactions with specific tau isoforms.

Other tau interactome mapping studies utilized the lysis/co-IP approach coupled to MS analysis to identify tau PPIs, followed by a more targeted approach to confirm and study the biological relevance of some of the novel tau interactors. In one study, WT mouse brain lysates were co-immunoprecipitated using three tau antibodies (Tau5, Tau21, and Tau24). Wang and colleagues identified 204 proteins as tau interactors and this included members of the dynactin complex, heat shock proteins, and members of the ubiquitin-proteasome system (P. Wang et al., 2017). Otub1 was identified as a novel tau deubiquitinase that significantly promoted phosphorylation and oligomerization of tau P301S *in vivo* and *in vitro* in transgenic models expressing TauP301S, an effect that was dependent on the catalytic domain of Otub1.

In another study, tau protein interacting partners were immunoprecipitated (Tau13 antibody) from frontal cortex lysate of 2.5-month-old uninduced (control) and induced rTg4510 tauopathy mouse model expressing the 0N4R tau isoform with the P301L mutation (Maziuk et al., 2018a). Doxycycline induction increases the expression level of the mutant tau protein. Interacting partners belonging to nucleotide binding, heat shock, and phosphoproteins were upregulated in the induced rTg4510 mice while proteins associated with the ribonucleoprotein complex, RNA binding, and mitochondria proteins were decreased in P301L expressing mice. Furthermore, nucleotide binding proteins including hnRNPA0, EWSR1, RPL7, and PABP colocalized with phosphorylated tau (pS202 tau, CP13 antibody) primarily in the neuronal soma and formed insoluble aggregates in the frontal cortex of 8 months old rTg4510 mice. Pathological deposits of RNA binding proteins (hnRNPA0, DDX60) were also observed adjacent (but not colocalized) to NFTs in the temporal cortex of human AD patients (Braak stage V and VI).

Phosphorylated tau accumulation is a key characteristic for tauopathies. Tau phosphorylation alters tau structure and function. A recent study used two phospho-tau antibodies, the AT8 and PHF1, to identify interacting partners via traditional IP approaches (Drummond et al., 2020). The hippocampus and entorhinal cortex of AD patients was used to purify AT8-positive tau and then used MS analysis to identify co-IPed proteins. The 542 proteins identified included APOE, GAPDH, CDK5, and ubiquitin. Samples from the frontal cortex of AD patients were immunoprecipitated with the PHF1 antibody and co-IPed proteins were identified by MS analysis. Utilizing this approach, 125 proteins were identified as potential interactors with phosphorylated tau. Among these, 75 proteins were also identified in AT8-purified samples, including ubiquitin, 14-3-3

protein family members, nucleotide binding proteins (e.g. HNRNPK, HNRNPA2B1, and HNRNPA1), and members of phagosome maturation protein family (e.g ATP6V0D1, NSF, PRDX5, PRDX6, and VAMP2).

Enzyme-mediated proximity labeling: A novel approach to study protein-protein interactions

Traditional methods for studying protein-protein molecular interactions relied mainly on antibody-based affinity purification coupled to MS analysis. These approaches allow for the identification of interacting partners that form a relatively stable complex with the protein of interest. However, the main limitations of this approach are the requirement of the non-physiological cell lysis which is susceptible to losing transient and low-affinity PPIs, the potential to artificially induce interactions, lysis and IP buffer-mediated effects, and a critical dependence on the availability of a high-quality antibodies. Other methods used to identify PPIs include the yeast two-hybrid system and coupling cross-linking to antibody affinity purification, however, they are prone to increased rate of false positives and yeast may not effectively recapitulate physiological interactions in mammalian cells (reviewed in (Berggård et al., 2007; Hayes et al., 2016)).

Over the past decade, proximity labeling (PL) techniques have emerged as a complementary approach that overcome several of the limitations of the traditional techniques. PL approaches involve the fusion of a protein of interest to an engineered enzyme which allow *in situ* biotin labeling of the proximal proteins (proximity-dependent biotinylation). The biotinylated proteins interacting with or in close proximity to the protein of interest are affinity captured using streptavidin-coated beads (leveraging the highly specific and strong biotin/streptavidin interaction) and identified using mass spectrometry.

To date, the engineered enzymes are either biotin ligases such as BioID, BioID2, BASU, TurboID, and miniTurbo, or peroxidases such as APEX, APEX2, and HRP. Biotin ligases catalyze the reaction between biotin and ATP to create the activated easter biotinyl-5'-AMP intermediate, which binds to lysine residues on the proximal proteins. Peroxidases oxidize biotin-phenol substrates in the presence of hydrogen peroxide to generate biotin-phenoxyl radical which reacts with tyrosine residues in the proximal proteins. The biotinylation radius of the enzymes (~10 nm in living cells) as well as the short half-life of the intermediates favors the labeling of the proximal proteins over the distant proteins that do not interact with the protein of interest (comprehensively reviewed in (Gingras et al., 2019; Qin et al., 2021; Zhou & Zou, 2021)).

The BioID biotin ligase (named for biotin identification) utilizes the *Escherichia coli* (*E. coli*) biotin ligase BirA. BioID is a mutated form of BirA which includes the R118G missense mutation. The mutated BioID overcomes the biotinylation specificity of BirA for the biotin carboxyl carrier protein subunit of acetyl-CoA carboxylase and allows BioID to promiscuously biotinylate all proximal lysine resides (Roux et al., 2012, 2013b). BioID2 was identified as an improved smaller form of BioID developed from the *Aquifex aeolicus* biotin ligase. BioID2 has the R40G mutation for promiscuous biotinylation of proximal lysines in interacting proteins in live cells. For efficient biotin labeling of proteins, BioID2 requires biotin supplementation and incubation for several hours (~16 -18 hours) or days as the protein labeling accumulates over time in living cells (Kim et al., 2016).

APEX is a cytosolic plant ascorbate peroxidase (hence APEX) that was first engineered as a tag for electron microscopy (Martell et al., 2012) and was first used for proteome labeling in living cells to identify mitochondrial matrix proteins (Rhee et al.,

2013). In 2014, APEX2 was developed from APEX to include the A134P mutation which improved the kinetics, stability, and cellular activity of the enzyme (Lam et al., 2014). The main difference between APEX2 and BioID2 is the significantly shorter time (~ 1 min) utilized for protein labeling by APEX2 in live cells, which allows for a shortened cross-sectional snapshot of the interactome in live cells. Also, APEX2 is a peroxidase which requires the addition of toxic hydrogen peroxide to the cells which limits its *in vivo* and long-term application (Qin et al., 2021; Samavarchi-Tehrani et al., 2020).

In APEX2 antibody-based recent study, the approach and an immunoprecipitation approach were used to study the tau protein interactome in human induced pluripotent stem cell (iPSC)-derived glutamatergic neurons (i³Neurons) (Tracy et al., 2022). The i³Neurons were modified to express one of the following proteins a) APEX2-Tau, b) Tau-APEX2, c) APEX2- α Tubulin, d) WT-Tau-Flag, e) TauP301L-Flag, and f) TauV337M-Flag. The APEX2-based PL experiments was used to identify tau PPIs by fusing APEX2 to either the N-terminus or the C-terminus of the 2N4R human tau protein. An APEX2-α-tubulin was used as the control fusion protein. This PL approach identified a total of 246 tau interacting partners, of which 136 were identified in APEX2-Tau and Tau-APEX2, 68 were unique to APEX2-Tau, and 42 were identified only with Tau-APEX2. This interactome snapshot identified proteins localized to the cytoskeleton. synapse, ribonucleoprotein complex, somatodendritic compartment, autophagosome, ubiquitin proteasome system, and synaptic vesicles. The antibody-based affinity purification experiment was used to study the effects of the FTD mutations P301L and V337M on the tau protein interactome. Protein lysates were immunoprecipitated using the Flag tag antibody and identified by mass spectrometry. Compared with WT-Tau,

TauP301L exhibited increased interaction with 14 proteins and decreased interaction with 108 proteins. While TauV337M showed increased interaction with 69 proteins and decreased interaction with 184 proteins. The enriched proteins with TauP301L were involved in nucleoside metabolism while those enriched with TauV337M were members of the synaptic vesicle membrane and spliceosome complex. Interestingly, the decreased interactions with both TauP301L and TauV337M included ribosomal and mitochondrial proteins which were presumably disrupted by the two FTD mutations.

THESIS OBJECTIVE

This thesis aims to develop a method to identify the protein interactome of tau. The microtubule-dependent and -independent functions of the tau protein are mediated by its interacting partners under physiological and pathological conditions. The identified tau protein interactome provides a comprehensive mapping of tau's growing cellular functions in neurons which could help to develop novel tau-targeted therapeutic strategies for the tau-mediated neurodegenerative processes.

I utilized the BioID2 biotin ligase approach which allows for the *in situ* biotin labeling in living neurons. The biotinylated proteins can then be identified by biotin-targeted pulldown with streptavidin and identified using mass spectrometry. I created fusion proteins between BioID2 and tau. BioID2 was fused to either the N-terminus of the 2N4R human tau protein (BioID2-Tau) or the C-terminus (Tau-BioID2). Both constructs featured a 13x-linker between BioID2 and tau which adds flexibility between the two proteins and minimizes the undesired interactions between them. Two control constructs were created, the Myc-BioID2 was used as a control for BioID2-Tau while the BioID2-HA was used as a control for Tau-BioID2. Lentiviruses expressing the BioID2 proteins were generated and used to transduce E18 TKO primary cortical mouse neurons. The long-term goal of this project is to provide an approach that will facilitate the detection of bona fide tau interactors that may be transient/weak interactors and/or difficult to detect using more traditional approaches.

Aim Statement

Develop a novel Tau-BioID2 assay to map tau protein-protein interactions which mediate the cellular functions of tau under normal physiological conditions.

Hypothesis

Tagging BioID2 to either the N-terminus or C-terminus of full-length 2N4R human tau protein will reveal known as well as novel tau interacting partners in primary cortical neurons.

MATERIALS AND METHODS

Creating Tau-BioID2 expression plasmids using Restriction Cloning

The below methods were used to create plasmids that express the Tau-BioID2 fusion proteins. The BioID2-expressing plasmids MCS-13X Linker-BioID2-HA (BioID2-HA, Addgene, #80899) and Myc-BioID2-13X Linker-MCS (Myc-BioID2, Addgene, #92308) were a kind gift from the Kyle Roux lab (Kim et al., 2016). MCS-13X Linker-BioID2-HA plasmid was used to fuse BioID2 to the C-terminus of the tau protein (Tau-BioID2) while the mycBioID2-13X Linker-MCS plasmid was used to fuse BioID2 to the N-terminus of the tau protein (BioID2-Tau). Both plasmids feature a 13x-linker which is a serine-glycine repeat sequence that acts as a flexible spacer sequence which could increase the biotinylation range (Kim et al., 2016). The BioID2 constructs were cloned into the pFIN vector (Addgene, #44352) to generate lentiviruses for primary neuron transductions. The longest tau isoform, hT40 or the 2N4R isoform (Tau, 441 amino acids) was used for all experiments. All plasmid constructs were validated by restriction digestion, Sanger sequencing, and western blotting.

Site-directed mutagenesis

Single-site and multi-site mutagenesis reactions were performed using QuikChange Lightning site-directed mutagenesis Kit (Agilent Technologies, #210518 and #210516). The BioID2-HA plasmid was mutated to include a KpnI restriction site upstream of the BioID2 sequence and then again to include an EcoRV site and a Kozak sequence

uprstream of the KpnI site. Then a NotI restriction site was inserted downstream of the BioID2 sequence. The following primers were used:

- Kpnl site insertion:
 - 5'- cggattcgaattcggatccGGTACCttttcggaattcggatccg-3'
- EcoRV site and Kozak sequence insertion:
 5'-cggtcgtacgtctccgGATATCAAGCCACCATGggtaccttttcg-3'
 - NotI site insertion: 5'-gatgtaccggattacgcatagGCGGCCGCcgctgatcagcctc-3'

The Myc-BioID2 plasmid was mutated to insert an EcoRV restriction site upstream of the BioID2 sequence and an NdeI restriction site downstream of the BioID2 sequence, and to delete the endogenous NdeI resitriction site upstream of the BioID2 sequence. The following primers were used:

- EcoRV site insertion: 5'- cactatagggagacccaagcGATATCgccaccatggaac-3'
- Ndel site insertion: 5'- gtggatcggcgcgcgtCATATGaacctcgagc-3'
- Ndel site deletion: 5'- gcagtacatcaagtgtatcCGCGgccaagtacgcccctattgacg-3'

The following mutagenesis reaction protocol was used: $19.25 \,\mu$ l nuclease-free H₂O, $2.5 \,\mu$ l QCL buffer, $0.75 \,\mu$ l Quiksolution reagent, $0.5 \,\mu$ l dNTP mix, $0.5 \,\mu$ l ($10 \,\mu$ M) primers, $25 \,\mu$ l ng DNA template, and $0.5 \,\mu$ l QCL enzyme. The mutagenesis reaction was transferred into a thermal cycler (Applied Biosystems, #4375786) and the cycling parameters in Table 1 were used. After mutagenesis, $2 \,\mu$ l of Dpn I restriction enzyme was added to the reaction and incubated for 10 minutes at 37 °C. Dpn I enzyme digests the template double stranded DNA (i.e. methylated) in the reaction.

Table 1: Cycling parameters for mutagenesis reactions

Step	Number of Cycles	Temperature	Time
1	1	95 °C	2 minutes
2	30	95 °C	30 seconds
		55 °C	30 seconds
		65 °C	30 seconds/kilobase of plasmid
			length
3	1	65 °C	5 minutes
4	1	4 °C	Infinity

Preparation of LB/agar plates and LB broth medium

The LB/agar was prepared by dissolving 10 grams of LB broth base (Sigma-Aldrich, #L3522), 7.5 grams of Agar (Sigma-Aldrich, #A1296) in 500 ml double-distilled water (ddH₂O) and autoclave using a liquid cycle. LB/agar was cooled at room temperature, 50 mg ampicillin (Sigma-Aldrich, #A9518) were added while still warm, and approximately 20 ml of LB/agar were poured into petri dishes and left at room temperature to solidify. LB/agar plates were used directly or stored at 4°C. LB broth base was prepared by dissolving 10 grams of LB in 500 ml ddH₂O.

Transformation of XL10-Gold ultracompetent cells

XL10-Gold ultracompetent cells (provided with QuikChange Lightning kit) were thawed on ice and then 40 µl of cells and 4 µl of DNA were transferred into a microcentrifuge tube and incubated on ice for 10 minutes. Cells were heat-shocked for 30 seconds at 42 °C and left on ice for 2 minutes. Pre-heated LB broth (360 µl) was added to the tube and cells were incubated for 1 hour at 37 °C with shaking at 300 rpm. The entire culture was

poured on one LB/agar plate, streaked to cover the plate, and incubated at 37 °C for 12-16 hours.

Transformation of Stbl3 competent E.coli

For each transformation reaction, one vial of one shot Stbl3 cells (ThermoScientific, #C7373-03) was thawed on ice. 5 µl DNA were added to the cells and left on ice for 30 minutes. Stbl3 cells were heat-shocked at 42 °C for 45 seconds and placed on ice for 2 minutes. S.O.C medium (250 µl) was added to the Stbl3 cells, and the transformation reaction was incubated for 1 hour at 37 °C with shaking at 225 rpm. The entire culture was streaked to cover an LB/agar plate, and the plate was incubated at 37 °C for 12-16 hours.

Plasmid DNA Miniprep

Single colonies (5-10 colonies/construct) from the streaked LB/agar plates were picked using a micropipette tip and inoculated into a culture of 5 ml LB containing ampicillin (100 µg/ml) in a sterile glass test tube and incubated for 12-16 hours at 37 °C with shaking at 225 rpm. Bacterial cells were centrifuged at 8000 x g for 3 minutes at room temperature and supernatant was discarded. Plasmid DNA extraction was performed using QIAprep spin miniprep kit (Qiagen, #27104) following the manufacturer's instructions. Plasmid DNA concentration was measured using NanoDrop spectrophotometer (ThermoScientific, #ND-2000). Validation of plasmid DNA was done by both restriction digestion and Sanger sequencing (Genewiz).

Plasmid DNA Maxiprep

A single colony was picked from LB/agar plate, inoculated into a 5 ml LB sterile glass test tube containing ampicillin (100 μg/ml), and incubated overnight at 37 °C with shaking at 225 rpm. The 5ml bacterial culture was inoculated into 250 ml LB containing ampicillin (100 μg/ml) in a flask. The bacterial culture was left to grow overnight at 37 °C with shaking at 225 rpm. The bacterial cells were harvested by centrifugation at 6,000 x g for 15 minutes at 4 °C, and the plasmid DNA maxiprep was performed using the Qiagen plasmid maxi kit (Qiagen, #12162) following the manufacture's protocol.

Restriction Digestion

Digestion reactions were prepared by adding 500 ng plasmid DNA samples, 1 μl of each restriction enzyme, 2 μl fast digest green buffer and nuclease-free H₂O to a total volume of 20 μl. Digestion reaction was incubated for 1 hour at 37°C. Restriction enzymes used for the plasmids created were fast digest EcoRV (ThermoScientific, #FD0303), Kpnl (ThermoScientific, #FD0524), Ndel (ThermoScientific, #FD0584), Notl (ThermoScientific, #FD0596), and Xhol (ThermoScientific, #FD0694).

DNA Gel Electrophoresis

One liter of 50X TAE buffer stock solution was prepared by adding 242.28 g Tris-base (Sigma-Aldrich, #10708976001), 57.2 ml glacial acetic acid, 100 ml of 500 mM EDTA buffer (pH 8.0) and adjusting the volume to one liter by adding ddH₂O. One liter 0.5X TAE

buffer working solution was prepared by adding 10 ml 50X TAE buffer to 990 ml ddH₂O. Agarose gel (1%) was prepared by dissolving 2 grams of agarose (Bio-Rad, #1613101) in 200 ml 0.5X TAE buffer and microwaving for 2-4 minutes until fully dissolved, and adding 20 μl ethidium bromide (Bio-Rad, #1610433). The agarose gel was poured into a gel electrophoresis system (ThermoScientifc, #09-528-110B), and left to polymerize for 30-40 minutes at room temperature. 20 μl of 1kilobase DNA ladder (NEB, #N3232S) was added to the first well then 20 μl digestion reaction was added. The gel was run at 150 constant volts for 45-60 minutes and the DNA bands were visualized under a UV transilluminator (Accuris, #E3100).

Gel purification and DNA ligation

The DNA gels were placed on a UV transilluminator and the desired DNA band was cut out using a razor blade and placed it into a microcentrifuge tube. DNA gel extraction was performed using QIAquick Gel Extraction Kit (Qiagen, #28706) following manufacturer's instructions. Then, the ligation reaction was prepared by adding 2 µl of open plasmid backbone, 8 µl of the desired insert (with compatible overhangs), 1 µl of 10X T4 buffer, 1 µl of T4 DNA ligase enzyme (ThermoScientific, #EL0011), adjusting the final volume to 20 µl with ddH₂O, and incubating overnight at 16 °C. The ligation reaction was used to transform a bacterial strain, purified using QIAprep spin miniprep kit (Qiagen, #27104), and validated by restriction digestion and Sanger sequencing (Genewiz).

Human embryonic kidney (HEK293T) cell culture

Complete Dulbecco's Modified Eagle Medium (DMEM) (500 ml Gibco, DMEM #11995073, 5% fetal bovine serum (FBS), and 1% penicillin-streptomycin Sigma-Aldrich, #P0781) was prepared. Complete DMEM was filtered through a disposable vacuum 0.22 µm filter (Corning, #097611) and stored at 4 °C for up to one month. HEK293T cells were retrieved by thawing 2 x 10^6 cells in 37°C bead bath, centrifuged at 200 x g for 2 minutes, supernatant was discarded, and the cell pellet was resuspended in 5 ml complete DMEM. Cells were transferred to a T25 flask (ThermoScientific, #156340), and maintained for 4 days at 37 °C, 5% CO₂ in a humidified incubator. For routine maintenance of cells, old medium was discarded, and monolayers of 80-90% confluent cells were detached by adding 1 ml 0.5% trypsin (Gibco, #15400054) and incubating for 5 minutes at 37 °C in the humidified incubator. Detached cells were collected in a 15 ml conical tube (Fisher scientific, #22010075), centrifuged at 200 x g for 2 minutes. Cell pellet was resuspended in 10 ml complete DMEM, split 1:10 in a new T75 flask (ThermoScientific, #156472), and maintained at 37°C, 5% CO₂ in a humidified incubator.

Transfection of HEK293T cells

HEK293T cells (4.8 x 10^6) were plated in a poly-d-lysine-coated 12-well plate (Corning, #354470) and left overnight in a humidified incubator. Transfection reactions for each well in a 12-well plate were prepared by adding 1 μg plasmid DNA (expressing BioID2-only controls or Tau-BioID2 fusion proteins), 10 μl polyethylenimine, 200 μl of 150 mM NaCl, and was kept at room temperature for 20 minutes. HEK293T Cells were transected at

~80% confluency by adding drops of the transfection mixture and were maintained for 24 hours in a humidified incubator. Finally, 100 µM biotin (Sigma-Aldrich, #B4501) was supplemented in complete DMEM and cells were incubated for 24 hours before collecting cell lysates.

HEK293T protein lysate collection

Cell culture media was removed, and cells were washed twice with 1x Dulbecco's phosphate-buffered saline (DPBS) (Gibco, #14200075). Cell lysates were collected in lysis buffer containing 50 mM Tris pH 7.4, 150 mM NaCl, 0.4% SDS, 1% NP-40, 1 mM EGTA, and 1.5 mM MgCl₂ supplemented with 1x protease inhibitors added immediately before use (pepstatin A, leupeptin, bestatin, aprotinin, and PMSF all purchased from ThermoScientific). Cell lysates were sonicated for 3 x 10 seconds (Misonix XL-2000 series) and centrifuged at 12,000 x g for 10 minutes at 4°C. Protein concentration was measured using Pierce rapid gold BCA protein assay kit (ThermoScientifc, #A53225) following manufacturer's instructions and protein lysates were stored at -80 °C until use.

SDS-PAGE and Western blotting

Lysates were prepared in 1x sample buffer (containing 2% Sodium dodecyl sulfate (SDS), 5% 2-mecaptoethanol, 10% glycerol, 0.002% bromophenol blue, 20 mM Tris-HCl pH 6.8) and heated to 95 °C for 5 minutes. Precast SDS-PAGE gels (Bio-Rad, #4561095) were used to separate proteins via electrophoresis in 1x running buffer (25 mM Tris base pH 8.3, 190 mM glycine, 0.1% SDS). Protein lysates (20 µg/lane) and protein standard

markers (1.5 μl/lane; Bio-Rad #1610373) were run for 32 minutes at constant 250 volts. Gels and nitrocellulose transfer membrane (Bio-Rad, #1620213) were soaked for 5 minutes in 1x transfer buffer (25 mM Tris pH 8.3, 192 mM glycine, and 20% methanol). Proteins were transferred from the gel onto a nitrocellulose membrane by running the transfer cassette for 50 minutes at constant 400 milliampere. Membranes were blocked in 2% non-fat milk for 1 hour at room temperature. Membranes were incubated in primary antibodies diluted in the blocking buffer overnight at 4 °C. Membranes were washed three times in 1x TBS-T (50 mM Tris, 150 mM NaCl, pH 7.4, 1% Tween-20) and then incubated in secondary antibodies IRDye 680LT goat anti-mouse IgG and IRDye 800CW goat anti-rabbit IgG, diluted in the blocking buffer (1:20,000). Membranes were washed three times in 1x TBST and imaged using LI-COR Odyssey® infrared system.

Generation of Lentiviruses that express the BioID2 proteins

Lentiviruses production in HEK293T cells

For each lentiviral preparation, 4 x 150 mm cell culture dishes (Corning, #430599) were plated at density 1 x 10^6 cells/dish in 25 ml complete DMEM. Culture dishes were incubated overnight in a humidified incubator. Two hours prior to transfection, DMEM was removed, and fresh DMEM was added. The following transfection reactions were then prepared for each 150 mm culture dish: 45 µg plasmid DNA (22.5 µg of the BioID2 plasmid DNA, 15 µg of pNHP packaging vector (Addgene, #22500), 7.5 µg of pHEF-VSVG envelope vector (Addgene, #22501), 300 µl polyethylenimine and 6 ml of 150 mM NaCl. The transfection reagent was incubated for 20 minutes at room temperature, slowly

added to each culture dish, then transfected HEK293T cells were maintained overnight in a humidified incubator. Complete DMEM was substituted by freshly prepared viral medium (98% DMEM, 1% FBS, and 1% penicillin-streptomycin) and transfected HEK293T cells were maintained for 48 hours in a humidified incubator. Medium containing lentiviruses was transferred to a 50 ml conical tube, centrifuged at 675 x g for 5 minutes and the supernatant containing lentiviruses was filtered through a 0.45 µm filter. Lentiviruses were harvested by layering on 20% sucrose solution, and ultracentrifugation at 82,700 x g for 2 hours at 4°C using Sorvall™ WX+ ultracentrifuge (ThermoScientific, #75000100). The lentiviral pellets were resuspended in 500 µl sterile PBS, aliquoted, snap-frozen in crushed dry ice, and stored at -80°C until use.

Immunocytochemistry (ICC)

HEK293T cells were plated in a 24-well plate at a density of 75,000 cells/well and incubated overnight. Cells were fixed in 4% paraformaldehyde (Electron Microscopy Sciences, #15714) prepared in 1x cytoskeleton buffer (10 mM MES, 138 mM KCl, 3 mM MgCl₂, 4 mM EGTA pH 6.1, all from Sigma-Aldrich). Cells were rinsed four times by 1x TBS and incubated for 1 hour at room temperature in blocking buffer containing 5% goat serum (GS, VWR#10152-212),1% bovine serum albumin (Gemini Bio Labs#700-101P), 0.2% Triton-X100 (Bio-Rad, #161-0407) prepared in 1x TBS. Cells were incubated in primary antibodies diluted in 2% GS-1x TBS and maintained overnight at 4 °C. Cells were rinsed four times by 1x TBS and were incubated for one hour in biotinylated secondary antibodies diluted 1:500 in 2% GS. Avidin-biotinylated horseradish peroxidase (HRP) complex (ABC, ThermoScientific, #32020) was prepared by adding 1 drop of each

reagent A and B to 10 ml 1x TBS and incubating for 30 minutes at 4 °C. Cells were rinsed four times in 1x TBS and were incubated in ABC solution or 1 hour at room temperature. The peroxidase substrate was prepared by adding 2.5 mg DAB (Sigma-Aldrich, #281751) to 5 ml 1x TBS and then adding 0.5 µl 30% H₂O₂. Cells were rinsed four times in 1x TBS and the peroxidase substrate was added for 5 minutes at room temperature. The assay development was stopped by removing the substrate and rinsing four times in 1x TBS. Cells were visualized under inverted light microscope Nikon eclipse TE2000-U.

Lentiviral functional titer determination using ICC

HEK293T cells were transduced by lentiviruses expressing either the fusion proteins Tau-BioID2, BioID2-Tau or the respective controls BioID2-HA, Myc-BioID2. Cells were transduced by lentiviruses at 10-fold dilutions from 1:10^2 to 1:10^9 and maintained for 72 hours in a humidified incubator. Cells were fixed in 4% paraformaldehyde and the ICC protocol was followed as described above. HA-tag and Myc-tag primary antibodies were used at dilutions 1:4,000 in 2% GS. Biotinylated goat anti-mouse IgG and goat anti-rabbit IgG secondary antibodies were diluted 1:500 in 2% GS. The lentiviral functional titer was calculated by multiplying the number of transduced cells at the highest viral dilution by the dilution factor.

Lentivirus functional titer (transducing unit/µI) = # transduced cells in the highest viral dilution x the dilution factor

Embryonic day 18 mouse primary cortical neuron culture preparation

Timed-pregnant female TKO mice (JAX, 007251) were euthanized by intraperitoneal injection of 50-100 mg sodium pentobarbital diluted in saline per kg. Mouse pups were collected on embryonic day 18 (E18) and kept in ice-cold 0.9% saline. Pups were decapitated and heads were isolated and placed on a 60 mm dish containing ice-cold saline and placed under a dissecting microscope. Skin and skull were removed, and the brain tissue was extracted. The cerebellum was discarded, the two hemispheres were separated, and the cerebral cortices were dissected. Cortices from all pups were cut into small pieces and collected in a tube containing ice-cold calcium- and magnesium-free solution (CMF; contains 1x DPBS, 1x amphotericin B (Gibco, #15290018), 1x gentamicin (Gibco, #15750060), and 10% glucose (Sigma-Aldrich, #G8270)). Where indicated, E18 WT C57/BL6 (BrainBits LLC, C57ECX) cortical tissue was used where indicated.

The E18 cortical tissue pieces were washed four times in CMF and incubated in 0.25% trypsin solution (Gibco, #15090046) for 15 minutes at 37 °C. Trypsin was removed and cortices were washed two times in CMF. Trypsin inactivation solution (3 ml) was added containing 2.1 ml Hank's Balanced Salt Solution (GibcoTM#24020117), 0.6 ml newborn calf serum (GibcoTM#16010167), and 0.3 ml DNase solution (Worthington# LS002006). A homogenous cell suspension was obtained by gentle trituration of the tissue (30 x 14-gauge needle, 30 x 15-gauge needle, 20 x 16-gauge needle, 20 x 18-gauge needle, and 15 x 21-gauge needle). Cell suspensions were layered onto 5 ml sterile-filtered FBS and centrifuged at 200 x g for 5 minutes. Primary neuron cell pellets were resuspended in 1ml complete neurobasal medium containing 96% neurobasal media (NBM; Gibco, #21103049), 1% L-glutamine (Gibco, #25030081), 1% amphotericin

B (Gibco, #15290018), 1% B-27 Supplement (Gibco, #17504044), and 1% gentamicin (Gibco, #15750060). Cell counts were determined using Countess™ 3 automated cell counter (Invitrogen, #AMQAX2000), primary neurons were plated at density 3.6 x 10^6 cells per plate and maintained in a humidified incubator by adding 10% NBM twice a week.

Immunocytofluorescence (ICF)

Primary neurons were fixed in 4% paraformaldehyde for 20 minutes, washed three times in 1x TBS, and blocked for one hour in blocking buffer (5% GS, 1% bovine serum albumin, 0.2% Triton-X100 diluted in 1xTBS). Cells were then incubated overnight in primary antibodies diluted in 2% GS. Cells were washed three times in 1xTBS then incubated in secondary antibodies diluted 1:500 in 2%GS for one hour at room temperature. Cells were washed three times in 1xTBS and counterstained using DAPI counterstain diluted 1:10,000 in 1xTBS. Cells were visualized under inverted microscope Nikon eclipse Ti2.

Lentivirus transduction efficiency

E18 WT primary cortical mouse neurons were transduced on 4th day *in vitro* (DIV) by lentiviruses expressing the BioID2 proteins (Tau-BioID2, BioID2-Tau, Myc-BioID2, and BioID2-HA). For each lentiviral construct, primary neurons were transduced at multiplicity of infection (MOI) of 50,100, and 200. On DIV9, primary neurons were fixed and ICF was performed as described above. Primary antibodies used were HA-tag or Myc-tag antibodies (diluted 1:800 in 2%GS), and Tau13 antibody diluted (1:5,000 in 2%GS).

Secondary antibodies used were Alexa Fluor 568 goat anti-mouse IgG or Alexa Fluor 488 goat anti-rabbit IgG (diluted 1:500 in 2%GS). Transduction efficiency was calculated by dividing the number of transduced cells by the total number of cells (identified by the DAPI nuclear counterstain).

$$Transduction \ efficiency = \frac{number \ of \ transduced \ cells}{total \ number \ of \ cells}$$

Lentiviral transduction in neurons

On DIV4, primary neurons were treated with lentiviruses expressing the fusion proteins BioID2-Tau, Tau-BioID2 or the respective controls Myc-BioID2, and BioID2-HA. Lentiviruses were diluted in complete NBM, and primary neurons were transduced at MOI 200. Every other day, 10% NBM was supplemented, and the primary neuronal culture was checked for the toxicity of the lentiviral vectors expressing the BioID2 proteins. The neuronal culture was maintained for four days before supplementing exogenous biotin. This allows sufficient time for the lentiviral genome reverse transcription, integration into the host cell DNA and expression of the proteins of interest using the host cell transcription and translation machinery.

Endogenous tau vs lentiviral tau expression levels

E18 WT and TKO primary cortical neurons were plated at density 150,000 cells/well in a 24-well plate (n=3 technical replicates). On DIV4, TKO neurons were transduced by lentivirus expressing Tau-BioID2. Both neuronal cultures were maintained by adding 10%

NBM every other day. On DIV12, primary neurons were fixed and ICF was performed as described above with Tau5 primary antibody (diluted 1:5,000 in 2%GS) and Alexa Fluor 568 goat anti-mouse IgG secondary antibody (diluted 1:500 in 2%GS). To quantify tau protein expression level, fluorescent signals were imaged at 20x magnification (0.9 mm field of view). Images were randomly selected within the well (5 images/well and 3 wells/condition) using identical image acquisition settings (1 second exposure, all other parameters at the default). Image analysis was preformed using FiJi software (Schindelin et al., 2012) by setting the minimum intensity threshold at 12,000 and the maximum intensity threshold at 60,000. Signal intensity was assessed within each image using the analyze particles function and taking the average pixel intensity values for comparison between WT cells and Tau-BioID2 transduced TKO neurons.

Mass Spectrometry identification of biotinylated proteins

Optimization of Biotin dose and incubation time

E18 TKO primary cortical neurons were transduced on DIV4 by lentivirus expressing BioID2-Tau. On DIV8, exogenous biotin prepared in neurobasal medium was supplemented in the following doses 0, 50, or 100 μM. Cells were incubated for either 24, 48 or 96 hours in a humidified incubator. Three biological replicates were performed for each biotin dose and incubation time condition. Protein lysates were collected and 10 μg was used for western blotting. Membranes were blocked in 2% non-fat milk for 1 hour at room temperature and incubated in anti-biotin primary antibody diluted 1:1,000 overnight at 4°C. Membranes were washed three times in 1x TBS-T and incubated in Li-cor IRDye

800CW goat anti-rabbit secondary antibody diluted 1:20,000. The blots were imaged using LI-COR Odyssey® infrared system. The biotin signal was quantified using LI-COR Image Studio™ lite version 5.2.

Primary neurons protein lysate collection

E18 TKO primary cortical neurons were plated at density 3.6 x 10^A6 cells per plate. On DIV4, each plate was transduced by lentivirus at MOI 200 (n=3 independent experimental replicates for each lentiviral transduction). On DIV8, 100 μM biotin was supplemented. On DIV12, cells were washed twice in 1x DPBS and protein lysates were collected in 1ml lysis buffer (50 mM Tris pH 7.4, 150 mM NaCl, 0.4% SDS, 1% NP-40, 1 mM EGTA, and 1.5 mM MgCl₂ supplemented with 1x protease inhibitors immediately before use (pepstatin A, leupeptin, bestatin, aprotinin, and PMSF). Lysates were sonicated 3 x 10 seconds and centrifuged at 12,000 x g for 10 minutes at 4°C. Protein concentration was measured using PierceTM rapid gold BCA protein assay kit.

Biotin-streptavidin affinity pulldown

Ethanol-clean low retention microcentrifuge tubes (ThermoScientific, #3453) were placed in a magnetic separation stand. Streptavidin magnetic Dynabeads C1 (400 μl; Invitrogen, #65002) were used per condition. The beads were washed twice in 1ml lysis buffer and then 1 mg of protein lysate was added to the beads and rotated overnight at room temperature. The following day unbound supernatant proteins were collected as the post-pulldown sample and stored at 4°C until further analysis. The beads containing bound

biotinylated proteins were washed twice in lysis buffer, then resuspended in 1ml 50 mM TrisCl, pH 7.4. 900 μ l was transferred to a new low retention tube for mass spectrometry analysis while the remaining 100 μ l was transferred to another tube for western blotting validation.

The tube containing the 100 µl for western blotting was placed on a magnetic separation stand and the supernatant was discarded. The beads were resuspended in elution buffer containing 25 mM biotin prepared in lysis buffer. Efficient elution of biotinylated proteins was performed by competition with free biotin in the elution buffer and heating to 95°C for 15 minutes. The tube was placed on a magnetic separation stand and the supernatant containing biotinylated proteins was transferred to a new tube and western blotting validation was performed as described above using anti-biotin antibody.

Liquid Chromatography-MS/MS

The tube containing the 900 µl was placed on magnetic separation stand and the supernatant was discarded. The beads were washed six times in 25 mM ammonium bicarbonate (pH 8) and then resuspended in 150 µl of 25 mM ammonium bicarbonate - 50% acetonitrile (ACN). On-bead protein digestion was performed by adding 100 ng of rlys-C enzyme (Promega, #V1671) and incubating for 90 minutes at 37°C then adding 3 µg trypsin (Promega, #V5280) and incubating for 16-18 hours at 37°C. The tubes were placed on magnetic separation band and the digestion solution was collected in a new low retention tube. The samples were dried to completion in a speed vacuum centrifuge

at 30 °C and the samples were resuspended in 50 µl of 25 mM ammonium bicarbonate /5% ACN.

NanoLC-MS/MS separations were performed with a Thermo Scientific™ Ultimate™ 3000 RSLCnano System. Peptides were desalted in-line using a 3 µm diameter bead, C18 Acclaim™ PepMap™ trap column (75 µm × 20 mm) with 2% ACN, 0.1% formic acid (FA) for 5 min with a flow rate of 5 µl/min at 40°C. The trap column was then brought in line with a 2 µm diameter bead, C18 EASY-Spray™ column (75 µm × 250 mm) for analytical separation over 60 min with a flow rate of 350 nl/min at 40°C. The mobile phase consisted of 0.1% FA (buffer A) and 0.1% FA in ACN (buffer B). The separation gradient was as follows: 5 min desalting, 40 min 4-40% B, 2 min 40-65% B, 2 min 65-95% B, 7 min 95% B, 1 min 95-4% B, 3 min 4% B. One microliter of each sample was injected. Top 20 data-dependent mass spectrometric analysis was performed with a Q Exactive™ HF-X Hybrid Quadrupole-Orbitrap™ Mass Spectrometer. MS1 resolution was 60K at 200 m/z with a maximum injection time of 45 ms, AGC target of 3e6, and scan range of 300-1500 m/z. MS2 resolution was 30K at 200 m/z, with a maximum injection time of 54 milliseconds, AGC target of 1e5, and isolation range of 1.3 m/z. HCD normalized collision energy was 28. Only ions with charge states from +2 to +6 were selected for fragmentation, and dynamic exclusion was set to 30 s. The electrospray voltage was 1.9 kV at a 2.0 mm tip to inlet distance. The ion capillary temperature was 280°C and the RF level was 55.0. All other parameters were set as default.

Mass spectrometry protein identification

Raw mass spectrometry data were searched with Sequest HT against the reviewed Mus musculus Uniprot proteome database (UP000000589, 25285 unique sequences) with Thermo Scientific Proteome Discoverer software (version 2.5). Enzyme specificity was set to trypsin with an MS1 tolerance of 10 ppm and a fragment tolerance of 0.02 Da. Oxidation (M), biotinylation (K), acetylation (protein N-term), methionine loss (protein N-term), and biotinylation (protein N-term) were set as dynamic modifications. Peptides and proteins were filtered by 1% false discovery rate with threshold determined via decoy search using the Percolator algorithm. At least two peptide identifications were required to identify a protein. All other parameters were set at the defaults.

Label-free quantification of identified proteins

Label-free quantification was performed using Proteome Discoverer software (version 2.5). Peptide abundance was calculated based on the peak intensity of the peptide spectral matches. Peptide abundance was normalized to the sample group with highest peptide abundance. The protein abundance ratio was calculated using the pairwise ratio approach by measuring the abundance ratios for each peptide observed in both the tau sample and its respective control and selecting the median ratio as the protein abundance ratio. The following criteria were used to define proteins as Tau-BioID2 or BioID2-Tau interactors: 1) being identified in at least two of the independent replicates, and 2) being detected at ≥1.5-fold increase compared to the respective BioID2 control. Proteins identified in only one independent replicate as well as background proteins including

keratins, and endogenously biotinylated carboxylases were removed from further analysis.

Functional protein association networks

Functional protein-protein interaction networks were visualized by the Search Tool for the Retrieval of Interacting Genes/Proteins (STRING) analysis. STRING V11.5 was used to visualize the protein interactome network including both functional associations retrieved from published databases, text mining, computational prediction methods and physical interactions retrieved from experimental data (genetic, biochemical, and biophysical techniques) with a minimum required confidence interaction score set at 0.7 and above (high confidence interaction) (Szklarczyk et al., 2015). The network map was then imported to the stringApp (Doncheva et al., 2019) (a built-in app in Cytoscape V.3.9.1) (Cline et al., 2007; Paul Shannon et al., 1971), the Cytoscape app ClusterMaker Cluster Network (J. H. Morris et al., 2011) was used to perform Markov Clustering (MCL) (Brohée & van Helden, 2006) with inflation value of 3.0 to reduce the cluster size. The string enrichment app (Cytoscape) was used to retrieve the functional enrichment analysis visualized on the protein network map with false discovery rate set at 1%, for simplicity. GO cellular component was added to the map to visualize the intracellular localization of the mapped proteins (Doncheva et al., 2019).

Gene Ontology enrichment analysis

GO enrichment analyses were performed using ClueGo (V.2.5.8) (Bindea et al., 2009) app plugged in Cytoscape V.3.9.1. I performed ClueGO cellular component, molecular function pathways and KEGG pathways with GO interval minimum level of 3 and maximum level of 9 showing only pathways with p-value ≤0.05. For KEGG pathway analysis, only diseases with more than 26 identified proteins were included. All other parameters were set at the defaults.

Validation of tau protein interacting partners

TKO primary cortical neurons (E18) were cultured at density 150,000 cells/well in a 24-well plate. Primary neurons were transduced by lentiviruses at MOI 200 on DIV4. Transduced neurons were maintained in a 37°C, 5% CO₂ humidified incubator. Protein lysates were collected on DIV12 in the high-concentration detergent lysis buffer and protein concentration was measured using Pierce rapid gold BCA protein assay kit (ThermoScientifc, #A53225). For each neuronal lysate, 250 μg proteins were rotated overnight at room temperature with 200 μl streptavidin magnetic Dynabeads C1 (Invitrogen, #65002). Validation of captured biotinylated proteins was done by probing for potential tau interacting partners in the elution samples using standard SDS-PAGE and western blotting. The protein lysate collection, biotin-streptavidin affinity pulldown, and western blotting were performed as described above.

Antibodies

Primary antibodies used were anti-biotin (Cell Signaling Technology Cat# 5597, RRID: AB_10828011), anti-BioID2 (Abcam, #ab232733), HA-tag antibody (Cell Signaling Technology Cat#3724, RRID: AB_1549585), Myc-tag antibody (Cell Signaling Technology Cat#2276, RRID:AB_331783), and GAPDH (Cell Signaling Technology Cat#5174, RRID:AB_10622025). Tau antibodies used were produced in-house, including Tau13 (Combs et al., 2016; García-Sierra et al., 2003) (amino acids 8-9, 13-21; in-house, RRID: AB_2721193), and Tau5 (Carmel et al., 1996; Kanaan & Grabinski, 2021; LoPresti et al., 1995; Porzig et al., 2007) (amino acids 218-225; in-house, RRID: AB_2721194). For validation experiments of identified proteins, antibodies used were MAP2 (Cell Signaling Technology Cat#8707, RRID: AB_2722660), and MAP6 (Cell Signaling Technology Cat#4265, RRID: AB_2140993). Secondary antibodies used were IRDye 680LT goat anti-mouse IgG (LI-COR Biosciences Cat#926-68020, RRID:AB 10706161), **IRDye** 800CW goat anti-rabbit IgG (LI-COR Biosciences Cat#926-32211, RRID:AB 621843), Alexa Fluor 568 goat anti-mouse IgG (Thermo Fisher Scientific Cat#A-11031, RRID:AB_144696), Alexa Fluor 488 goat anti-rabbit IgG (Thermo Fisher Scientific Cat#A-11034, RRID:AB_2576217), biotinylated goat anti-mouse IgG (Jackson ImmunoResearch Labs Cat#115-065-166, RRID:AB 2338569), and biotinylated goat anti-rabbit (Vector Laboratories Cat#BA-1000, RRID:AB 2313606). For western blotting, Tau13 and Tau5 were used at dilution 1:100,000 while all commercial antibodies were used at dilution 1:1000. For ICC, HA-tag, and Myc-tag antibodies were diluted 1:800. For ICF, Tau13 and Tau5 were diluted 1:5,000 while HA-tag and Myc-tag antibodies were diluted 1:800.

Data representation and statistical analysis

Statistical tests and bar graphs were done using GraphPad Prism (V.8.0.1), GraphPad Software, La Jolla California USA, www.graphpad.com. Fluorescent microscopy images were taken using NIS-Elements BR (V.5.02.00, 64-bit) software, image analysis and quantification was preformed using FiJi (Schindelin et al., 2012). Western blot quantification was performed using LI-COR Image Studio Mass spectrometry label free quantification was performed using Thermo Scientific Proteome Discoverer software (PD; V 2.5). Lists of identified proteins were curated and filtered according to the defined criteria using RStudio (V.1.4.1717) (RStudio Team, 2021). Schematic figures were created with BioRender.com.

RESULTS

Generation and validation of Tau-BioID2 expression plasmids and lentiviruses

The BioID2-HA plasmid was used to create the Tau-BioID2 construct with BioID2 fused to the C-terminus of the longest human tau isoform (Tau, 2N4R or hT40 isoform with 441 amino acids) and served as the control protein. The Myc-BioID2 plasmid was used to create the BioID2-Tau construct with BioID2 fused to the N-terminus of Tau and served as the control protein (Figure 1). All plasmid DNA sequences were validated by restriction digestion and Sanger sequencing (GENEWIZ).

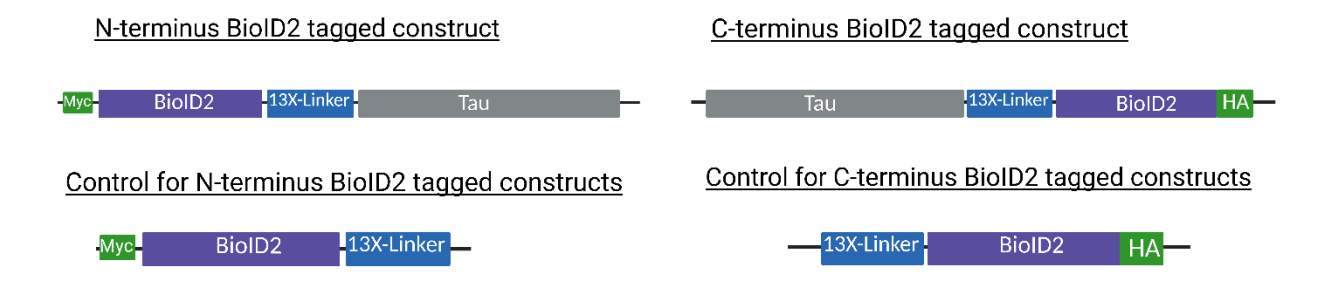


Figure 1: Design of the BioID2 constructs. Two fusion and two BioID2-only control constructs were created. Fusion constructs are BioID2 tagged to either the N-terminus or the C-terminus of Tau sequence to create BioID2-Tau or Tau-BioID2, respectively. The control constructs were designed to express only the BioID2 protein. The Myc-BioID2 construct was used as a control for BioID2-Tau and the BioID2-HA construct was used as a control for Tau-BioID2. All constructs featured a 13xlinker between tau and BioID2. BioID2-Tau and Myc-BioID2 had a Myc tag on the N-terminus. Tau-BioID2 and BioID2-HA had an HA tag on the C-terminus.

Mutagenesis of the BioID2 expression plasmids and creating the Tau-BioID2 fusion proteins

The BioID2-HA plasmid was mutated to insert EcoRV, Kozak sequence, and KpnI restriction sites upstream of the 13xLinker-BioID2 sequence and NotI restriction site downstream of the BioID2-HA sequence as shown in Figure 2A. Mutagenesis reactions were validated by restriction digestion to confirm the presence of newly inserted sites (Figure 2A). Plasmid DNA from two bacterial colonies were screened first for KpnI and NotI restriction sites insertion, one plasmid DNA had only the NotI site insertion while the other plasmid DNA had both restriction sites inserted (Figure 2A, red box). Then, the plasmid DNA was screened for EcoRV restriction site insertion. DNA gel shows successful insertion of all restriction sites (Figure 2A). Single cut plasmid DNA shows the linearized plasmid compared to the uncut supercoiled plasmid while the double cut plasmid shows the 13xLinker-BioID2 region of interest at 973 base pairs (Figure 2A, bottom panel red box). The final BioID2-HA plasmid that passed restriction digestion analysis was further confirmed by Sanger sequencing.

To create the Tau-BioID2 fusion protein, both pCMV-Tau and the mutated BioID2-HA plasmids were cut by KpnI and NotI (Figure 2B). DNA bands of the open pCMV plasmid and the BioID2-HA insert were extracted from the gel, ligated, and transformed into XL10-Gold ultracompetent cells. Plasmid DNA from two colonies were extracted and screened using EcoRV and NotI restriction digestion, one plasmid DNA showed successful ligation of the Tau-BioID2 sequence at 2,293 base pairs (Figure 2B, red box). The final Tau-BioID2 plasmid that passed restriction digestion analysis was further confirmed by Sanger sequencing.

The Myc-BioID2 plasmid was mutated to insert an EcoRV restriction site upstream of the BioID2-13xLinker sequence and an Ndel restriction site downstream of the BioID2-13xLinker sequence, then the endogenous Ndel restriction site upstream of the BioID2-13xLinker sequence was deleted as shown in Figure 2C. Plasmid DNA was screened first for EcoRV and Ndel restriction sites insertion. The DNA gel EcoRV/Ndel single cut shows two bands for the open plasmid and the region between the inserted EcoRV/Ndel sites and the endogenous Ndel site (Figure 2C). The DNA plasmid was then validated for the deletion of the endogenous Ndel restriction site. Ndel single cut shows only the linearized plasmid which indicates the deletion of the endogenous Ndel site, while the EcoRV and Ndel double cut shows the BioID2-13xLinker region of interest (Figure 2C, red box). The final Myc-BioID2 plasmid that passed restriction digestion analysis was further confirmed by Sanger sequencing.

To create the BioID2-Tau fusion protein, the pT7c-Tau and the mutated Myc-BioID2 plasmids were cut with NdeI and XhoI (Figure 2D). The tau band (from the pT7c plasmid) and the open Myc-BioID2 plasmid were extracted from the gel, ligated, and transformed into XL10-Gold ultracompetent cells. Plasmid DNA was extracted and screened using EcoRV and NotI restriction digestion. Plasmid DNA showed successful ligation of the BioID2-13xLinker-Tau sequence at 2,320 base pairs (Figure 2D, red box). The final BioID2-Tau plasmid that passed restriction digestion analysis was further confirmed by Sanger sequencing.

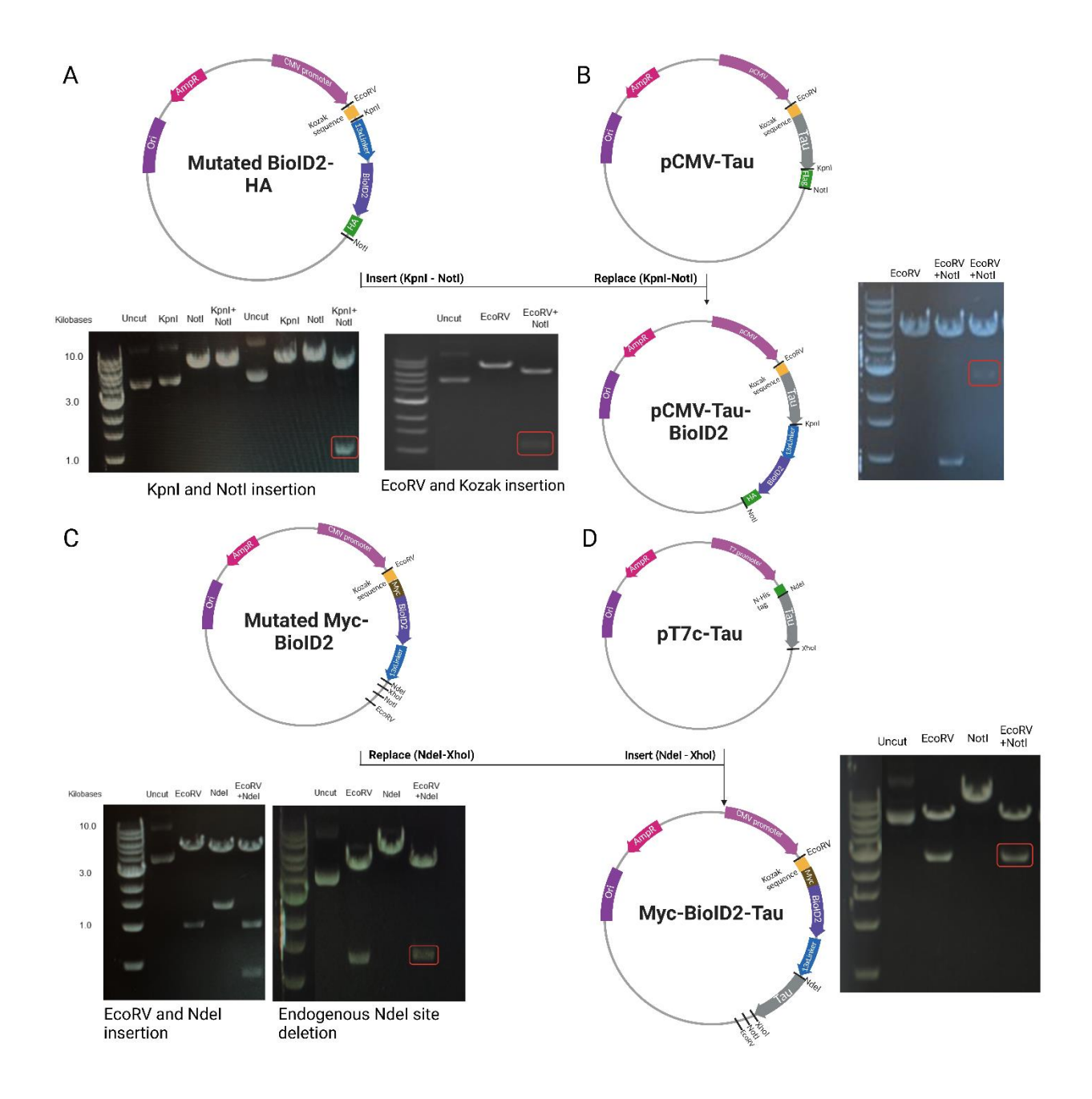


Figure 2: Restriction cloning of the BioID2 fusion proteins. A) Map illustrations for the mutated BioID2-HA plasmid show the insertion of the EcoRV, Kozak and KpnI sites. Restriction digestion validation gels show a purified plasmid that does not contain both restriction sites (lanes 2-5) and the plasmid used for further construct generation that correctly included both KpnI and NotI restriction sites (lanes 5-8). Lane 1 is the DNA

Figure 2 (cont'd)

size ladder. The red box shows the expected digestion product with both sites inserted. The other validation gel shows the insertion of the EcoRV restriction, and the final expected digestion product is shown in the red box. B) Cloning of the Tau-BioID2 construct. The fusion protein was created by replacing the Flag tag in the pCMV-Tau plasmid by the BioID2-HA sequence. The pCMV-Tau and the BioID2-HA plasmids were cut by KpnI and NotI, the insert and open plasmid were extracted and ligated. Restriction digestion validation gel shows the purified ligated plasmid containing the Tau-BioID2 fusion protein (red box). C) Map illustrations for the mutated Myc-BioID2 plasmids show the insertion of EcoRV and Ndel restriction sites, and deletion of endogenous Ndel site. The red box shows the final expected digestion product with insertion of both EcoRV and Ndel restriction sites and deletion of the endogenous Ndel restriction site. D) Cloning of the BioID2-Tau construct. The fusion protein was created by inserting the tau sequence from the pT7c-Tau plasmid into the mutated Myc-BioID2 plasmid. Both plasmids were cut by Ndel and Xhol, the tau insert and the Myc-BioID2 open plasmid were ligated. Restriction digestion validation gel shows the purified ligated plasmid containing the BioID2-Tau fusion protein (red box). All plasmid DNA sequences were further validated by Sanger sequencing (GENEWIZ).

Creating BioID2 lentiviral transfer plasmids

The Tau-BioID2 fusion proteins and the respective BioID2-only controls were cloned into the pFIN vector to generate lentiviruses. The pFIN vector is the lentiviral transfer plasmid which encodes the protein of interest as well as the human immunodeficiency virus-1 Gag, RRE, and WPRE sequences flanked by the 5'- and 3'- long terminal repeats. The pFIN-CBA-Tau plasmid was cut by EcoRV and NotI to open the pFIN-CBA plasmid backbone and remove the tau sequence, allowing ligation of the the Tau-BioID2 and BioID2-Tau inserts as well as the BioID2-HA and Myc-BioID2 control inserts.

To create the pFIN-BioID2-HA and the pFIN-Tau-BioID2, the BioID2-HA and Tau-BioID2 sequences were cut by EcoRV and NotI from the mutated BioID2-HA plasmid and the pCMV-Tau-BloID2 plasmid respectively (Figure 2 A and B). The DNA bands of the pFIN open plasmid, the BioID2-HA and the Tau-BioID2 inserts were extracted from the gel, ligated, and transformed into StbI3 competent *E. coli* which reduce the homologous recombination events of the long terminal repeats in the pFIN vector. The ligated plasmid DNA was extracted and screened by EcoRV and NotI restriction digestion. Plasmid DNA showed successful ligation of the BioID2-HA and Tau-BioID2 into the pFIN plasmid backbone (Figure 3A, red box). The final pFIN-BioID2-HA and pFIN-Tau-BioID2 plasmids that passed restriction digestion analysis were further confirmed by Sanger sequencing.

To create the pFIN-Myc-BioID2 and the pFIN-BioID2-Tau, the Myc-BioID2 and BioID2-Tau sequences were cut by EcoRV and NotI from the mutated Myc-BioID2 plasmid and the Myc-BioID2-Tau plasmid respectively (Figure 2 C and D). The DNA bands of the pFIN open plasmid, the Myc-BioID2 and the BioID2-Tau inserts were extracted from the gel, ligated, and transformed into Stbl3 competent *E. coli*. The ligated

plasmid DNA was extracted and screened by EcoRV and NotI restriction digestion. Plasmid DNA showed successful ligation of the Myc-BioID2 and BioID2-Tau into the pFIN plasmid backbone (Figure 3B, red box). The final pFIN-Myc-BioID2 and pFIN-BioID2-Tau plasmids that passed restriction digestion analysis were further confirmed by Sanger sequencing.

Prior to packaging into lentiviruses, the pFIN plasmids were further validated for the mammalian cell expression of the BioID2 constructs. HEK293T cells were transfected with either pFIN-BioID2-HA, pFIN-Tau-BioID2, pFIN-Myc-BioID2 or pFIN-BioID2-Tau plasmids and were maintained overnight. The next day, biotin (100 μM) was supplemented and the HEK293T cells were maintained overnight before collecting the protein lysates. Expression and functionality of the BioID2 proteins were validated by western blotting and probing the membranes with BioID2 and biotin antibodies. As expected, BioID2 antibody showed reactive bands were for Myc-BioID2, BioID2-Tau, BioID2-HA and Tau-BioID2 at ~37, ~90, ~37, and ~90 kiloDaltons, respectively (Figure 3C). In addition, biotin antibody showed that the expressed BioID2 proteins were functional (Figure 3C).

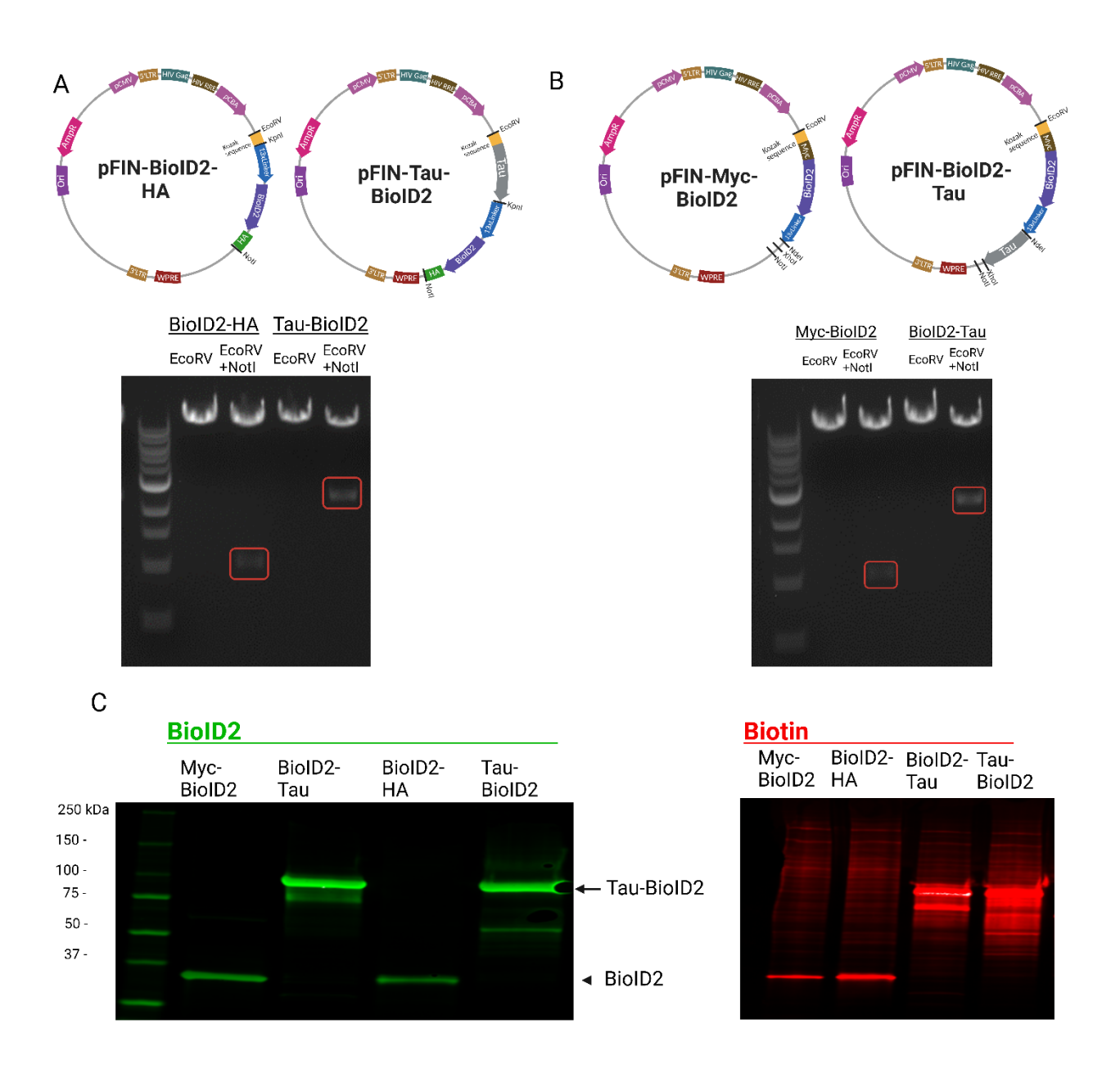


Figure 3: Validation the lentiviral transfer plasmids expressing the BioID2 constructs. A) Cloning of the BioID2-HA and the Tau-BioID2 sequences into the pFIN plasmid backbone. pFIN-BioID2-HA and pFIN-Tau-BioID2 plasmids were created by replacing tau sequence in the pFIN-Tau plasmid with the BioID2-HA and the Tau-BioID2 sequences. pFIN-Tau, mutated BioID2-HA, and pCMV-Tau-BioID2

Figure 3 (cont'd)

plasmids were cut by EcoRV and Notl. The pFIN open plasmid, the BioID2-HA insert, and the Tau-BioID2 insert DNA bands were extracted from the gel and ligated. EcoRV and NotI restriction digestion validation gel shows the purified ligated plasmids containing the BioID2-HA and the Tau-BioID2 fusion protein (red boxes). B) Cloning of the Myc-BioID2 and the BioID2-Tau sequences into the pFIN plasmid backbone. pFIN-Myc-BioID2 and pFIN-BioID2-Tau plasmids were created by replacing tau sequence in the pFIN-Tau plasmid by the Myc-BioID2 and the BioID2-Tau sequences. pFIN-Tau, mutated Myc-BioID2, and Myc- BioID2-Tau plasmids were cut by EcoRV and Notl. The pFIN open plasmid, the Myc-BioID2 insert, and the BioID2-Tau insert DNA bands were extracted from the gel and ligated. EcoRV and Notl restriction digestion validation gel shows the purified ligated plasmids containing the Myc-BioID2 and the BioID2-Tau fusion protein (red boxes). C) HEK293T cells were transfected by pFIN-Myc-BioID2, pFIN-BioID2-Tau, pFIN-BioID2-HA, and pFIN-Tau-BioID2 plasmids. Exogenous biotin was supplemented to validate the functionality of the BioID2 proteins. The expression and functionality of the BioID2 proteins was confirmed by western blotting. Antibodies used were anti-BioID2 (green) and anti-biotin (red) primary antibodies.

Lentiviruses generation and determination of the functional titer

To generate lentiviruses (LV) expressing the BioID2 proteins, HEK293T cells were transfected with the lentiviral transfer plasmids (encodes BioID2 proteins), the pNHP packaging vector (encodes for Gag, Pol, Rev, and Tat), and the pHEF-VSVG envelope vector (encodes VSV-G envelope protein). Lentiviruses were harvested by centrifugation and the lentiviral functional titer was determined by ICC of transduced HEK293T cells. The functional titer for each lentivirus was as follows: a) the Tau-BioID2 LV was 3.70x10⁷ TU/µl, b) BioID2-HA LV was 3.45x10⁷ TU/µl, c) BioID2-Tau LV was 2.85x10⁷ TU/µl, and d) Myc-BioID2 LV was 1.42x10⁷ TU/μI (Figure 4A-B). To further validate the expression of the BioID2 proteins, HEK293T cells were transduced at MOI of 50 by Myc-BioID2, BioID2-HA, BioID2-Tau, or Tau-BioID2 lentiviruses. Lysates were analyzed using western blotting with Myc tag and HA tag antibodies and the protein bands for Myc-BioID2, BioID2-HA, BioID2-Tau, and Tau-BioID2 were found at the predicted molecular weights ~37, ~37. ~90, and ~90 kiloDaltons, respectively (Figure 4C). Moreover, to validate the expression of tau protein, HEK293T cell lysates were analyzed using western blotting with Tau13 antibody. The protein bands for BioID2-Tau and Tau-BioID2 show that lentiviruses express tau protein at similar levels (Figure 4D).

Collectively, these data suggest that the molecular cloning of the BioID2 lentiviral transfer plasmids (pFIN vector) was successful as validated by restriction digestion, Sanger sequencing, and western blotting. Also, the lentiviral production and purification was successful in generating viable viral particles capable of transducing and expressing the BioID2 proteins in HEK293T cells.

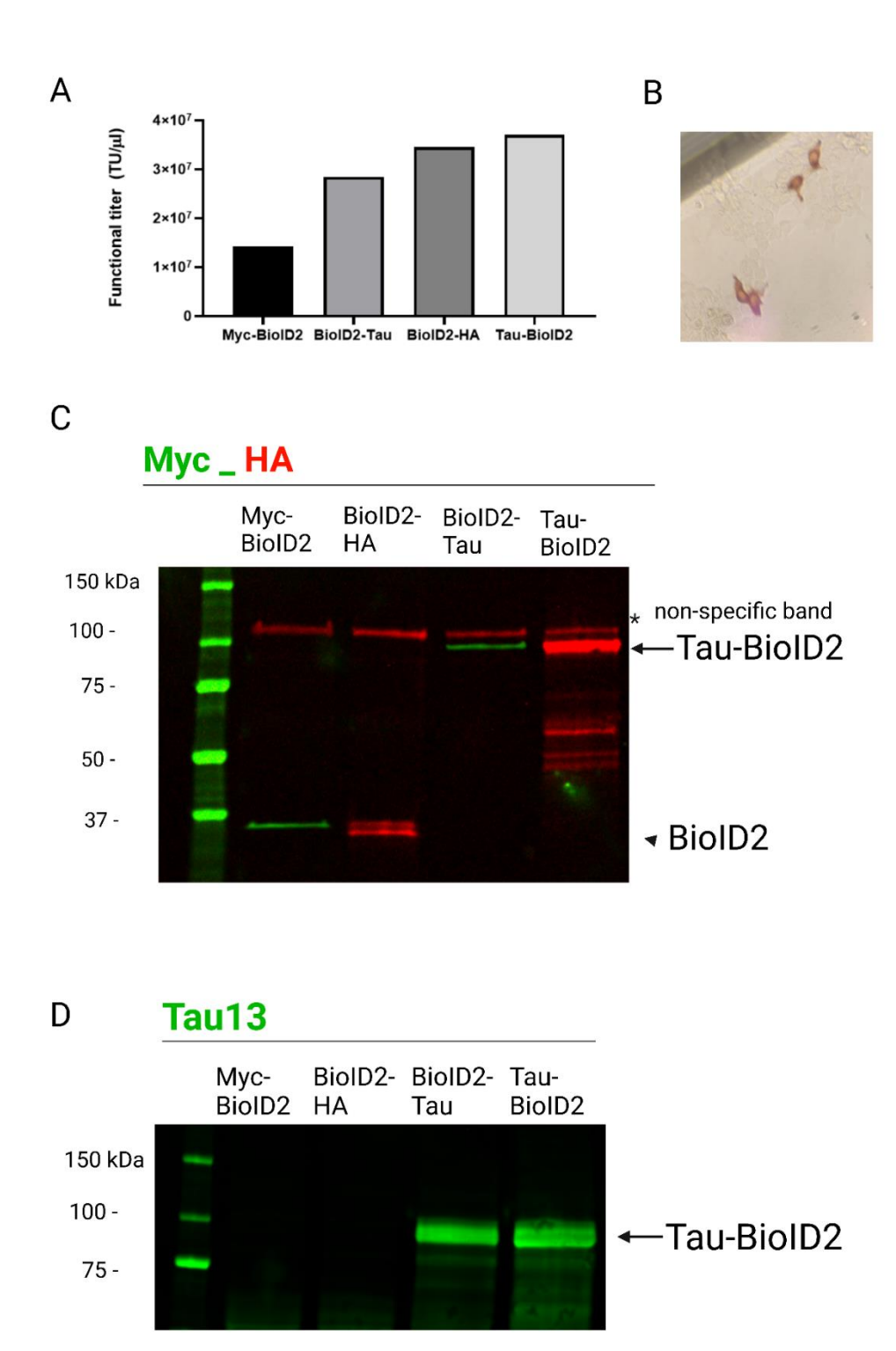


Figure 4: Lentiviruses functional titer and validation. A) For each lentiviral construct, HEK293T cells were transfected by lentiviral plasmids (pFIN transfer plasmids expressing

Figure 4 (cont'd)

the BioID2 protein, pNHP packaging plasmid, and pHEF-VSVG envelope plasmid). Functional titer of the generated lentiviruses was assessed by immunocytochemistry (ICC). The functional titer was calculated by multiplying the number of transduced cells at the highest viral dilution by the respective dilution factor. B) Representative image for the ICC of the lentiviral transduction of HEK293T cells at the lowest viral concentration that was used to calculate the functional titer. C) HEK293T cells were transduced by lentiviruses at MOI 50 to validate the viability of the created lentiviruses. Lysates were analyzed by western blot which shows the expression of all four BioID2 proteins at the expected molecular weights. Antibodies used were Myc tag and HA tag primary antibodies. Note the BioID2-Tau and Tau-BioID2 bands are indicated by the arrow, the Myc-BioID2 and BioID2-HA control bands by an arrowhead, and a non-specific band identified with the HA antibody with an asterisk. D) HEK293T cell lysates were validated for the expression of tau protein. Western blotting with Tau13 antibody shows the expression of BioID2-Tau and Tau-BioID2 proteins (arrow) at the expected molecular weight and at a similar expression level. MOI; multiplicity of infection, TU; transducing unit

Optimizing lentiviral transduction of primary cortical neurons

Three important optimizations were performed for lentivirus-mediated expression of the BioID2 proteins in E18 WT and TKO primary cortical neurons. First, a range of multiplicity of infections were used to optimize the amount of mouse E18 cortical neurons transduced. Second, the level of exogenous tau expression was measured to determine whether near-physiological or supraphysiological levels were expressed. Third, a dose response for exogenous biotin supplemented into the medium was tested. These optimization steps were critical to ensure sufficient transduction efficiency in primary neurons, establish whether overexpression artifacts may cloud interpretation, and determine the functionality of the BioID2 enzymes.

Determining optimal titer for primary neuron transduction

The E18 WT primary cortical neurons were transduced by the BioID2 lentiviruses on DIV 4 at MOI of 50,100, and 200. Primary neurons were maintained five days post-transduction (DIV 9) and the transduction efficiency was determined by ICF. Quantification of the ICF images showed increased lentiviral transduction efficiency at higher MOI achieving ~50% transduction efficiency at MOI 200 (Figure 5A). Accordingly, MOI of 200 was used for the lentiviral transduction of primary neurons in all the downstream experiments. Representative images show successful expression of the BioID2 proteins in WT primary cortical neurons probed by Myc tag, HA tag, and Tau13 antibodies (Figure 5B). The BioID2-Tau and Tau-BioID2 proteins were probed by the Tau13 antibody, which binds to an epitope in the N-terminus of the human tau protein (amino acids 8-9, 13-21) not present in rodent tau (i.e. Tau13 is human tau-specific) (Combs et al., 2016; García-Sierra et al., 2003). The Tau13 antibody will only bind to the

human expressed by lentiviral transduction (Figure 5B). For the downstream experiments, TKO primary cortical neurons were used to avoid the competition with the endogenous mouse tau.

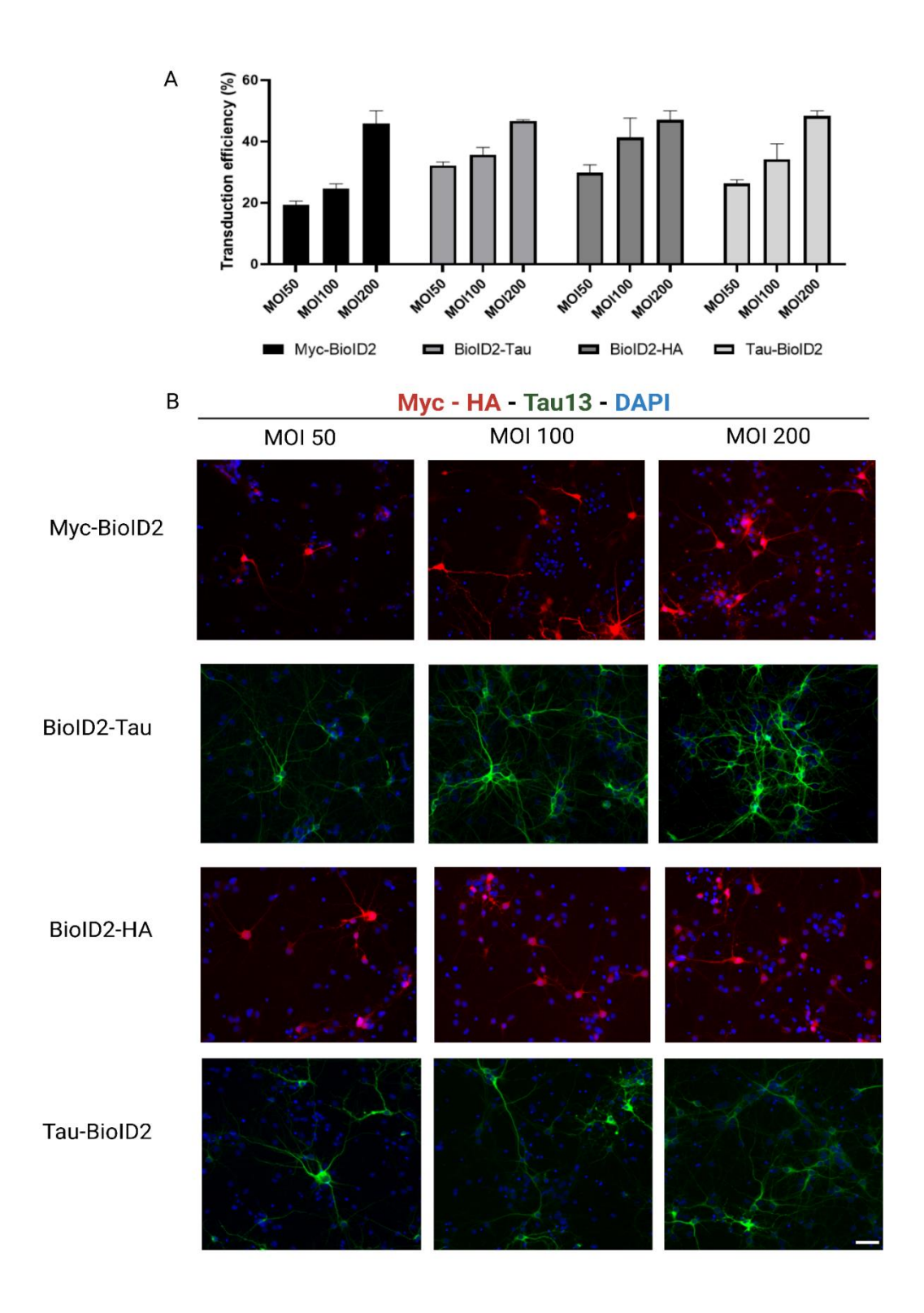


Figure 5: Expression of the BioID2 proteins in primary cortical neurons. A) E18 WT primary cortical neurons were transduced by lentiviruses expressing Myc-BioID2, BioID2-Tau, BioID2-HA, and Tau-BioID2 proteins. Lentiviral transduction was done at a range of

Figure 5 (cont'd)

multiplicity of infections (MOI 50, MOI 100, and MOI 200). For each lentiviral transduction, ICF was performed, and the transduction efficiency was calculated at each MOI by dividing the number of transduced neurons by the total number of neurons. Myc-BioID2 positive cells were analyzed by Myc tag antibody, BioID2-HA positive cells were analyzed by HA tag antibody while BioID2-Tau and Tau-BioID2 positive cells were analyzed by Tau13 antibody which does not bind mouse tau. The bar graph shows the quantification transduction efficiency for each lentivirus and at each MOI (5 images/well used for analysis). Primary neurons transduced at MOI 200 showed the highest transduction efficiency for all lentiviruses (~50%). Values are represented as mean ± SEM. B) Representative images showing the increased expression of the BioID2 proteins at increased lentiviral MOI. Antibodies used were Myc tag, HA tag, and Tau13. E18; embryonic day 18, DIV; days in vitro, MOI; multiplicity of infection, ICF; immunocytofluorescence. Scale bar, 50 µm (applies to all panels).

Lentiviruses express the Tau-BioID2 proteins at near physiological levels

Viral vector-mediated expression of exogenous proteins can lead to overexpression and subsequent artifacts. Thus, the level of lentivirus-mediated expression of the Tau-BioID2 protein in TKO mouse cortical neurons was assessed and compared to the expression levels of endogenous Tau in WT mouse cortical neurons. On DIV 4, TKO neurons were transduced by lentivirus expressing the Tau-BioID2 protein at MOI 200 and ICF was performed at DIV 12 along with WT neurons (untransduced) of the same age. Tau signal intensity was determined by densitometry measurements of Tau5 ICF. The Tau5 antibody binds to both the human and mouse tau protein (Kanaan & Grabinski, 2021). Quantification of the average pixel intensity of tau signal shows similar expression levels between the lentiviral expressed Tau-BioID2 and the WT Tau (Figure 6A-B).

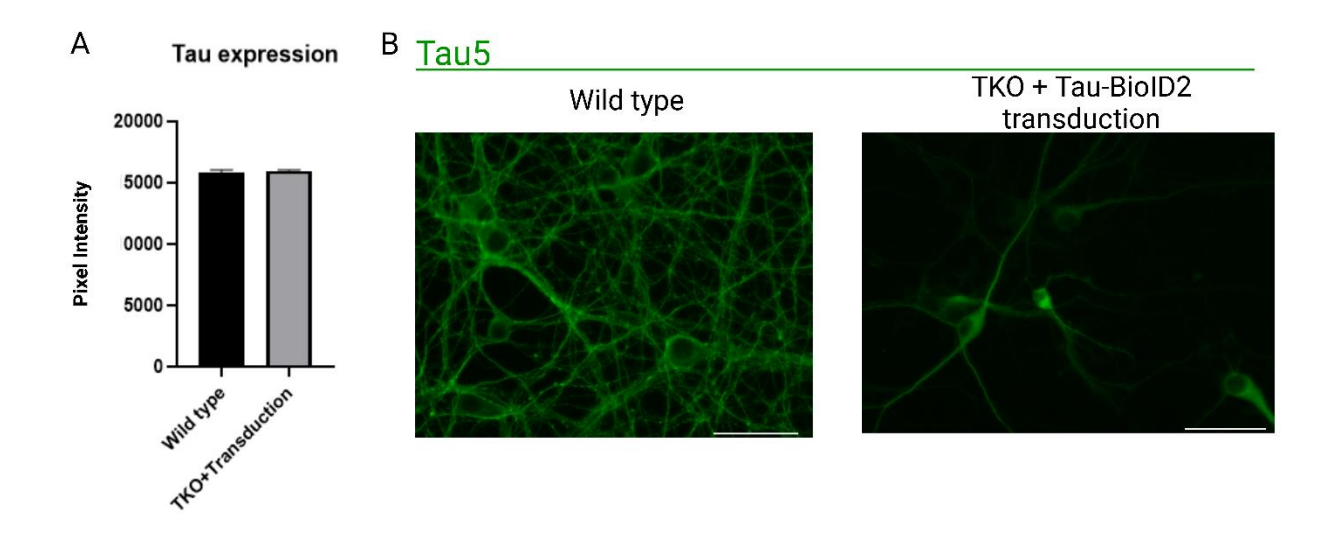


Figure 6: Lentiviral expression of Tau-BioID2 compared to WT Tau expression. A)

E18 TKO cortical neurons were transduced by Tau-BioID2 lentivirus on DIV 4. Transduced TKO neurons and WT cortical neurons were maintained until DIV 12. Cortical neurons were fixed and ICF was performed at DIV 12 using Tau5 antibody. Densitometry quantification of the average pixel intensity for tau signal shows similar expression between the Tau-BioID2 protein expressed in TKO primary cortical neurons and the WT mouse tau (n=3 wells/condition and 5 images/well). Values are represented as mean ± SEM. B) Representative images of the physiological tau in WT cortical neurons and the Tau-BioID2 expression (used as a representative lenti-tau construct) in transduced TKO cortical neurons of the same age. Scale bar, 50 μm. TKO; tau knockout, WT: wild type, E18; embryonic day 18, DIV; days in vitro, MOI; multiplicity of infection, ICF; immunocytofluorescence

Optimization of biotin dose and incubation time

E18 TKO primary cortical neurons were transduced on DIV 4 by the BioID2-Tau lentivirus (MOI 200) and on DIV 8 exogenous biotin was supplemented at 0, 50, or 100 μ M. Cells were analyzd 24, 48, or 96 hours after biotin supplementation. Quantification of the western blotting for biotinylated proteins showed a time- and dose-dependent increase in the biotinylation signal detected, with a maximum signal achieved at 100 μ M biotin for 96 hours (Figure 7A). The biotinylation signal observed at 0 μ M supplemented biotin dose was due to the presence of biotin in the B-27 supplement added to the neurobasal medium.

Taken together, the lentiviruses were effective at transducing \sim 50% of the primary cortical neurons at MOI 200. The expression level of the exogenous Tau-BioID2 protein was comparable to the expression level of endogenous WT mouse tau. Finally, optimal biotin supplementation was at 100 μ M followed by a four-day post-supplementation incubation period. Based upon these optimization experiments, an experimental paradigm was selected for all downstream studies (Figure 8).

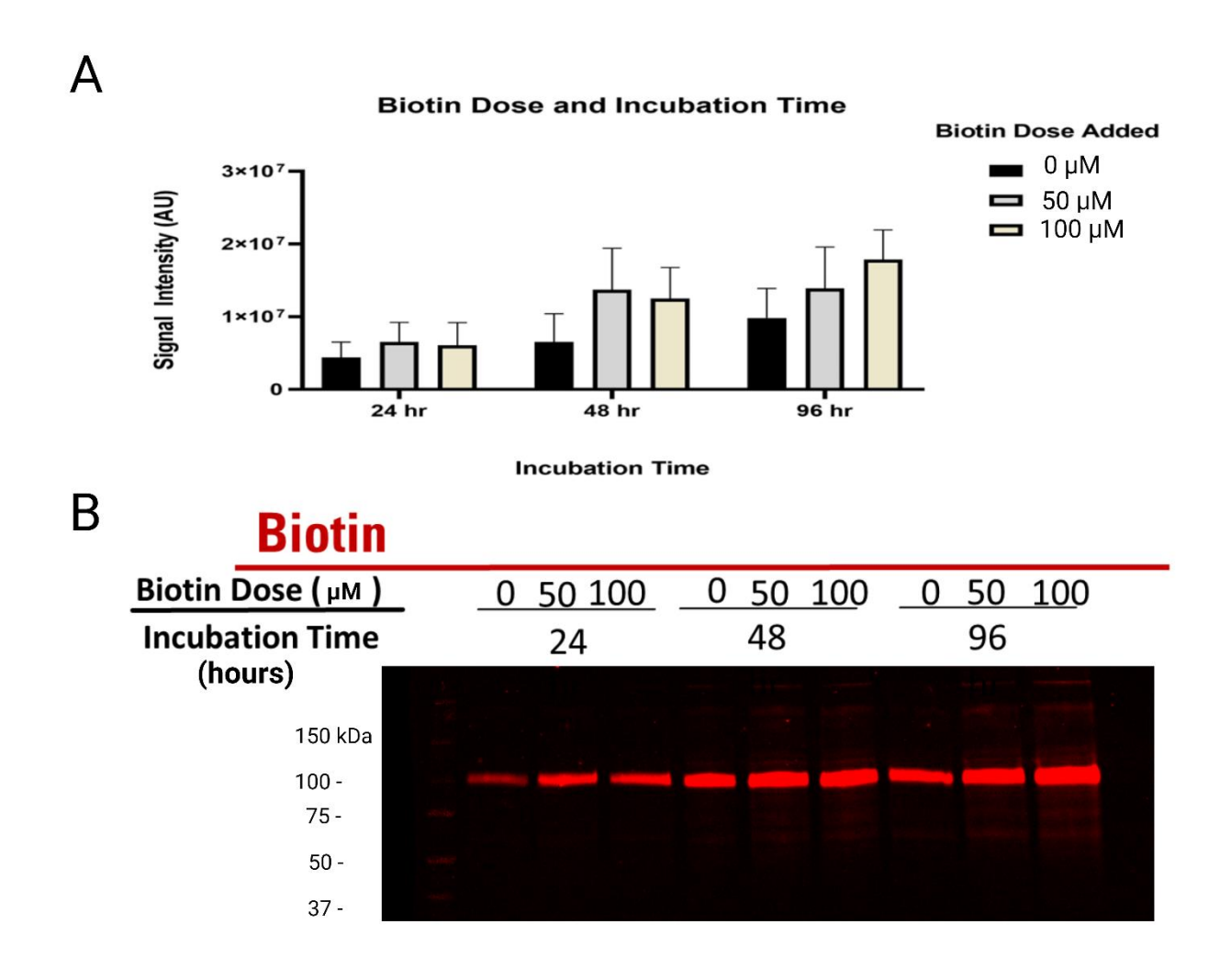


Figure 7: Optimization of biotin dose and incubation time. E18 TKO primary cortical neurons were transduced by lentivirus expressing the BioID2-Tau protein at MOI 200 on DIV 4. Lysates were collected on DIV 12 and western blotting was performed using biotin antibody. A) Quantification of the biotinylation signal detected by western blotting, values are represented as mean ± SEM (n=3 independent experiments). B) Representative image of the western blotting. TKO; tau knockout, E18; embryonic day 18, DIV; days in vitro, MOI; multiplicity of infection.

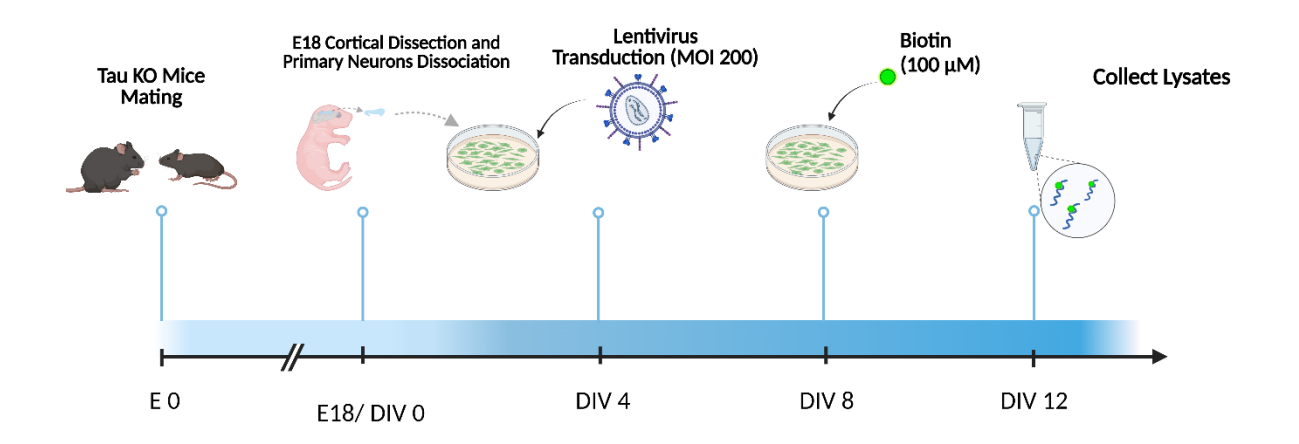


Figure 8: Schematic representation of the experimental paradigm selected for primary neurons affinity purification and mass spectrometry experiments. E18 TKO primary cortical neurons were transduced on DIV 4 (n=3 for each lentiviral transduction). Exogenous biotin (100 μ M) was supplemented on DIV 8 and protein lysates were collected on DIV 12. TKO; tau knockout, E; embryonic day, DIV; day in vitro.

Affinity pulldown and mass spectrometry identification of biotinylated tau interacting proteins

Protein lysates containing *in situ* biotin-labeled interacting proteins from TKO cortical neurons transduced with either BioID2-HA, Tau-BioID2, Myc-BioID2 or BioID2-Tau were collected on DIV 12 (Figure 8). The biotinylated proteins were captured by streptavidin-coated magnetic beads. The purified biotinylated protein samples were split into a) 10% for western blotting to confirm biotinylation and validate identified interacting proteins, and b) 90% for MS protein identification (Figure 9).

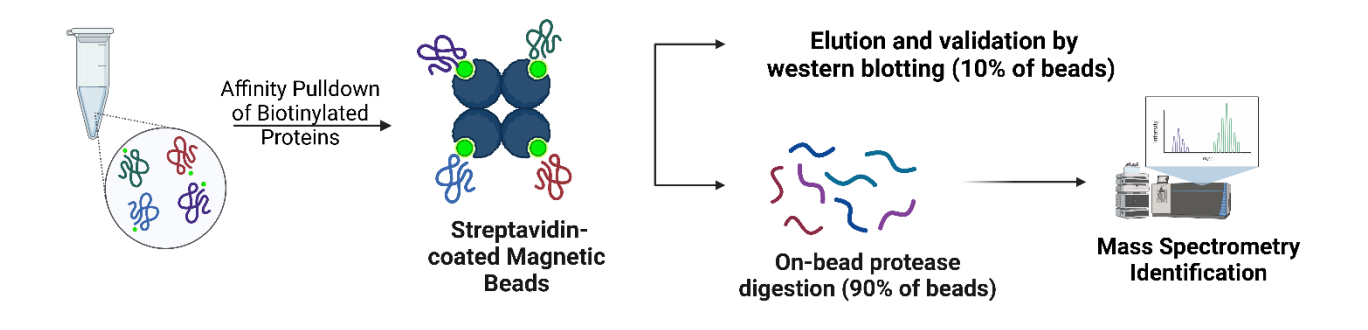


Figure 9: Affinity capture of biotinylated proteins using streptavidin Dynabeads.

Streptavidin-coated beads capture the biotinylated labeled proteins. Then 10% of the sample was used to validate effective pulldown of biotinylated proteins and the expression of exogenous proteins (BioID2-HA, Tau-BioID2, Myc-BioID2 and BioID2-Tau). The other 90% of the captured protein sample was used for MS identification of tau interacting proteins. MS; Mass spectrometry

Optimization of the biotin-streptavidin affinity pulldown using HEK293T cell lysates

The first set of affinity pulldown optimizations was performed using HEK293T cell lysates. HEK293T cells were transfected by pFIN-Myc-BioID2, pFIN-BioID2-Tau, and pFIN-Tau-BioID2 plasmids. First, the protein lysates containing the biotinylated proteins were collected in 1x co-immunoprecipitation (Co-IP) lysis buffer containing 20 mM Tris pH 7.5, 0.5 mM dithiothreitol, 150 mM NaCl, and 0.5% Triton X-100. The biotinylated proteins were eluted in 1x sample buffer. Capturing and eluting the biotinylated proteins was unsuccessful (Figure 10A). Next, a method adapted from (Roux et al., 2013a) was used, which includes a lysis buffer containing 50 mM Tris pH 7.4, 500 mM NaCl, 0.2% SDS, and 1 mM dithiothreitol and elution in 1x sample buffer. Again, capturing and eluting the biotinylated proteins was unsuccessful (Figure 10B). Finally, the method described in (Cheah & Yamada, 2017) was tested. A high concentration detergent lysis buffer was used that contained 50 mM Tris pH 7.4, 150 mM NaCl, 0.4% SDS, 1% NP-40, 1 mM EGTA, and 1.5 mM MgCl₂. Elution of the biotinylated proteins was performed by competition with high concentration of free biotin (25 mM) prepared in lysis buffer and heating the sample to 95°C for 15 minutes. This method showed efficient capturing and elution of the biotinylated proteins and the BioID2 proteins (Figure 10C). For these optimization experiments, the sample-bead incubation was set to four hours at room temperature. Based on these results, the high concentration detergent and biotin competition/heat elution method was used.

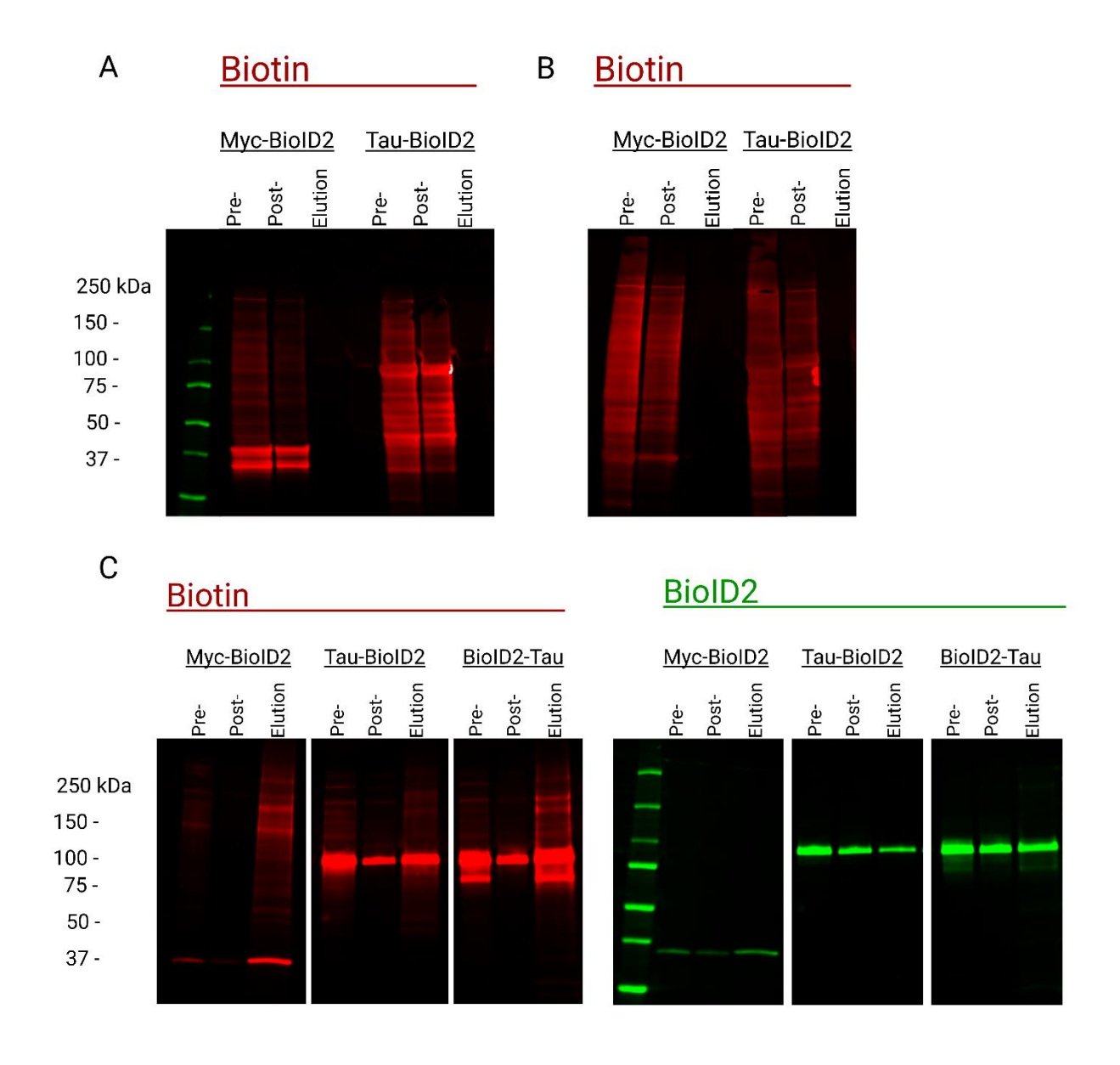


Figure 10: Optimization of affinity pulldown in HEK293T cell lysates. HEK293T cells were transfected by pFIN-Myc-BioDI2, pFIN-Tau-BioID2 plasmids, or pFIN-BioID2-Tau plasmids. Exogenous biotin (100 μM) was supplemented, and cells were maintained for 48 hours. Protein lysates were collected, and biotinylated proteins were captured by streptavidin-coated magnetic beads. Captured proteins were eluted and western blotting was performed. Three lysis buffers and three elution methods were

Figure 10 (cont'd)

performed to validate the optimal pulldown conditions. A) Co-IP lysis buffer was used, and biotinylated proteins were eluted in 1x sample buffer. No proteins were detected in the elution. B) Low concentration detergent lysis buffer was used, and elution was done in 1x sample buffer. No proteins were detected in the elution. C) High concentration detergent lysis buffer was used, and elution was done in 25 mM biotin with sample heating to 95°C showing successful capturing and elution of biotinylated proteins (elution lanes in western blots). Note the effective capture and elution of biotinylated proteins. Biotin and BioID2 antibodies were used for the western blotting. Pre- refers to the input lysate sample, Post- refers to the flow through after capturing, and Elution refers to the eluted sample from the beads. Co-IP; co-immunoprecipitation.

Optimization of the biotin-streptavidin affinity pulldown using primary cortical neurons lysates

The optimized affinity pulldown protocol was then tested with primary neurons lysates. Primary cortical neurons (E18) from TKO mice were transduced by lentiviruses to express BioID2-HA, BioID2-Tau, Myc-BioID2, or Tau-BioID2. Protein lysates containing the biotinylated proteins were collected on DIV 12 in the high-detergent concentration lysis buffer and elution was done in 25 mM biotin at 95°C. In this set of experiments, the sample-bead incubation time and temperature were optimized. Capturing and eluting biotinylated proteins was unsuccessful when samples were incubated with pulldown beads for four hours at room temperature (Figure 11A). Next, samples were incubated with beads overnight at 4°C, but this also was unsuccessful (Figure 11B). Finally, incubating the sample-bead mixture overnight at room temperature showed successful capturing and elution of the biotinylated proteins (Figure 11C).

Taken together, these optimization experiments demonstrated that the ideal pulldown and elution conditions for neuron lysates includes incubating samples with beads overnight at room temperature followed by elution in a high concentration detergent buffer, competition with free biotin and heat. These parameters were used in subsequent experiments described below.

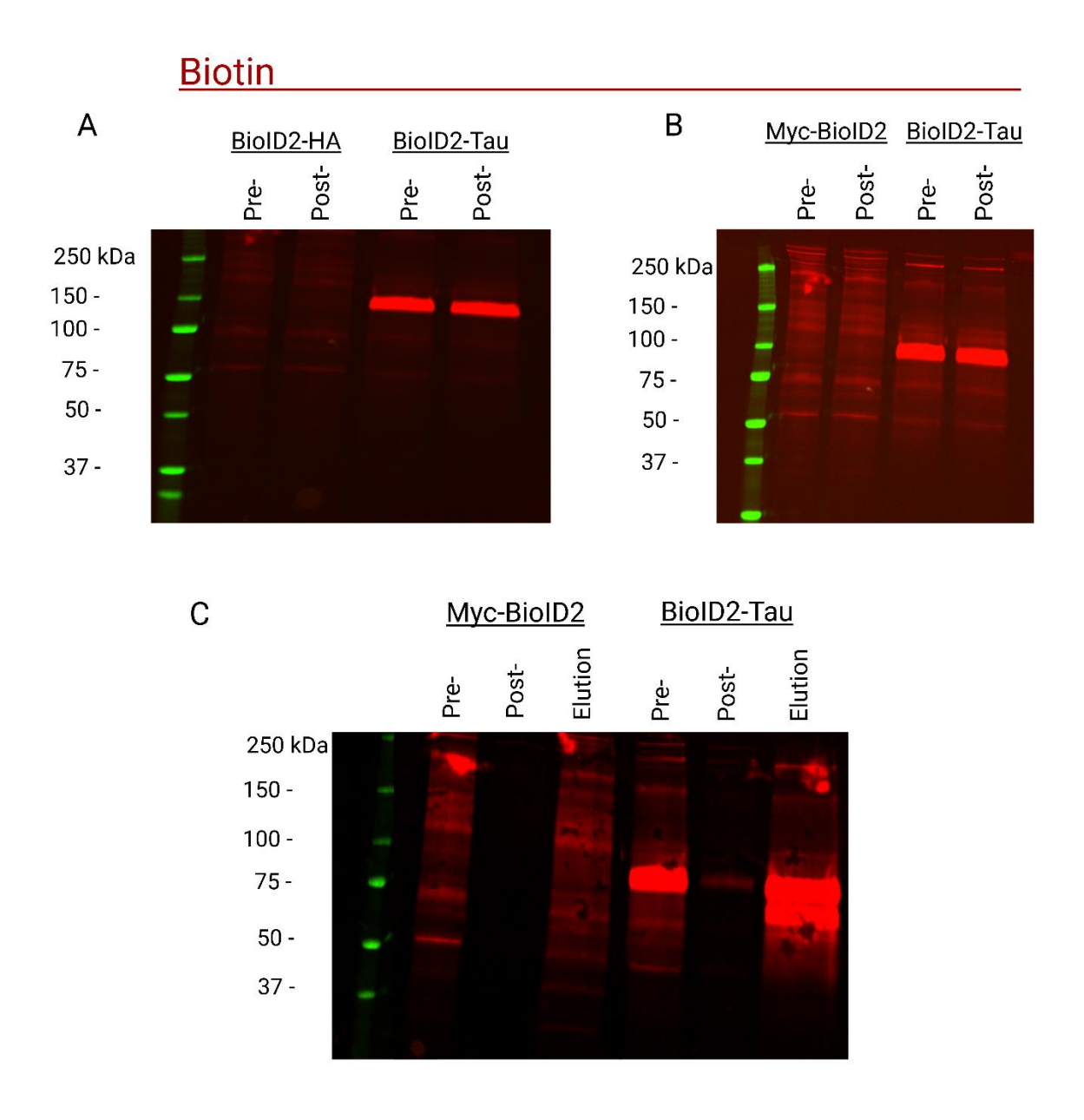


Figure 11: Optimization of affinity pulldown in primary neurons lysates. E18 TKO primary cortical neurons were transduced by BioID2-HA, BioID2-Tau, Myc-BioID2, or Tau-BioID2 lentiviruses on DIV4. Exogenous biotin (100 μM) was supplemented on DIV8, and cells lysates were collected on DIV12. Biotinylated proteins were captured by streptavidin-coated magnetic beads and western blotting was performed to validate the

Figure 11 (cont'd)

successful capturing and elution of tau interacting proteins. Three conditions were optimized for the successful capturing by the streptavidin-coated magnetic beads. A) Sample-bead incubation was done for four hours at room temperature, biotinylated proteins were not captured by the beads, as indicated by similar levels in both the input lysate (pre-) and the flow through (post-). B) Sample-bead incubation was done overnight at 4°C, biotinylated proteins were not captured by the beads, as indicated by similar levels in both the input lysate (pre-) and the flow through (post-). C) Sample-bead incubation was done overnight at room temperature. This method successfully captured biotinylated proteins and provided effective elution of biotinylated proteins (elution lanes in western blots). Biotin antibody was used. Pre- refers to the input lysate sample, Post- refers to the flow through after capturing, and Elution refers to the eluted sample from the beads

Identification of the tau protein interactome using mass spectrometry

To identify the interacting partners with Tau-BioID2 and BioID2-Tau proteins, label-free quantification analysis was performed on the mass spectrometry raw data files. Potential interactors with either Tau-BioID2 or BioID2-Tau were defined as follows: a) identified in at least two of the experimental replicates, and b) was ≥1.5-fold increased compared to the respective control. Following these criteria, 269 proteins were identified as potential interactors with the Tau-BioID2 protein (≥1.5-fold increase versus BioID2-HA control) and 219 showed < 1.5-fold change and were not considered potential interactors (Figure 12A). For the BioID2-Tau interactors, 169 proteins showed ≥1.5-fold increase compared to the Myc-BioID2 control, and 140 proteins showed < 1.5-fold change (Figure 12B). Out of the 269 preferential interactors with Tau-BioID2 and the 169 preferential interactors with the BioID2-Tau: 1) 66 proteins were identified as interactors, and 3) 103 proteins were identified only as Tau-BioID2 interactors, and 3) 103 proteins were identified only as BioID2-Tau interactors (Figure 12C). Taken together, a total of 372 proteins were identified as potential tau interacting partners.

STRING analysis was performed to map the functional and physical associations network of the identified tau protein interactome with MCL clustering inflation value of 3.0. Major cellular component categories of the identified interacting partners included mitochondrial proteins, cytoskeletal proteins, synaptic proteins, nuclear proteins and ribonucleoproteins ranked by the number of identified proteins in the cellular component (Figure 13). The full list of the identified proteins is shown in Appendix A.

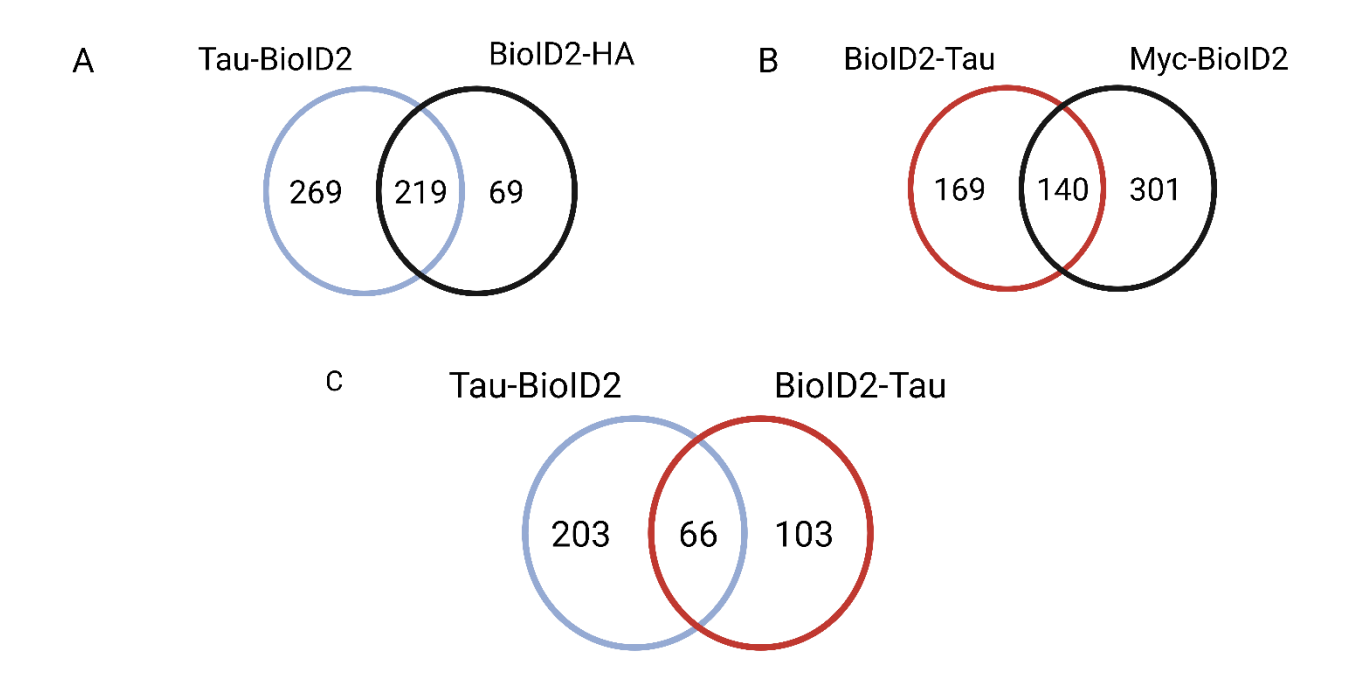


Figure 12: Venn diagrams of the identified preferential interacting proteins. A) Tau-BioID2 and BioID2-HA shows 269 proteins considered as preferential Tau-BioID2 interactors (>1.5-fold change compared to BioID2-HA). B) BioID2-Tau and Myc-BioID2 shows 169 proteins considered as BioID2-Tau interactors (>1.5-fold change compared to Myc-BioID2), C) Tau-BioID2 and BioID2-Tau interactors collectively showing 372 proteins considered potential members of the tau interactome.

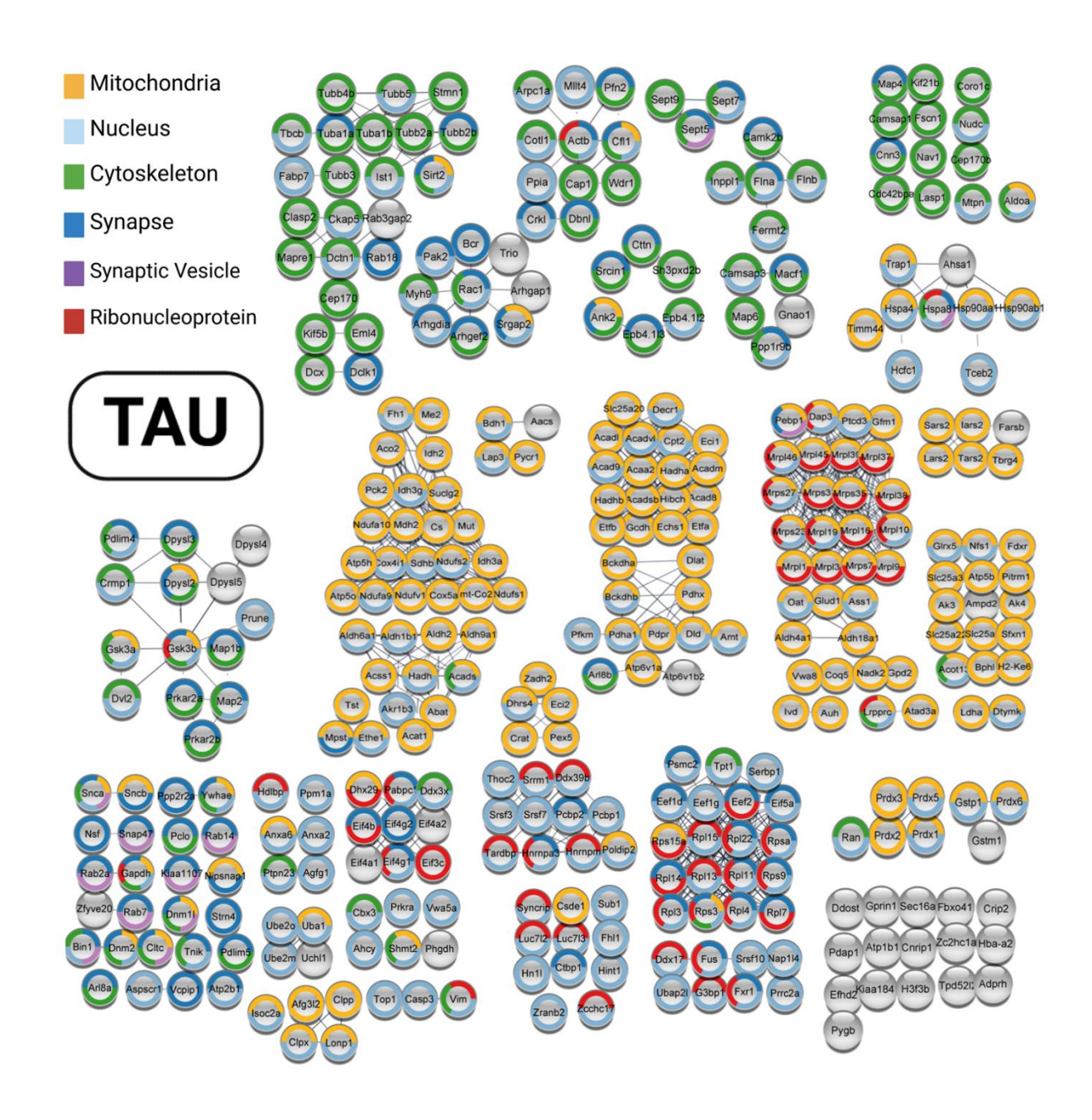


Figure 13: STRING analysis for the identified tau interactome. The network included both functional and physical associations with high confidence interaction score (>0.7). MCL Clustering was then performed using the String app with an inflation parameter of 3.0. Clustering was performed to reduce the complexity in the network to visualize the individual nodes. Major cellular component categories of the identified proteins are grouped by color.

Gene ontology enrichment analysis of tau interactome

ClueGO cellular component and molecular function pathways were analyzed for the list of tau interacting partners (Figure 14). Cellular component analysis mapped synaptic proteins localized to axonal growth cone, dendritic spine, pre-synapse, post-synapse and synaptic vesicle membrane. Cytoskeletal proteins belonging to the microtubule and actin cytoskeleton were identified. Mitochondrial proteins belonging to the mitochondrial respirasome, inner mitochondrial membrane, and the mitochondrial matrix were identified. The identified proteins were mapped to both the cytosolic and the mitochondrial ribosomal proteins, while proteins also were mapped to the peroxisome and the ribonucleoprotein granule (Figure 14A).

ClueGo molecular function pathway enrichment identified RNA binding proteins (dsRNA, mRNA, rRNA binding proteins), ribonucleoprotein complex binding proteins, cytoskeletal binding proteins (tau, microtubule, and actin binding proteins), kinase binding and ubiquitin ligase binding proteins. Proteins regulating translation initiation and nucleotide binding were also identified. Mitochondrial pathways included NADH dehydrogenase, oxidoreductase, peroxidase, FAD binding, fatty-acyl-coA binding, and electron transfer pathways were identified (Figure 14B). The full list of the identified proteins in cellular components and molecular function pathways are shown in Appendices B and C.

Interestingly, the GO KEGG pathways analysis revealed proteins involved in neurological diseases. Those included AD (26 proteins), Parkinson's disease (PD; 28 proteins), Amyotrophic lateral sclerosis (ALS; 31 proteins), HD (24 proteins), and prion diseases (25 proteins). The list of the associated proteins is shown in Table 2.

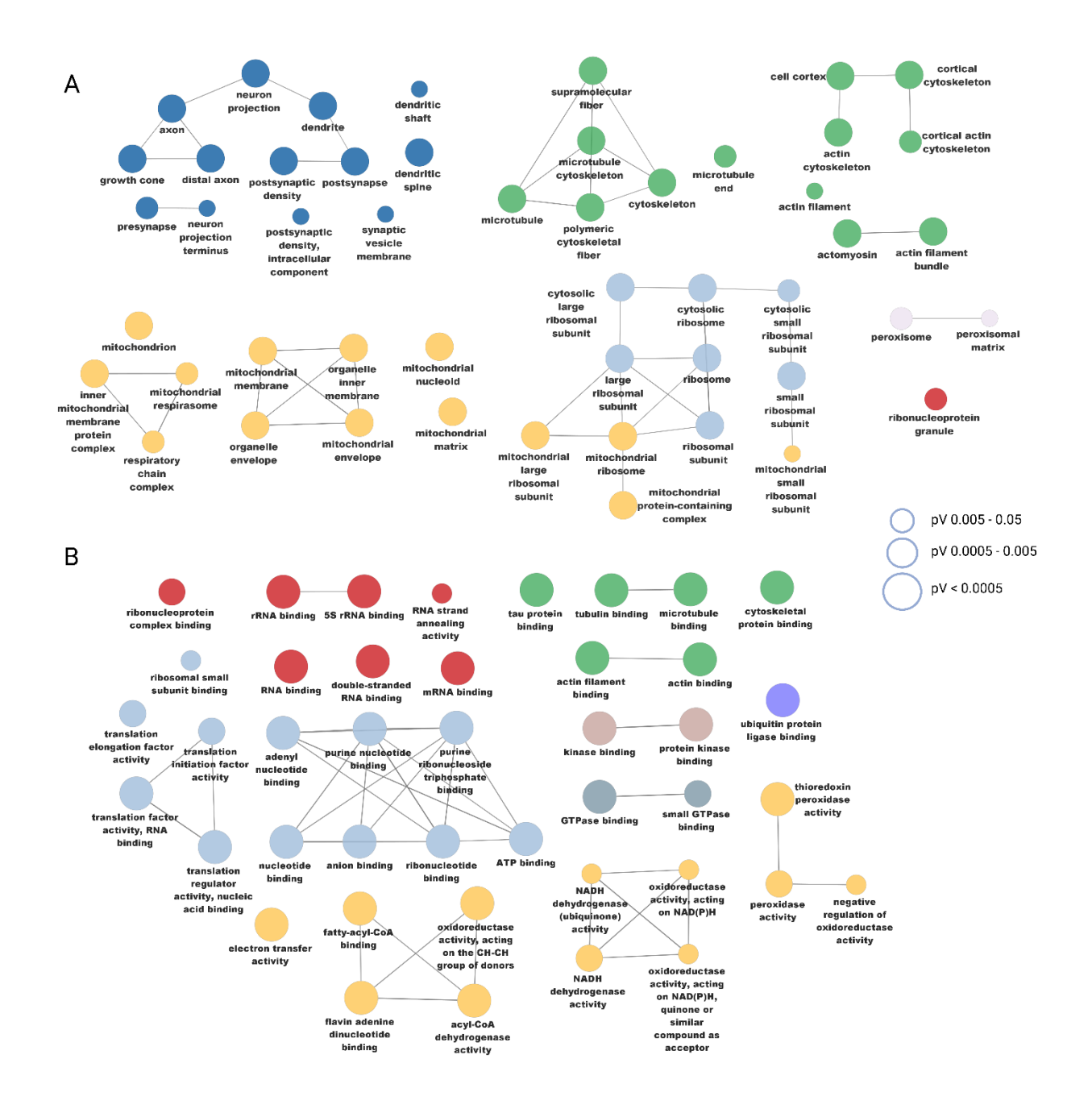


Figure 14: ClueGo gene ontology enrichment analysis for the identified tau interactome. A) Cellular component enrichment analysis, B) Molecular function pathways analysis. Only pathways with p-value ≤0.05 were included.

Table 2: KEGG pathway analysis associated proteins with neurological disorders

Disease	# of Proteins	% of Genes	Associated Genes
Alzheimer's Disease	26	7.05	[Atp5b, Atp5h, Atp5o, COX2, Casp3, Cox4i1, Cox5a, Dvl2, Gapdh, Gsk3b, Kif5b, Ndufa10, Ndufa9, Ndufs1, Ndufs2, Ndufv1, Psmc2, Sdhb, Snca, Tuba1a, Tuba1b, Tubb2a, Tubb2b, Tubb3, Tubb4b, Tubb5]
Parkinson's Disease	28	11.34	[Atp5b, Atp5h, Atp5o, COX2, Camk2b, Casp3, Cox4i1, Cox5a, Kif5b, Ndufa10, Ndufa9, Ndufs1, Ndufs2, Ndufv1, Psmc2, Sdhb, Septin5, Snca, Trap1, Tuba1a, Tuba1b, Tubb2a, Tubb2b, Tubb3, Tubb4b, Tubb5, Uba1, Uchl1]
Amyotrophic Lateral Sclerosis	31	8.40	[Actb, Atp5b, Atp5h, Atp5o, COX2, Casp3, Cox4i1, Cox5a, Dctn1, Fus, Hnrnpa3, Kif5b, Ndufa10, Ndufa9, Ndufs1, Ndufs2, Ndufv1, Pfn2, Psmc2, Rac1, Sdhb, Srsf3, Srsf7, Tardbp, Tuba1a, Tuba1b, Tubb2a, Tubb2b, Tubb3, Tubb4b, Tubb5]
Huntington Disease	24	7.95	[Atp5b, Atp5h, Atp5o, COX2, Casp3, Cltc, Cox4i1, Cox5a, Dctn1, Kif5b, Ndufa10, Ndufa9, Ndufs1, Ndufs2, Ndufv1, Psmc2, Sdhb, Tuba1a, Tuba1b, Tubb2a, Tubb2b, Tubb3, Tubb4b, Tubb5]
Prion Disease	25	9.33	[Atp5b, Atp5h, Atp5o, COX2, Casp3, Cox4i1, Cox5a, Gsk3b, Hspa8, Kif5b, Ndufa10, Ndufa9, Ndufs1, Ndufs2, Ndufv1, Psmc2, Rac1, Sdhb, Tuba1a, Tuba1b, Tubb2a, Tubb2b, Tubb3, Tubb4b, Tubb5]

GO enrichment analysis reveals distinct cellular components for Tau-BioID2 and BioID2-Tau interacting partners

ClueGO cellular component analysis was performed separately on: a) proteins identified in both Tau-BioID2 and BioID2-Tau (66 shared proteins), b) proteins identified in Tau-BioID2 but not BioID2-Tau (203 proteins), and c) proteins identified in BioID2-Tau but not Tau-BioID2 (103 proteins). The 66 shared proteins were localized to mitochondria, ribosomes, axonal growth cone, dendrites, and cytoskeleton (Figure 15A). The 203 proteins identified with only Tau-BioID2 were localized to the cytoskeleton, ribonucleoprotein granule, cytoplasmic stress granule, ribosomes, axonal growth cone, dendritic shaft, synapse, and synaptic vesicles (Figure 15B). The 103 proteins identified with only BioID2-Tau were primarily localized to mitochondria and ribosomal subunits (Figure 15C).

Taken together, the identified tau protein interactome mapped synaptic, nuclear mitochondrial, RNA binding, ribosomal, and cytoskeletal proteins. GO cellular component analysis revealed a preferential interaction of synaptic and RNA binding proteins with the C-terminus tagged tau protein (Tau-BioID2), while the mitochondrial proteins showed preferential interaction with the N-terminus tagged Tau protein (BioID2-Tau).

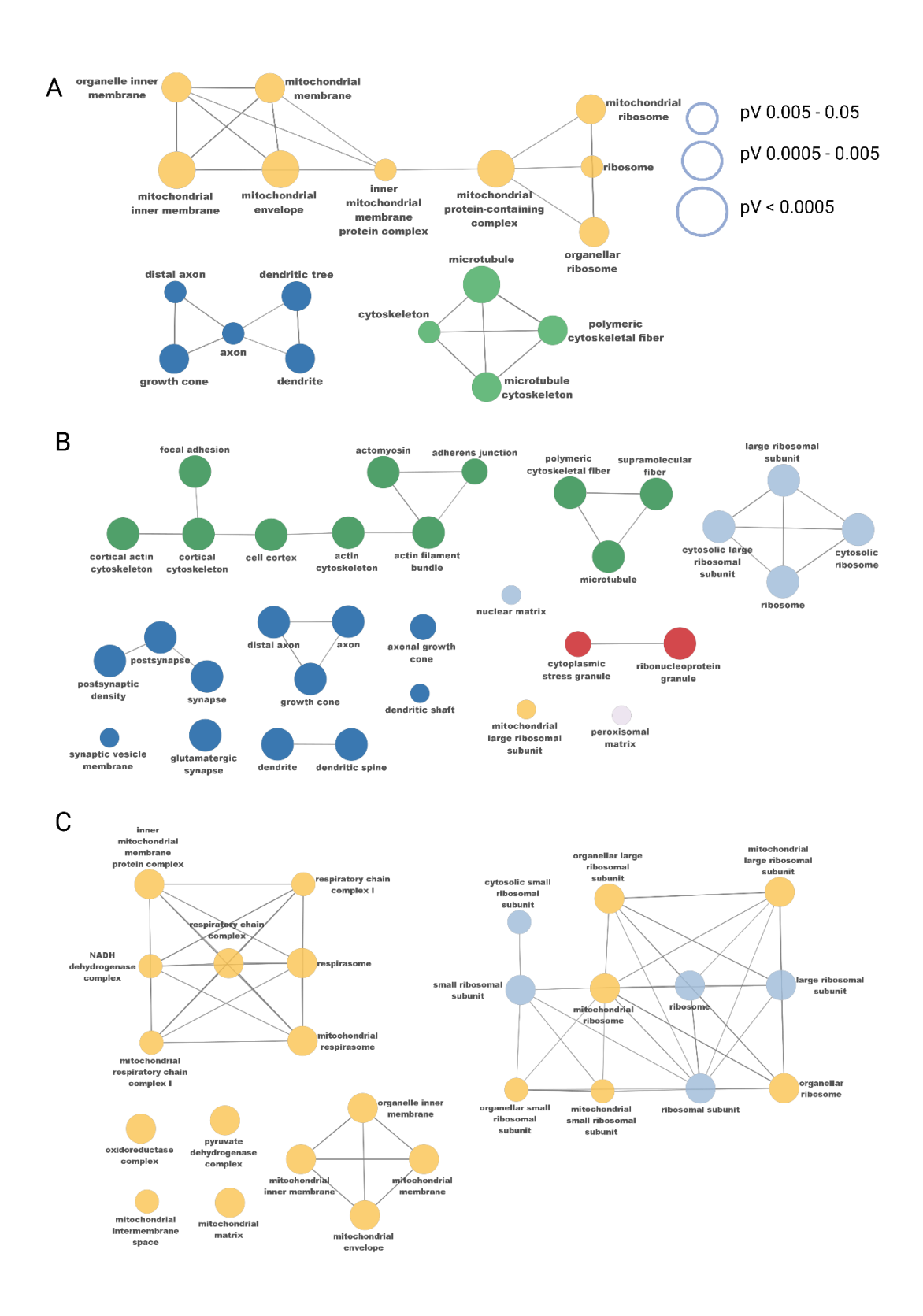


Figure 15: GO enrichment cellular component analysis. A) Proteins identified as interacting partners with both Tau-BioID2 and BioID2-Tau (66 proteins). B) Proteins

Figure 15 (cont'd)

identified as Tau-BioID2 only interacting partners (203 proteins). C) Proteins identified as BioID2-Tau only interacting partners (103 proteins). Only pathways with p-value ≤0.05 were included

Validation of the identified tau interacting partners

Primary E18 cortical neurons from TKO mice were transduced by lentiviruses expressing the BioID2 proteins and candidate tau interacting partners identified by mass spectrometry were validated by western blotting. Proteins identified by mass spectrometry as potential interactors with both Tau-BioID2 and BioID2-Tau proteins were chosen for validation experiments as these likely represent robust tau interactors. First, MAP2 was identified by mass spectrometry as an enriched protein in both Tau-BioID2 and BioID2-Tau when compared to their respective controls BioID2-HA and Myc-BioID2 (i.e. 3-fold increase in Tau-BioID2 compared to BioID2-HA and 2-fold increase in BioID2-Tau compared to Myc-BioID2). Immunoblotting confirmed that MAP2 shows an increased interaction with Tau-BioID2 and BioID2-Tau compared to the control samples (Figure 16A). Second, MAP6 was identified by mass spectrometry as a specific interactor with both BioID2-Tau and Tau-BioID2 proteins and was not detected in either Myc-BioID2 or BioID2-HA control proteins. Immunoblotting confirms that MAP6 was uniquely found with both tau proteins and was undetectable in the controls (Figure 16B).

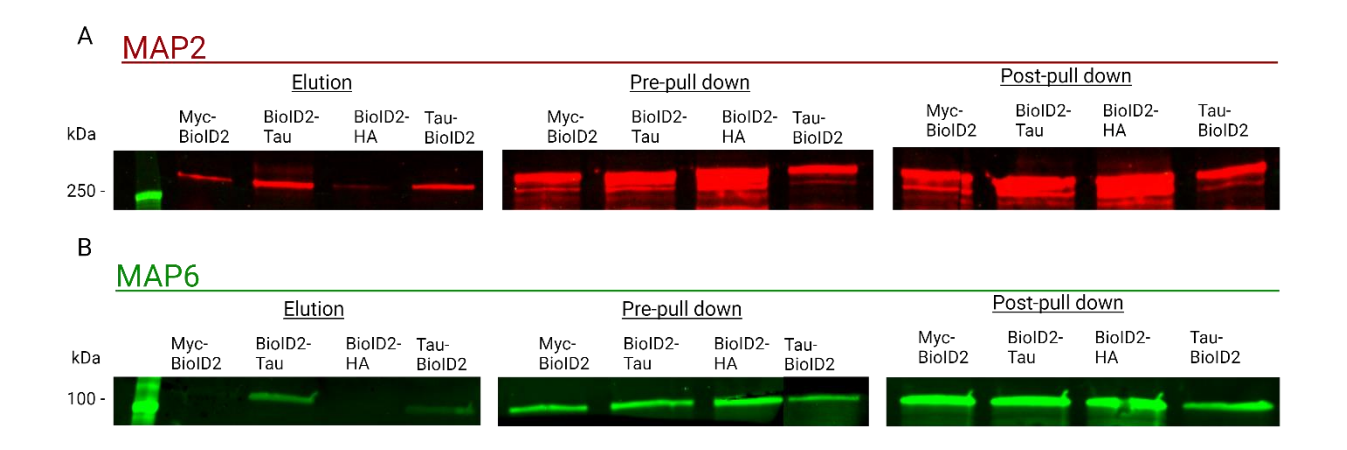


Figure 16: Validation of candidate Tau interacting partners by western blotting.

TKO primary cortical neurons (E18) were transduced by BioID2-HA, Tau-BioID2, Myc-BioID2, and BioID2-Tau lentiviruses. Biotinylated Tau interacting partners were captured by streptavidin-coated magnetic beads. Western blotting was performed to validate the mass spectrometry results by probing with potential tau interacting partners that were enriched in either Tau-BioID2 or BioID2-Tau samples compared to their respective controls BioID2-HA and Myc-BioID2. Western blots were probed for A) MAP2, and B) MAP6. MAP2 and MAP6 antibodies were used.

DISCUSSION

Accumulating evidence suggests there are physiological microtubule-dependent and - independent functions of the tau protein. Understanding the diverse biological processes in which the tau protein participates is critical to advancing our understanding of normal tau physiology and potentially tau's role in pathological mechanisms of tauopathies. The work presented in this thesis provides a novel *in situ* labeling approach to study tau protein-protein interactions in living neurons.

Tau interactome mapping

Utilizing the BioID2 *in situ* labelling approach, 372 proteins were identified that are candidate members of the tau protein interactome. The cellular localization of the identified tau protein interactions was consistent with previous findings and included proteins mapped to the mitochondria, cytoskeleton, synaptic vesicles, ribosomes, the ribonucleoprotein complex as well as heat shock proteins and regulators of the ubiquitin-proteasome system (Geeth Gunawardana et al., 2015; C. Liu et al., 2016; Tracy et al., 2022; P. Wang et al., 2017). Moreover, the BioID2 approach identified tau protein interactions previously reported in the literature including PP1α, GSK3β (Combs et al., 2021; Kanaan et al., 2011b), EFhd2 (Ferrer-Acosta et al., 2013), Annexins A2, and A6 (Gauthier-Kemper et al., 2018b), and α-synuclein (Esposito et al., 2007). These results provide supportive evidence of the various physiological functions of the tau protein and demonstrate the capability of the BioID2 approach in mapping the tau protein interactome.

Interestingly, the identified tau interactome revealed proteins associated with neurodegenerative diseases including AD, PD, ALS, HD, and prion disease. Among which; a) GSK3β, Dvl2, α-synuclein and GAPDH associated with AD, b) α-synuclein, Camk2b, Trap1, Uba1, Uchl1, and Septin5 are associated with PD, c) Actb, Dctn1, Hnrnpa3, Fus, Srsf3, Srsf7, and Tardbp are associated with ALS, d) Hspa8, and Rac1 are associated with prion disease, and e) Atp5b, Atp5h, Atp5o, Cox2, Cox4i1, Cox5a, Casp3, Kif5b, Ndufa10, Ndufa9, Ndufs1, Ndufs2, Ndufv1, Psmc2, Sdhb, Tuba1a, Tuba1b, Tubb2a, Tubb2b, Tubb3, Tubb4b, and Tubb5 are associated with all five diseases. These results align with a previous study showing that a tau protein consisting of amino acids 151-391 interacted with 39 proteins associated with AD, 10 associated with PD, and 22 associated with both diseases (Sinsky et al., 2020). However, the associated interactions detected here were different. One possible explanation for the difference in specific proteins identified is the experimental strategy used. Sinsky et al., utilized a rat brainstem crosslinking approach coupled to mass spectrometry to identify the interactome of a truncated version of tau expressing amino acids 151-391, while here the *in situ* labeling BioID2 approach with full-length tau was used.

Distinct and overlapping interactions between BioID2-Tau and Tau-BioID2

I reported distinct interactions between the N- versus C- terminus tagged tau proteins, BioID2-Tau and Tau-BioID2. The preferential interactors with BioID2-Tau (103 proteins) were mapped to the mitochondria and ribosomal subunits while the preferential interactors with Tau-BioID2 (203 proteins) were mapped to cytoplasmic stress granule, ribosomes, cytoskeleton, axonal growth cone, dendritic shaft, synapse, and synaptic vesicles. This is possibly due to where the interactors bind tau as BioID2 labeling will be influenced by the physical distance and/or orientation of binding partners. The labeling radius of the BioID2 protein is estimated at ~10 nm (Kim et al., 2014). Adding a 25 nm

13xlinker between BioID2 and the protein of interest was suggested to increase the biotinylating range of the BioID2 protein (Kim et al., 2016). The length of the tau protein was estimated to be ~63-70 nm with the longest average length of human tau estimated at 96.2 nm (Hagestedt et al., 1989; Ruben et al., 1991; Tracy et al., 2022). Thus, the placement of the BioID2 may facilitate or restrict access to specific sets of interacting partners.

Tracy et al., used APEX2 in situ labeling fused to either the N-terminus (APEX-Tau) or C-terminus (Tau-APEX2) of full-length human tau in human neurons derived from a human induced pluripotent stem cell line (WTC11) (Tracy et al., 2022). The APEX2 is a proximity labeling enzyme similar in principle to BioID2, both proteins involve biotin labeling in a ~10-20 nm labeling radius. A major difference is that APEX2 is peroxidase which requires adding toxic hydrogen peroxide and accordingly biotinylates proteins in a ~1 min time frame identifying the interactome as a cross-sectional snapshot that can be utilized to study tau dynamics (i.e. tau secretion during activity-dependent neuron excitability). Similar to our results, they found enrichment of different interactors with each protein. They reported synaptic, dendritic, mRNA binding, and proteasomal proteins interacting preferentially with APEX2-Tau, while Tau-APEX2 preferentially interacted with proteins involved in heat shock response, vesicle mediated transport, and transport along microtubules. Out of the 372 proteins identified with the BioID2 approach, only 62 proteins were also identified in the APEX2 approach and were mapped to the cytoskeleton, synapse, somatodendritic compartment and mitochondria. Importantly, out of the 62 overlapping proteins between both APEX2 and BioID2 approaches, 10 proteins (αsynuclein, Rac1, Pfn2, Cltc, Hspa8, Psmc2, Tubb2a, Tubb2b, Tubb3, and Tubb4b) were annotated to neurodegenerative diseases including AD, PD, HD, ALS, and prion disease.

In addition, BioID2 identified 66 overlapping proteins between both BioID2-Tau and Tau-BioID2 and were mapped to mitochondria, and mitochondrial ribosomes (e.g. Timm44, Tbrg4, Pdhx, Ak4, Mut, Cox4i1, Fdxr, MrpI19, MrpI37, and MrpI38), somatodendritic compartment, and axonal growth cone (Dcx, β-synuclein, α-synuclein, PcIo, and MAP6), and the microtubule cytoskeleton (e.g. Map2, Map6, Stmn1, Map1b, Kif2a, Map4, Camsap3, and Tbcb). While Tracy et al., identified 136 overlapping proteins between APEX2-Tau and Tau-APEX2 and included tubulin binding, actin binding, nucleic acid binding, as well as members of the SNARE complexes (Tracy et al., 2022). Again, differences in specific proteins identified between Tracy et al. and this work might be due to the experimental approaches and cellular models utilized. Neither study can assign the differences to where in the tau protein the interactors bind, but they indicate that *in situ* labeling may require tagging both ends of a protein to effectively label the full spectrum of interactors.

The use of truncated portions of the full-length tau protein are more likely to facilitate the identification of tau domain-specific interactors. Geeth Gunawardana et al., utilized a crosslinking approach to identify tau interactors with an N-terminal tau construct (amino acids 1-255) and a C-terminal tau construct (amino acids 256-441) in the human neuroblastoma SH-SY5Y cell model. The Tau1-255 protein showed interactions with histones, RNA binding, and translation proteins, while the Tau256-441 protein interacted with heat shock proteins, actin binding proteins, and members of the proteasomal system

(Geeth Gunawardana et al., 2015). A natural extension of this work is to utilize the BioID2 approach to identify tau domain-specific interactors in neurons.

Tau protein interactions in various cellular localizations

GO cellular component analysis revealed tau protein interactions in the mitochondria, cytoskeleton, synaptic vesicles, ribosomes, and the ribonucleoprotein complex. Perhaps not surprisingly, several tubulin cytoskeleton-related proteins were identified as interactors with tau using the BioID2 approach, but additional and potentially important other interactions were identified. Tau protein was traditionally described as a microtubule stabilizing protein. This finding was later challenged, and tau was reported to regulate microtubule dynamics rather than stabilizing them (Qiang et al., 2018). Tau, as well as other MAPs, were suggested to crosslink the actin and microtubules cytoskeletons (reviewed in (Mohan & John, 2015)). This aligns with our finding that tau interacts with proteins involved in tubulin, and actin binding, as well as the interaction with other MAPs including MAP2, MAP1b, MAP4, MAP6, EML4, MAPRE1, and JPT2. I provided additional support that the tau-cytoskeletal protein interactions exist, which might modulate the various functions of tau in regulating cytoskeletal dynamics as well as tau's role as a scaffolding protein that may localize binding partners to cytoskeleton.

The interaction between tau and mitochondria is extensively reported in literature. Early studies examined the effect of tau binding to the microtubules on the mitochondria kinesin-mediated axonal transport (Ebneth et al., 1998), a process potentially regulated by GSK3β (Llorens-Martin et al., 2011; Tatebayashi et al., 2004). More recent studies reported the effect of mitochondria dysfunction on tau pathology (Du et al., 2022; Terada et al., 2021), while others correlated tau mutations and accumulation to mitochondria

reduction and/or dysfunction (Cummins et al., 2019; Li et al., 2016; Rodríguez-Martín et al., 2016; Tracy et al., 2022). However, it's not well characterized whether tau accumulation leads to mitochondrial dysfunction, or whether mitochondrial dysfunction is a major contributor to tau pathology. Much less is known about a potential physiological role for tau in mitochondrial function, but it is notable that 164 proteins involved in mitochondria function were found in this work. Those included proteins involved in mitochondria respirasome, mitochondrial large and small ribosomal subunits, mitochondrial oxidoreductase activity, electron transfer, NADH dehydrogenase activity, and FAD binding. Future studies may investigate the physiological tau-mitochondria interaction which will further our understanding of the pathological mechanisms that involve tau accumulation and mitochondrial dysfunction.

Tau was also reported to bind RNA-binding proteins in the dendrites which regulates the formation of stress granules as well as tau pathological misfolding (Apicco et al., 2018; Jiang et al., 2021; Maziuk et al., 2018b; Vanderweyde et al., 2016). Tau interaction with RNA binding proteins and members of the ribonucleoprotein complex was observed in this work. The identified proteins included HNRNPA3, HNRNPM, HNRNPQ, TARDBP, FARSB, FUS, FXR1, among others. Oligomeric tau was reported to inhibit translation by increasing the tendency of RNA stress granules formation, a process mediated by tau binding to HNRNPA2/B1(Jiang et al., 2021). Other RNA binding proteins (i.e. TIA1) were also found to mediate tau toxicity and increase the tendency of tau aggregation and neurodegeneration. The role of physiological tau in binding to RNA binding proteins and localization to the dendrites is a relatively new area of investigation and not well-understood (Maziuk et al., 2018a; Vanderweyde et al., 2016). Studying the

molecular mechanisms involved in tau localization to the dendrites and binding to RNA binding proteins may elucidate the physiological roles and the pathological mechanisms involved in stress granules formation and pathologic tau accumulation in neurodegenerative diseases. The BioID2 approach identified small and large ribosomal proteins (RPL11, RPL13, RPL14, RPL3, RPL4, RPS15a, RPS3, RPS9, RPSa), translation initiation factors (EIF4b, EIF4a2, EIF5a, among others), and proteins localized to the dendrites (DCX, PP1r9b, PCLO, SNAP47, NSF, NAP1I4, among others). These findings provide additional evidence of microtubule-independent functions of the tau proteins which require further investigation to understand the molecular mechanisms mediated by tau protein-protein interactions.

Tau also localizes to the synapses in both physiological and pathological states. Tau is suggested to play a role in synaptic plasticity. For instance, tau knockout mice show impairment in long-term potentiation (Ahmed et al., 2014) and long-term depression (Kimura et al., 2014). Physiological tau undergoes activity-dependent translocation to the post-synaptic compartment where it acts as a scaffolding protein by binding to Fyn kinase and PSD-95 localizing Fyn kinase to phosphorylate and stabilize NMDA receptors, a process critical to long-term potentiation (Ittner et al., 2010; Mueller et al., 2021). In AD, pathological tau accumulates in the synaptic terminals causing synaptic loss and impairment of synaptic plasticity (Wu et al., 2021; Yoshiyama et al., 2007). Pathological tau can induce presynaptic dysfunction by binding synaptogrin-3 on synaptic vesicles which leads to accumulation of synaptic vesicles and blocking exocytosis in the presynaptic terminals (McInnes et al., 2018). The localization of tau to the synapses is consistent with the findings presented in this thesis. Tau interactions were reported in the

presynaptic terminals (e.g. Bin1, PCLO, FXR1, α-synuclein, β-synuclein, Srcin1, Tnik, among others), post synapses (e.g. Neurabin-2, srGAP2, DCLK1, DNM2, ARHGEF2, CFL1, FUS, PRKAR2B, PSMC2, Ank2, among others), and synaptic vesicles membrane (e.g. ATP2b1, CLTC, DNM1L, Rab14, Rab2a, Rab7, Snap47, and α-synuclein). Understanding the signaling mechanisms of synaptic tau protein-protein interactions will help us better identify and study various roles of synaptic tau in both health and disease states.

Taken together, the BioID2 proximity labeling approach provides an effective route to map the tau interactome highlighting the broad physiological functions mediated by the tau protein. Understanding the molecular signaling pathways mediated by the physiological tau interactome may help elucidate the pathological mechanisms involved in the switch from physiologic-to-insoluble aggregated pathologic tau in the neurodegenerative tauopathies.

Technical development of the approach

The proposed experimental framework involved four main phases; a) molecular cloning to create fusion proteins between the BioID2 biotin ligase and tau followed by the production of the fusion proteins in lentiviruses, b) culturing TKO primary cortical neurons and expression of the BioID2 proteins via lentiviral-mediated transduction, c) affinity capturing and mass spectrometry identification of the biotinylated tau-interacting proteins, and d) validation of the identified proteins by affinity capturing and immunoblotting.

Cloning of BioID2 and Tau fusion proteins

To map the total tau protein interactome, I tagged BioID2 to the N-terminus (BioID2-Tau) or the C-terminus (Tau-BioID2) of the 2N4R human tau isoform. The two fusion proteins were cloned from the Myc-BioID2-13xlinker and the 13xlinker-BioID2-HA plasmids respectively. The two plasmids are different in the place of the tag and the 13xlinker sequence. Accordingly, the Myc-BioID2-13xlinker was used as a control protein for BioID2-Tau and the 13xlinker-BioID2-HA was used as a control for Tau-BioID2. This step is critical for proper elimination of background proteins (proteins identified due to non-specific interactions or direct interactions with BioID2 and/or the 13x linker), endogenously biotinylated proteins (e.g. carboxylases), and contaminant proteins (e.g. streptavidin, trypsin, keratins).

Fusion proteins Tau-BioID2, BioID2-Tau and the respective controls BioID2-HA and Myc-BioID2 were cloned into a pFIN vector backbone which encodes for essential elements for the lentiviral production including Gag, RRE, and WPRE sequences. The pFIN plasmids are prone to homologous recombination events between the 5'- and 3'-long terminal repeats which makes it challenging to produce the constructs. To avoid this, I used Stbl3 competent *E. coli* to produce the DNA constructs. Stbl3 cells are known to reduce the homologous recombination events. I also noted that incubating transformed Stbl3 cells for the least amount of time (~12 hours) increases the chances of successful viral plasmid preparations. To ensure proper cloning of the DNA construct, the created pFIN plasmids were validated by restriction digestion and Sanger sequencing for the correct insertion of the BioID2 protein sequences. These steps are important to the generation of high-quality lentiviral preparations.

Lentiviruses production

The BioID2 proteins were produced in lentiviruses by transfection of HEK293T cells by pFIN transfer plasmids carrying the BioID2 sequences, pNHP packaging vector, and pHEF-VSVG envelope vector. Lentiviruses were harvested by centrifugation and the functional titer was determined by immucnocytochemistry in HEK293T cells. The functional titer protocol is based on the ability of the functional viruses in infecting the cells and expressing the protein of interest. I determined the lentiviral functional titer in HEK293T cells which is time and cost effective. HEK293T cells were then transduced at a similar MOI of 50 by BioID2-Tau and Tau-BioID2 lentiviruses to establish whether the functional titers were accurate. The results showed that the lentiviruses expressed the fusion proteins at nearly similar levels validating the functional titer protocol. Ensuring that the lentiviruses achieved similar expression levels in mammalian cells facilitates a more robust interpretation of the identified Tau-BioID2 and BioID2-Tau protein interactomes by mitigating expression level differences as a potential driver of disparate interactors identified between each tau protein.

Lentiviral-mediated transduction of primary cortical mouse neurons

The second phase of the project involved a series of optimizations to define an experimental paradigm before affinity capturing and MS identification of biotinylated proteins. First, I identified the lentiviral transduction efficiency by transuding E18 TKO primary cortical neurons at a varying range of multiplicity of infections (50, 100, and 200). I found that all four lentiviruses expressing Tau-BioID2, BioID2-Tau, Myc-BioID2, and

BioID2-HA are capable of infecting ~50% of primary neurons at MOI 200. Although increasing the titer further may have produced higher efficiency, this may also increase the chance or extent of non-physiological overexpression leading to unwanted artifacts.

Next, the level of lentiviral-mediated tau expression was measured to determine whether near-physiological or supraphysiological levels of expression occurred. Similar expression levels of the physiological WT tau and lentiviral-expressed Tau-BioID2 were determined. This optimization step was important to ensure that the identified tau protein interactions represented the physiological state and were not identified due to the high levels of expression of the Tau-BioID2 proteins by lentiviruses. Although gene therapy-based approaches are effective at delivering exogenous expression systems to neurons, the potential artifacts induced by overexpression can be difficult to address. Fortunately, densitometry analyses suggest that the level of lentiviral-mediated tau expression was similar to WT neuron tau levels. These results suggested the approach used here was unlikely to be affected significantly by overexpression artifacts.

Finally, I showed that the highest biotinylation signal was achieved by supplementing 100 μM biotin and incubating for 96 hours. This allows sufficient time for the BioID2 *in situ* biotin labeling of the proximal proteins. Our experimental paradigm involved the lentiviral transduction (MOI 200) of 3.6 x 10^6 E18 TKO primary cortical neurons on DIV4, supplementing biotin (100 μM) on DIV8 and collecting the lysates of biotinylated proteins on DIV 12. Notably, I could have revisited these optimization steps if I were not able to detect biotinylated proteins by mass spectrometry. This could have included, a) increasing the number of TKO primary cortical neurons per lentiviral

transduction, b) transducing TKO neurons at a higher MOI (i.e. 300), and/or c) supplementing a higher biotin dose and/or increasing the incubation time.

Mass spectrometry identification of tau interacting proteins

The third phase involved affinity capturing of the biotinylated proteins using streptavidin conjugated magnetic beads and identification of the labelled proteins by mass spectrometry. For efficient capturing of biotinylated proteins, I performed two rounds of optimizations using lysates from HEK293T cells and primary cortical neurons. Although the interaction between biotin and streptavidin is one of the strongest known biological interactions (Haugland & You, 2008), the most efficient capturing was with a highconcentration detergent lysis buffer. One possible explanation for this might be that denaturing the secondary structures of the proteins by a high concentration of detergents (i.e. SDS and NP-40) was required to expose the biotinylated residues and allow binding to the streptavidin magnetic beads. Importantly, the *in situ* labeling of interactors prior to cell lysis affords harsher conditions that traditional IP-type approaches would not allow. Due to the high affinity interaction between biotin and streptavidin, elution of biotinylated proteins bound to the magnetic beads required competition with a high concentration of free biotin (25 mM) and heat. Furthermore, when I used lysates from primary neurons, the sample-bead incubation time (overnight) and temperature (room temp) were critical for the efficient capturing of the biotinylated proteins. This might be due to the lower lentiviral-mediated expression of the BioID2 proteins (hence lower biotinylation levels) compared to the expression in HEK293T cells mediated by pFIN plasmids transfection and similar approaches others have used (Kim et al., 2016; Roux et al., 2013b).

For the mass spectrometry identification, I performed label free quantification to determine the abundances of the identified proteins in the Tau-BioID2 and BioID2-Tau samples compared to the respective controls BioID2-HA and Myc-BioID2. I set the following criteria for defining proteins as tau interactors: 1) Proteins must be identified in at least two out of the three independent replicates, and 2) proteins should be detected at \geq 1.5-fold increase compared to the respective BioID2 control. These criteria were chosen to balance minimizing false positives and false negatives. I chose the abundance ratio based on the previously reported enrichment ratios in the antibody-based affinity purification experiments such as \geq 1.2 in (Geeth Gunawardana et al., 2015), \geq 1.1 in (C. Liu et al., 2016), and \geq 1.5 in (Tracy et al., 2022). I identified 372 tau-interacting partners by MS using these criteria, however, MS identification ultimately requires validation to confirm whether these proteins are bona fide tau interactors.

Validation of identified tau interacting partners

Finally, I chose some of the identified interactors for proof-of-concept validation by western blotting. I successfully validated MAP2 and MAP6 as tau interactors using this approach. Notably, the validation of interacting proteins by western blotting is limited to the amount of biotinylation on the protein, and subsequently the amount that will be captured by the beads. Mass spectrometry is more sensitive at identifying low levels of biotinylated proteins compared to western blotting. Future experiments are planned to validate additional novel tau interactors that were identified using the BioID2 approach using tau antibody-based affinity purification coupled with the use of brain lysates from either human tau knock-in mouse brains and/or post-mortem human brain tissue.

Reversal of the co-immunoprecipitation using antibodies against the identified tau interacting partners will help to strengthen the confirmation as a bona fide interactor. Finally, the use of *in situ* labeling immunostaining techniques, such as proximity ligation assays, are viable means to further validate not only the interaction but where in neurons the proteins interact.

Limitations of the approach

Enzyme-mediated proximity labeling approaches, including the BioID2 approach, provide a complementary framework for studying protein-protein interactions. The proximity labeling approaches overcome several of the limitations of the traditional lysis and antibody-based techniques. However, some limitations remain that should be considered when planning experiments and interpreting results. First, proximity labeling techniques are based on creating relatively bulky fusion proteins which might directly interfere with protein interactions. Fusion proteins can alter the functionality and/or folding of the target protein. However, our group has worked with Tau-GFP fusion proteins and found that microtubule binding and in vitro aggregation are unaffected (Kanaan et al., 2020). Also, biotinylation of the fused target protein (i.e. tau) may affect its interactions. Moreover, labeling is dependent on the biotinylating radius of the enzyme (~10 nm) as well as the surface-exposed lysine residues available for biotinylation by the BioID2 enzyme. Thus, the orientation and/or accessibility of an interactor may impact whether it is effectively biotinylated. Indeed, we and others (Tracy et al., 2022) noted differences in the set of interactors identified in the BioID2 or APEX2 fusions are on the N- or C-terminus of fulllength tau. Another limitation is that the BioID2 enzyme not only biotinylates the stable and transient/weak interactions but could also label proteins that are in close proximity

either in a complex (i.e. indirectly interacting) or not interacting (i.e. non-specific detection) with the target protein. Nonetheless, the *in situ* labeling of interactors provided by BioID2 approach is advantageous and provides a robust addition to the toolkit available for studying tau protein-protein interactions, but these caveats require consideration and identified interactors require validation.

Identifying protein interactions using this approach is also limited by the tau isoform used, solubility of the proteins in the lysis buffer, and the neuronal model. In the adult human brain, six tau isoforms are expressed due to the alternative splicing of exons E2, E3, and E10 of the *MAPT* gene. In this study, I tagged BioID2 to the longest isoform of the tau protein (2N4R isoform). Thus, the identified tau interacting partners are limited to potential interactors with the 2N4R isoform. Liu and colleagues previously reported preferential interactions to specific mouse tau isoforms (C. Liu et al., 2016). To better represent candidates of the physiological tau protein interactome, BioID2 could be tagged to all six tau isoforms.

Solubility of the proteins is another limiting factor. I used lysis buffer containing 50 mM Tris pH 7.4, 150 mM NaCl, 0.4% SDS, 1% NP-40, 1 mM EGTA, and 1.5 mM MgCl₂. The identified proteins are those soluble in SDS and NP-40 detergents, non-soluble pelleted proteins were not identified using this approach as the pellet was not analyzed. A more comprehensive assessment to try capturing the full set of interacting partners would include analysis of biotinylated proteins in the lysate pellet.

Tau knockout primary cortical neurons were transduced on the 4th day *in vitro*. TKO mice display a compensatory upregulation of other MAPS (MAP1A, MAP1B and MAP2), but whether this occurs in TKO primary neurons is unknown. (Harada et al., 1994; G. Liu

et al., 2019; Ma et al., 2014). The increased expression levels of MAPs in TKO neurons might interfere or compete with the physiological interacting partners of the DIV 4 expressed lenti-tau. However, this requires further investigation to study the crosstalk between lenti-tau and compensatory mechanisms such as changes in other MAPs. Finally, the model system used here is a developing neuron in culture, which may influence the tau interactome. Indeed, developmental-dependent differences in tau expression are well known (i.e. 0N3R is expressed in early development and later additional isoforms are expressed) (Y. Wang & Mandelkow, 2016). The influence of an actively developing neuron on tau interactions is an area of high interest as it has not been well-studied. Confirming the identified tau interactors in adult CNS tissue sources (as discussed above) could help clarify whether the interactors identified here are relevant to the adult nervous system. Taken together, I identified candidate members of the tau interactome using the BioID2 approach and several of the identified proteins overlapped with prior work and some of the proteins were further confirmed by immunoblotting. However, due to the limitations discussed abover, there might be other physiological tau interacting partners that were not effectively detected using this approach or were due to specific technical aspects and the model system used.

Future directions

I demonstrated that the BioID2 *in situ* labeling approach facilitates the detection of tau interactors. Future studies can adapt this technique to address several questions regarding tau proteins interactions at both the physiological and pathological states. I plan on dissecting the role of each tau domain in protein interactions by creating BioID2 fusion proteins with the following tau domains: a) 1-224 amino acids (Nterm-BioID2), b) 225-380

amino acids (MTBR-BioID2), c) 381-441 amino acids (Cterm-BioID2), d) 1-380 amino acids (Nterm-MTBR-BioID2), and e) 225-441 amino acids (MTBR-Cterm-BioID2). This approach will help further our understanding of the various physiological functions of the tau protein mediated by the protein-protein interactions of its different domains. Moreover, this technique can be adapted to identify tau protein interactions at the level of the disease-related modifications including pathogenic post-translational modifications and mutations of the *MAPT* gene involved in the neurodegenerative tauopathies.

The BioID2 approach was successfully adapted by others to identify protein interactions *in vivo* (Feng et al., 2020; Pronobis et al., 2021). Thus, the presented approach can be utilized to study *in vivo* tau protein-protein interactions in tauopathy mouse models. This could help us better understand the spatiotemporal development of the disease-causing mechanisms mediated by tau protein interactions. If adapted to a normal physiological model, perhaps by fusing to normal tau in mice, the "physiological" tau interactome during neurodevelopment and/or in specific brain regions or cell types may be elucidated. The approach adapted in this thesis is a discovery-based approach in which I was interested in identifying candidates of the physiological tau interactome. Future studies may couple the discovery-based approach to a more targeted approach to study the downstream signaling pathways of the novel tau protein interactions identified. This could help reveal novel regulatory mechanisms of the various biological functions of the tau protein which may reveal novel therapeutic targets to counteract tau-mediated neurodegenerative processes.

APPENDICES

APPENDIX A

Table 3: List of the identified tau protein interacting partners

Accession ID	Gene	Protein Description	Tau- BioID2	BioID2- Tau
P19783	Cox4i1	Cytochrome c oxidase subunit 4 isoform 1	Yes	Yes
P28740-1	Kif2a	Isoform 1 of Kinesin-like protein KIF2A	Yes	Yes
P31324	Prkar2b	cAMP-dependent protein kinase type II- beta regulatory subunit	Yes	Yes
P46460	Nsf	Vesicle-fusing ATPase	Yes	Yes
Q07417	Acads	Short-chain specific acyl-CoA dehydrogenase	Yes	Yes
Q3UHX2	Pdap1	28 kDa heat- and acid-stable phosphoprotein	Yes	Yes
Q61191	Hcfc1	Host cell factor 1	Yes	Yes
Q7TSJ2	Map6	Microtubule-associated protein 6	Yes	Yes
Q80Y14	Glrx5	Glutaredoxin-related protein 5	Yes	Yes
Q8BJZ4	Mrps35	28S ribosomal protein S35	Yes	Yes
Q91YT0	Ndufv1	NADH dehydrogenase [ubiquinone] flavoprotein 1	Yes	Yes
Q9WUR9	Ak4	Adenylate kinase 4	Yes	Yes
O88712	Ctbp1	C-terminal-binding protein 1	Yes	Yes
P35293	Rab18	Ras-related protein Rab-18	Yes	Yes
P85094	Isoc2a	Isochorismatase domain-containing protein 2A	Yes	Yes
Q60875	Arhgef2	Rho guanine nucleotide exchange factor 2	Yes	Yes
Q6NS60	Fbxo41	F-box only protein 41	Yes	Yes
Q80VC9	Camsap3	Calmodulin-regulated spectrin- associated protein 3	Yes	Yes

Q8BK64	Ahsa1	Activator of 90 kDa heat shock protein ATPase homolog 1	Yes	Yes
Q8K0D5	Gfm1	Elongation factor G	Yes	Yes
Q91YM4	Tbrg4	Transforming growth factor beta regulated gene 4; Protein TBRG4; May play a role in cell cycle progression; Belongs to the FAST kinase family	Yes	Yes
Q921S7	Mrpl37	39S ribosomal protein L37	Yes	Yes
Q99LB2	Dhrs4	Dehydrogenase/reductase SDR family member 4	Yes	Yes
Q9D1E6	Tbcb	Tubulin-folding cofactor B	Yes	Yes
Q9D338	Mrpl19	39S ribosomal protein L19	Yes	Yes
Q9DCX2	Atp5h	ATP synthase subunit d	Yes	Yes
Q80TK0	Kiaa1107	AP2-interacting clathrin-endocytosis protein	Yes	Yes
P27546-4	Map4-4	Isoform 4 of Microtubule-associated protein 4	Yes	Yes
Q9ER88	Dap3	28S ribosomal protein S29	Yes	Yes
P20357	Map2	Microtubule-associated protein 2	Yes	Yes
Q6A065	Cep170	Centrosomal protein of 170 kDa	Yes	Yes
P54227	Stmn1	Stathmin	Yes	Yes
O88809	Dcx	Neuronal migration protein doublecortin	Yes	Yes
P27546	Map4	Microtubule-associated protein 4	Yes	Yes
Q9ERD7	Tubb3	Tubulin beta-3 chain	Yes	Yes
Q61578	Fdxr	NADPH:adrenodoxin oxidoreductase	Yes	Yes
Q9CPY7	Lap3	Cytosol aminopeptidase	Yes	Yes
Q8BH04	Pck2	Phosphoenolpyruvate carboxykinase	Yes	Yes
Q91ZZ3	Sncb	Beta-synuclein	Yes	Yes
P99024	Tubb5	Tubulin beta-5 chain	Yes	Yes
Q8BJH1	Zc2hc1a	Zinc finger C2HC domain-containing protein 1A	Yes	Yes
P14873	Map1b	Microtubule-associated protein 1B	Yes	Yes

г	_			
P16332	Mut	Methylmalonyl-CoA mutase	Yes	Yes
Q9CQR4	Acot13	Acyl-coenzyme A thioesterase 13	Yes	Yes
O35857	Timm44	Mitochondrial import inner membrane translocase subunit TIM44	Yes	Yes
Q9QYX7	Pclo	Protein piccolo	Yes	Yes
Q9JLM8	Dclk1	Serine/threonine-protein kinase DCLK1	Yes	Yes
Q8K2M0	Mrpl38	39S ribosomal protein L38	Yes	Yes
Q8JZN5	Acad9	Complex I assembly factor ACAD9	Yes	Yes
Q99KE1	Me2	NAD-dependent malic enzyme	Yes	Yes
Q8CFA2	Amt	Aminomethyltransferase	Yes	Yes
Q8BIJ6	lars2	IsoleucinetRNA ligase	Yes	Yes
Q8JZQ2	Afg3l2	AFG3-like protein 2	Yes	Yes
Q9JJV2	Pfn2	Profilin-2	Yes	Yes
Q8JZU2	Slc25a1	Tricarboxylate transport protein	Yes	Yes
Q91WD5	Ndufs2	NADH dehydrogenase [ubiquinone] iron- sulfur protein 2	Yes	Yes
Q9R0U0	Srsf10	Serine/arginine-rich splicing factor 10	Yes	Yes
Q7TSQ8	Pdpr	Pyruvate dehydrogenase phosphatase regulatory subunit	Yes	Yes
Q9Z2I8	Suclg2	SuccinateCoA ligase [GDP-forming] subunit beta	Yes	Yes
Q8BKZ9	Pdhx	Pyruvate dehydrogenase protein X component	Yes	Yes
O55042	Snca	Alpha-synuclein	Yes	Yes
Q9CZU6	Cs	Citrate synthase	Yes	Yes
Q91V41	Rab14	Ras-related protein Rab-14	Yes	Yes
Q8BH95	Echs1	Enoyl-CoA hydratase	Yes	Yes
Q8K411	Pitrm1	Presequence protease	Yes	Yes

Q9JJL8	Sars2	SerinetRNA ligase	Yes	Yes
O08788	Dctn1	Dynactin subunit 1	Yes	No
O09012	Pex5	Peroxisomal targeting signal 1 receptor	Yes	No
P10630	Eif4a2	Eukaryotic initiation factor 4A-II	Yes	No
P35235-1	Ptpn11	Isoform 2 of Tyrosine-protein phosphatase non-receptor type 11	Yes	No
P47857	Pfkm	ATP-dependent 6-phosphofructokinase	Yes	No
P49443	Ppm1a	Protein phosphatase 1A	Yes	No
P62245	Rps15a	40S ribosomal protein S15a	Yes	No
P62774	Mtpn	Myotrophin	Yes	No
P83510	Tnik	Traf2 and NCK-interacting protein kinase	Yes	No
P97447	Fhl1	Four and a half LIM domains protein 1	Yes	No
Q0KL02	Trio	Triple functional domain protein	Yes	No
Q3UMY5	Eml4	Echinoderm microtubule-associated protein-like 4	Yes	No
Q61990	Pcbp2	Poly(rC)-binding protein 2	Yes	No
Q6PIU9		Uncharacterized protein FLJ45252 homolog	Yes	No
Q80U49	Cep170b	Centrosomal protein of 170 kDa protein B	Yes	No
Q80X90	Flnb	Filamin-B	Yes	No
Q8BHG2	Czib	CXXC motif containing zinc binding protein	Yes	No
Q8BL97	Srsf7	Serine/arginine-rich splicing factor 7	Yes	No
Q8CIB5	Fermt2	Fermitin family homolog 2	Yes	No
Q8CIN4	Pak2	Serine/threonine-protein kinase PAK 2	Yes	No
Q8R570	Snap47	Synaptosomal-associated protein 47	Yes	No
Q8VBT9	Aspscr1	Tether containing UBX domain for GLUT4	Yes	No

Q99KC8	Vwa5a	von Willebrand factor A domain- containing protein 5A	Yes	No
Q99N95	Mrpl3	39S ribosomal protein L3	Yes	No
Q99N96	Mrpl1	39S ribosomal protein L1	Yes	No
Q9CQI6	Cotl1	Coactosin-like protein	Yes	No
Q9D0E1	Hnrnpm	Heterogeneous nuclear ribonucleoprotein M	Yes	No
Q9DCT8	Crip2	Cysteine-rich protein 2	Yes	No
Q9QXZ0	Macf1	Microtubule-actin cross-linking factor 1	Yes	No
A2AAY5	Sh3pxd2b	SH3 and PX domain-containing protein 2B	Yes	No
O08709	Prdx6	Peroxiredoxin-6	Yes	No
O35098	Dpysl4	Dihydropyrimidinase-related protein 4	Yes	No
O35685	Nudc	Nuclear migration protein nudC	Yes	No
O54734	Ddost	Dolichyl-diphosphooligosaccharide protein glycosyltransferase 48 kDa subunit	Yes	No
O88342	Wdr1	WD repeat-containing protein 1	Yes	No
P00405	mt-Co2	Cytochrome c oxidase subunit 2	Yes	No
P06151	Ldha	L-lactate dehydrogenase A chain	Yes	No
P14094	Atp1b1	Sodium/potassium-transporting ATPase subunit beta-1	Yes	No
P14148	Rpl7	60S ribosomal protein L7	Yes	No
P14824	Anxa6	Annexin A6	Yes	No
P16460	Ass1	Argininosuccinate synthase	Yes	No
P39054	Dnm2	Dynamin-2	Yes	No
P40124	Cap1	Adenylyl cyclase-associated protein 1	Yes	No
P45376	Akr1b3	Aldo-keto reductase family 1 member B1	Yes	No
P46471	Psmc2	26S proteasome regulatory subunit 7	Yes	No
P47941	Crkl	Crk-like protein	Yes	No
P50247	Ahcy	Adenosylhomocysteinase	Yes	No

P50516	Atp6v1a	V-type proton ATPase catalytic subunit A	Yes	No
P56959	Fus	RNA-binding protein FUS	Yes	No
P58404	Strn4	Striatin-4	Yes	No
P61082	Ube2m	NEDD8-conjugating enzyme Ubc12	Yes	No
P62814	Atp6v1b2	V-type proton ATPase subunit B	Yes	No
P63001	Rac1	Ras-related C3 botulinum toxin substrate 1	Yes	No
P63028	Tpt1	Translationally-controlled tumor protein	Yes	No
P63242	Eif5a	Eukaryotic translation initiation factor 5A-1	Yes	No
P67984	Rpl22	60S ribosomal protein L22	Yes	No
P70271	Pdlim4	PDZ and LIM domain protein 4	Yes	No
P70677	Casp3	Caspase-3	Yes	No
P97930	Dtymk	Thymidylate kinase	Yes	No
Q2NL51	Gsk3a	Glycogen synthase kinase-3 alpha	Yes	No
Q3UU96	Cdc42bpa	Serine/threonine-protein kinase MRCK alpha	Yes	No
Q52Kl8	Srrm1	Serine/arginine repetitive matrix protein 1	Yes	No
Q61316	Hspa4	Heat shock 70 kDa protein 4	Yes	No
Q61584	Fxr1	Fragile X mental retardation syndromerelated protein 1	Yes	No
Q68FF0	Kiaa1841	Uncharacterized protein KIAA1841	Yes	No
Q6NZJ6	Eif4g1	Eukaryotic translation initiation factor 4 gamma 1	Yes	No
Q6P1F6	Ppp2r2a	Serine/threonine-protein phosphatase 2A 55 kDa regulatory subunit B alpha isoform	Yes	No
Q8K1M6	Dnm1l	Dynamin-1-like protein	Yes	No
Q8K2K6	Agfg1	Arf-GAP domain and FG repeat- containing protein 1	Yes	No
Q8R1B4	Eif3c	Eukaryotic translation initiation factor 3 subunit C	Yes	No

Q921F2	Tardbp	TAR DNA-binding protein 43	Yes	No
Q9CYZ2	Tpd52l2	Tumor protein D54	Yes	No
Q9CZM2	Rpl15	60S ribosomal protein L15	Yes	No
Q9D0G0	Mrps30	28S ribosomal protein S30	Yes	No
Q9D2R0	Aacs	Acetoacetyl-CoA synthetase	Yes	No
Q9EQI8	Mrpl46	39S ribosomal protein L46	Yes	No
Q9ESX4	Zcchc17	Nucleolar protein of 40 kDa	Yes	No
Q9WTX2	Prkra	Interferon-inducible double-stranded RNA-dependent protein kinase activator A	Yes	No
Q9WV60	Gsk3b	Glycogen synthase kinase-3 beta	Yes	No
Q9WV92	Epb4.1l3	Band 4.1-like protein 3	Yes	No
Q9CX00	lst1	IST1 homolog	Yes	No
Q9EQF6	Dpysl5	Dihydropyrimidinase-related protein 5	Yes	No
P52196	Tst	Thiosulfate sulfurtransferase	Yes	No
Q61166	Mapre1	Microtubule-associated protein RP/EB family member 1	Yes	No
Q8C8R3	Ank2	Ankyrin-2	Yes	No
Q9QXL1	Kif21b	Kinesin-like protein KIF21B	Yes	No
Q61792	Lasp1	LIM and SH3 domain protein 1	Yes	No
Q9CY58	Serbp1	Plasminogen activator inhibitor 1 RNA-binding protein	Yes	No
A2AGT5	Ckap5	Cytoskeleton-associated protein 5	Yes	No
Q8BRT1	Clasp2	CLIP-associating protein 2	Yes	No
Q8BGT8	Phyhipl	Phytanoyl-CoA hydroxylase-interacting protein-like	Yes	No
P97855	G3bp1	Ras GTPase-activating protein-binding protein 1	Yes	No
Q62418	Dbnl	Drebrin-like protein	Yes	No
P52480-2	Pkm-2	Isoform M1 of Pyruvate kinase PKM	Yes	No
-			•	

Q6ZPJ3	Ube2o	(E3-independent) E2 ubiquitin- conjugating enzyme UBE2O	Yes	No
Q8VDJ3	Hdlbp	Vigilin	Yes	No
Q8Cl94	Pygb	Glycogen phosphorylase	Yes	No
Q62448	Eif4g2	Eukaryotic translation initiation factor 4 gamma 2	Yes	No
Q8VE88- 2	Fam114a2	Isoform 2 of Protein FAM114A2	Yes	No
Q9JHI5	lvd	Isovaleryl-CoA dehydrogenase	Yes	No
Q9DAW9	Cnn3	Calponin-3	Yes	No
P07356	Anxa2	Annexin A2	Yes	No
Q62188	Dpysl3	Dihydropyrimidinase-related protein 3	Yes	No
Q9R0Q6	Arpc1a	Actin-related protein 2/3 complex subunit 1A	Yes	No
Q9DBT5	Ampd2	AMP deaminase 2	Yes	No
Q9WUM4	Coro1c	Coronin-1C	Yes	No
P63017	Hspa8	Heat shock cognate 71 kDa protein	Yes	No
Q8BMG7	Rab3gap2	Rab3 GTPase-activating protein non-catalytic subunit	Yes	No
Q60598	Cttn	Src substrate cortactin	Yes	No
Q8CDG3	Vcpip1	Deubiquitinating protein VCIP135	Yes	No
Q8VDQ8	Sirt2	NAD-dependent protein deacetylase sirtuin-2	Yes	No
P68369	Tuba1a	Tubulin alpha-1A chain	Yes	No
Q8CI51	Pdlim5	PDZ and LIM domain protein 5	Yes	No
Q6PGC1	Dhx29	ATP-dependent RNA helicase DHX29	Yes	No
P70296	Pebp1	Phosphatidylethanolamine-binding protein 1	Yes	No
P05064	Aldoa	Fructose-bisphosphate aldolase A	Yes	No
A2AHC3	Camsap1	Calmodulin-regulated spectrin-associated protein 1	Yes	No
Q9D8Y0	Efhd2	EF-hand domain-containing protein D2	Yes	No

B1AZI6	Thoc2	THO complex subunit 2	Yes	No
Q8CH77	Nav1	Neuron navigator 1	Yes	No
Q62417	Sorbs1	Sorbin and SH3 domain-containing protein 1	Yes	No
Q78ZA7	Nap1l4	Nucleosome assembly protein 1-like 4	Yes	No
P17742	Ppia	Peptidyl-prolyl cis-trans isomerase A	Yes	No
P05213	Tuba1b	Tubulin alpha-1B chain	Yes	No
Q8BTM8	Flna	Filamin-A	Yes	No
Q80Y56	Zfyve20	Rabenosyn-5	Yes	No
P68372	Tubb4b	Tubulin beta-4B chain	Yes	No
P62908	Rps3	40S ribosomal protein S3	Yes	No
Q6R891	Ppp1r9b	Neurabin-2	Yes	No
Q61171	Prdx2	Peroxiredoxin-2	Yes	No
P18872	Gnao1	Guanine nucleotide-binding protein G(o) subunit alpha	Yes	No
Q6PB44	Ptpn23	Tyrosine-protein phosphatase non- receptor type 23	Yes	No
P10649	Gstm1	Glutathione S-transferase Mu 1	Yes	No
O55131	7-Sep	Septin-7	Yes	No
G5E829	Atp2b1	Plasma membrane calcium-transporting ATPase 1	Yes	No
Q922W5	Pycr1	Pyrroline-5-carboxylate reductase 1	Yes	No
Q8BGC4	Zadh2	Prostaglandin reductase-3	Yes	No
Q9CWF2	Tubb2b	Tubulin beta-2B chain	Yes	No
Q9CQW2	Arl8b	ADP-ribosylation factor-like protein 8B	Yes	No
P19157	Gstp1	Glutathione S-transferase P 1	Yes	No
Q62167	Ddx3x	ATP-dependent RNA helicase DDX3X	Yes	No
P11031	Sub1	Activated RNA polymerase II transcriptional coactivator p15	Yes	No
P58252	Eef2	Elongation factor 2	Yes	No
Q8C8R3- 2	Ank2-2	Isoform 2 of Ankyrin-2	Yes	No

	1			
Q80X50	Ubap2l	Ubiquitin-associated protein 2-like	Yes	No
Q6PGH2	Hn1l	Jupiter microtubule associated homolog 2	Yes	No
Q8BG05	Hnrnpa3	Heterogeneous nuclear ribonucleoprotein A3	Yes	No
Q91W50	Csde1	Cold shock domain-containing protein E1	Yes	No
P97427	Crmp1	Dihydropyrimidinase-related protein 1	Yes	No
P53994	Rab2a	Ras-related protein Rab-2A	Yes	No
O08553	Dpysl2	Dihydropyrimidinase-related protein 2	Yes	No
O08539	Bin1	Myc box-dependent-interacting protein 1	Yes	No
P18760	Cfl1	Cofilin-1	Yes	No
P60843	Eif4a1	Eukaryotic initiation factor 4A-I	Yes	No
P07901	Hsp90aa1	Heat shock protein HSP 90-alpha	Yes	No
Q6P549	Inppl1	Phosphatidylinositol 3	Yes	No
Q9R0P9	Uchl1	Ubiquitin carboxyl-terminal hydrolase isozyme L1	Yes	No
Q61768	Kif5b	Kinesin-1 heavy chain	Yes	No
E9QAT4	Sec16a	Protein transport protein Sec16A	Yes	No
Q9D8E6	Rpl4	60S ribosomal protein L4	Yes	No
P35700	Prdx1	Peroxiredoxin-1	Yes	No
Q60838	Dvl2	Segment polarity protein dishevelled homolog DVL-2	Yes	No
P23198	Cbx3	Chromobox protein homolog 3	Yes	No
P29341	Pabpc1	Polyadenylate-binding protein 1	Yes	No
Q9WUA2	Farsb	PhenylalaninetRNA ligase beta subunit	Yes	No
P60710	Actb	Actin	Yes	No
P70349	Hint1	Histidine triad nucleotide-binding protein 1	Yes	No
Q7TMM9	Tubb2a	Tubulin beta-2A chain	Yes	No
P51880	Fabp7	Fatty acid-binding protein	Yes	No

Q02053	Uba1	Ubiquitin-like modifier-activating enzyme 1	Yes	No
O70318	Epb4.1l2	Band 4.1-like protein 2	Yes	No
Q7TMK9	Syncrip	Heterogeneous nuclear ribonucleoprotein Q	Yes	No
P11499	Hsp90ab1	Heat shock protein HSP 90-beta	Yes	No
Q6PAJ1	Bcr	Breakpoint cluster region protein	Yes	No
Q8VDD5	Myh9	Myosin-9	Yes	No
Q8CHT0	Aldh4a1	Delta-1-pyrroline-5-carboxylate dehydrogenase	Yes	No
Q9CR57	Rpl14	60S ribosomal protein L14	Yes	No
Q9D8N0	Eef1g	Elongation factor 1-gamma	Yes	No
Q80UG5	9-Sep	Septin-9	Yes	No
Q61753	Phgdh	D-3-phosphoglycerate dehydrogenase	Yes	No
P12367	Prkar2a	cAMP-dependent protein kinase type II- alpha regulatory subunit	Yes	No
P84244	H3f3b	Histone H3.3	Yes	No
P62259	Ywhae	14-3-3 protein epsilon	Yes	No
Q9QZQ1	Mllt4	Afadin	Yes	No
Q8BGD9	Eif4b	Eukaryotic translation initiation factor 4B	Yes	No
P57776	Eef1d	Elongation factor 1-delta	Yes	No
Q7TSC1	Prrc2a	Protein PRRC2A	Yes	No
Q9Z1N5	Ddx39b	Spliceosome RNA helicase Ddx39b	Yes	No
P62827	Ran	GTP-binding nuclear protein Ran	Yes	No
Q99PT1	Arhgdia	Rho GDP-dissociation inhibitor 1	Yes	No
P60335	Pcbp1	Poly(rC)-binding protein 1	Yes	No
Q9Z2Q6	5-Sep	Septin-5	Yes	No
P28652	Camk2b	Calcium/calmodulin-dependent protein kinase type II subunit beta	Yes	No

P54923	Adprh	[Protein ADP-ribosylarginine] hydrolase	Yes	No
P62869	Tceb2	Elongin-B	Yes	No
Q68FD5	Cltc	Clathrin heavy chain 1	Yes	No
P20152	Vim	Vimentin	Yes	No
P27659	Rpl3	60S ribosomal protein L3	Yes	No
P16858	Gapdh	Glyceraldehyde-3-phosphate dehydrogenase	Yes	No
Q61553	Fscn1	Fascin	Yes	No
Q9CXW4	Rpl11	60S ribosomal protein L11	Yes	No
Q8VEH3	Arl8a	ADP-ribosylation factor-like protein 8A	Yes	No
P50136	Bckdha	2-oxoisovalerate dehydrogenase subunit alpha	Yes	No
Q64521	Gpd2	Glycerol-3-phosphate dehydrogenase	No	Yes
Q8BG05- 2	Hnrnpa3-2	Isoform 2 of Heterogeneous nuclear ribonucleoprotein A3	No	Yes
Q8CC88	Vwa8	von Willebrand factor A domain- containing protein 8	No	Yes
Q8QZS1	Hibch	3-hydroxyisobutyryl-CoA hydrolase	No	Yes
Q99N93	Mrpl16	39S ribosomal protein L16	No	Yes
Q9CXI0	Coq5	2-methoxy-6-polyprenyl-1	No	Yes
Q9DCM0	Ethe1	Persulfide dioxygenase ETHE1	No	Yes
Q9JKF7	Mrpl39	39S ribosomal protein L39	No	Yes
P20108	Prdx3	Thioredoxin-dependent peroxide reductase	No	Yes
P47934	Crat	Carnitine O-acetyltransferase	No	Yes
P52825	Cpt2	Carnitine O-palmitoyltransferase 2	No	Yes
Q14C51	Ptcd3	Pentatricopeptide repeat domain- containing protein 3	No	Yes
Q3TBW2	Mrpl10	39S ribosomal protein L10	No	Yes
Q3UQ84	Tars2	ThreoninetRNA ligase	No	Yes
Q501J6	Ddx17	Probable ATP-dependent RNA helicase	No	Yes

Q5SUF2	Luc7l3	Luc7-like protein 3	No	Yes
Q60759	Gcdh	Glutaryl-CoA dehydrogenase	No	Yes
Q61425	Hadh	Hydroxyacyl-coenzyme A dehydrogenase	No	Yes
Q80X85	Mrps7	28S ribosomal protein S7	No	Yes
Q91Z67	Srgap2	SLIT-ROBO Rho GTPase-activating protein 2	No	Yes
Q99N94	Mrpl9	39S ribosomal protein L9	No	Yes
Q9D0Q7	Mrpl45	39S ribosomal protein L45	No	Yes
Q9D6M3	Slc25a22	Mitochondrial glutamate carrier 1	No	Yes
Q9DC69	Ndufa9	NADH dehydrogenase [ubiquinone] 1 alpha subcomplex subunit 9	No	Yes
Q9JLJ2	Aldh9a1	4-trimethylaminobutyraldehyde dehydrogenase	No	Yes
O88935-	Syn1	Isoform Ib of Synapsin-1	No	Yes
P12787	Cox5a	Cytochrome c oxidase subunit 5A	No	Yes
Q9R020	Zranb2	Zinc finger Ran-binding domain- containing protein 2		Yes
P42125	Eci1	Enoyl-CoA delta isomerase 1		Yes
P84104	Srsf3	Serine/arginine-rich splicing factor 3	No	Yes
Q7TNC4	Luc7l2	Putative RNA-binding protein Luc7-like 2	No	Yes
O08749	Dld	Dihydrolipoyl dehydrogenase	No	Yes
Q99JR1	Sfxn1	Sideroflexin-1	No	Yes
Q8VEM8	Slc25a3	Phosphate carrier protein	No	Yes
Q99J99	Mpst	3-mercaptopyruvate sulfurtransferase	No	Yes
Q8BK72	Mrps27	28S ribosomal protein S27	No	Yes
Q8BWT1	Acaa2	3-ketoacyl-CoA thiolase	No	Yes
P14206	Rpsa	40S ribosomal protein SA	No	Yes
P51174	Acadl	Long-chain specific acyl-CoA dehydrogenase	No	Yes

Q9JLZ3	Auh	Methylglutaconyl-CoA hydratase	No	Yes
Q99NB1	Acss1	Acetyl-coenzyme A synthetase 2-like	No	Yes
Q9D7B6	Acad8	Isobutyryl-CoA dehydrogenase	No	Yes
Q8VE22	Mrps23	28S ribosomal protein S23	No	Yes
Q9WTP7	Ak3	GTP:AMP phosphotransferase AK3	No	Yes
Q9JHS4	Clpx	ATP-dependent Clp protease ATP- binding subunit clpX-like	No	Yes
Q9QWI6	Srcin1	SRC kinase signaling inhibitor 1	No	Yes
Q9DBL1	Acadsb	Short/branched chain specific acyl-CoA dehydrogenase	No	Yes
Q99LC3	Ndufa10	NADH dehydrogenase [ubiquinone] 1 alpha subcomplex subunit 10	No	Yes
P29758	Oat	Ornithine aminotransferase	No	Yes
Q8C5H8	Nadk2	NAD kinase 2	No	Yes
Q9EQ20	Aldh6a1	Methylmalonate-semialdehyde dehydrogenase [acylating]	No	Yes
P47738	Aldh2	Aldehyde dehydrogenase	No	Yes
P70404	ldh3g	Isocitrate dehydrogenase [NAD] subunit gamma 1	No	Yes
Q9CZN7	Shmt2	Serine hydroxymethyltransferase	No	Yes
Q9CZS1	Aldh1b1	Aldehyde dehydrogenase X	No	Yes
Q6ZWN5	Rps9	40S ribosomal protein S9 OS	No	Yes
P50171	H2-Ke6	Estradiol 17-beta-dehydrogenase 8	No	Yes
P99029	Prdx5	Peroxiredoxin-5	No	Yes
Q925I1	Atad3a	ATPase family AAA domain-containing protein 3	No	Yes
Q9CQ62	Decr1	2,4-dienoyl-CoA reductase	No	Yes
Q9CQN1	Trap1	Heat shock protein 75 kDa	No	Yes
Q5M8N0	Cnrip1	CB1 cannabinoid receptor-interacting protein 1	No	Yes

Q5FWK3	Arhgap1	Rho GTPase-activating protein 1	No	Yes
Q04750	Top1	DNA topoisomerase 1	No	Yes
Q9D6R2	ldh3a	Isocitrate dehydrogenase [NAD] subunit alpha	No	Yes
Q6PB66	Lrpprc	Leucine-rich PPR motif-containing protein	No	Yes
Q8VH51- 2	Rbm39	Isoform 2 of RNA-binding protein 39	No	Yes
Q91VD9	Ndufs1	NADH-ubiquinone oxidoreductase 75 kDa subunit	No	Yes
Q6P3A8	Bckdhb	2-oxoisovalerate dehydrogenase subunit beta	No	Yes
P61922	Abat	4-aminobutyrate aminotransferase	No	Yes
Q9Z110	Aldh18a1	Delta-1-pyrroline-5-carboxylate synthase	No	Yes
O88696	Clpp	ATP-dependent Clp protease proteolytic subunit	No	Yes
P47963	Rpl13	60S ribosomal protein L13	No	Yes
Q9CQA3	Sdhb	Succinate dehydrogenase [ubiquinone] iron-sulfur subunit		Yes
P35486	Pdha1	Pyruvate dehydrogenase E1 component subunit alpha		Yes
Q99JY0	Hadhb	Trifunctional enzyme subunit beta		Yes
Q9Z2Z6	Slc25a20	Mitochondrial carnitine/acylcarnitine carrier protein		Yes
Q8R164	Bphl	Valacyclovir hydrolase	No	Yes
Q8BMF4	Dlat	Dihydrolipoyllysine-residue acetyltransferase component of pyruvate dehydrogenase complex		Yes
Q8CGK3	Lonp1	Lon protease homolog		Yes
Q8BIW1	Prune	Exopolyphosphatase PRUNE1		Yes
P54071	ldh2	Isocitrate dehydrogenase [NADP]	No	Yes
Q9DCW4	Etfb	Electron transfer flavoprotein subunit beta	No	Yes

P97807	Fh1	Fumarate hydratase	No	Yes
Q8BMS1	Hadha	Trifunctional enzyme subunit alpha	No	Yes
O55125	Nipsnap1	Protein NipSnap homolog 1	No	Yes
Q99KI0	Aco2	Aconitate hydratase	No	Yes
Q3UNH4	Gprin1	G protein-regulated inducer of neurite outgrowth 1	No	Yes
P08249	Mdh2	Malate dehydrogenase	No	Yes
Q9WUR2	Eci2	Enoyl-CoA delta isomerase 2	No	Yes
Q9Z1J3	Nfs1	Cysteine desulfurase	No	Yes
P45952	Acadm	Medium-chain specific acyl-CoA dehydrogenase	No	Yes
Q8QZT1	Acat1	Acetyl-CoA acetyltransferase	No	Yes
P56480	Atp5b	ATP synthase subunit beta	No	Yes
P01942	Hba-a2	Hemoglobin subunit alpha	No	Yes
Q8VDC0	Lars2	Probable leucinetRNA ligase	No	Yes
Q9DB20	Atp5o	ATP synthase subunit O	No	Yes
P26443	Glud1	Glutamate dehydrogenase 1	No	Yes
Q80XN0	Bdh1	D-beta-hydroxybutyrate dehydrogenase	No	Yes
Q99LC5	Etfa	Electron transfer flavoprotein subunit alpha	No	Yes
P50544	Acadvl	Very long-chain specific acyl-CoA dehydrogenase	No	Yes
Q91VA6	Poldip2	Polymerase delta-interacting protein 2	No	Yes
P51150	Rab7	Ras-related protein Rab-7a	No	Yes

APPENDIX B

Table 4: List of tau interacting partners identified in ClueGo cellular components

CO torm	Number of	0/ Accopiated	Accopiated games found
GO term	Number of	% Associated	Associated genes found
	genes	genes	
mitochondrion	164	8.627038002	Abat, Acaa2, Acad8, Acad9, Acadl, Acadm, Acads, Acadsb, Acadvl, Acat1, Aco2, Acot13, Acss1, Afg3l2, Ak3, Ak4, Aldh18a1, Aldh1b1, Aldh2, Aldh4a1, Aldh6a1, Aldh9a1, Aldoa, Amt, Ank2, Anxa6, Ass1, Atad3a, Atp5b, Atp5h, Atp5o, Atp6v1a, Auh, Bckdha, Bckdhb, Bdh1, Bphl, COX2, Cfl1, Clpp, Clpx, Cltc, Coq5, Cox4i1, Cox5a, Cpt2, Crat, Cs, Csde1, Dap3, Decr1, Dhrs4, Dhx29, Dlat, Dld, Dnm1l, Dnm2, Dpysl2, Dtymk, Echs1, Eci1, Eci2, Etfa, Etfb, Ethe1, Fdxr, Fh1, Gapdh, Gcdh, Gfm1, Glrx5, Glud1, Gpd2, Gsk3a, Gsk3b, Gstp1, H2-Ke6, Hadh, Hadha, Hadhb, Hibch, Hsp90aa1, Hsp90ab1, Hspa4, lars2, Idh2, Idh3a, Idh3g, Isoc2a, Ivd, Lap3, Lars2, Ldha, Lonp1, Lrpprc, Mdh2, Me2, Mmut, Mpst, Mrpl1, Mrpl10, Mrpl16, Mrpl19, Mrpl3, Mrpl37, Mrpl38, Mrpl39, Mrpl45, Mrpl46, Mrpl9, Mrps23, Mrps27, Mrps30, Mrps35, Mrps7, Nadk2, Ndufa10, Ndufa9, Ndufs1, Ndufs2, Ndufv1, Nfs1, Nipsnap1, Oat, Pck2, Pdha1, Pdhx, Pdpr, Pebp1, Pex5, Phyhipl, Pitrm1, Poldip2, Prdx1, Prdx2, Prdx3, Prdx5, Prdx6, Ptcd3, Pycr1, Rps15a, Rps3, Sars2, Sdhb, Sfxn1, Shmt2, Sirt2, Slc25a1, Slc25a20, Slc25a22, Slc25a3, Snca, Sncb, Srgap2, Suclg2, Tars2, Tbrg4, Timm44, Trap1, Tst, Uba1, Vwa8, Ywhae, Zadh2

mitochondrial matrix	83	23.78223419	Abat, Acaa2, Acadl, Acadm, Acads, Acadsb, Acadvl, Acat1, Acss1, Ak3, Ak4, Aldh1b1, Aldh2, Aldh4a1, Atad3a, Atp5b, Bckdha, Bckdhb, Bdh1, Clpp, Clpx, Coq5, Cs, Dap3, Dlat, Dld, Dtymk, Echs1, Eci1, Etfa, Etfb, Ethe1, Gcdh, Glrx5, Glud1, H2-Ke6, Hadh, Hadha, Hadhb, Iars2, Ivd, Lars2, Lonp1, Lrpprc, Mdh2, Me2, Mmut, Mrpl1, Mrpl10, Mrpl16, Mrpl19, Mrpl3, Mrpl37, Mrpl38, Mrpl39, Mrpl45, Mrpl46, Mrpl9, Mrps23, Mrps27, Mrps30, Mrps35, Mrps7, Ndufa10, Ndufa9, Nfs1, Oat, Pdha1, Pdhx, Pdpr, Pitrm1, Poldip2, Prdx1, Rps3, Sars2, Shmt2, Snca, Suclg2, Tars2, Tbrg4, Timm44, Trap1, Tst
mitochondrial membrane	59	8.452721596	Acaa2, Acad9, Acadl, Acadm, Acads, Acadvl, Acat1, Afg3l2, Aldh18a1, Ass1, Atad3a, Atp5b, Atp5h, Atp5o, Bckdhb, Bdh1, COX2, Cfl1, Clpx, Coq5, Cox4i1, Cox5a, Cpt2, Crat, Csde1, Dnm1l, Dnm2, Eci1, Fdxr, Gcdh, Glud1, Gpd2, Hadh, Hadha, Hadhb, Idh2, Ivd, Mdh2, Mpst, Ndufa10, Ndufa9, Ndufs1, Ndufs2, Ndufv1, Nipsnap1, Pebp1, Rps3, Sdhb, Sfxn1, Shmt2, Slc25a1, Slc25a20, Slc25a22, Slc25a3, Snca, Srgap2, Timm44, Trap1, Tst
mitochondrial envelope	63	8.333333015	Acaa2, Acad9, Acadl, Acadm, Acads, Acadvl, Acat1, Afg3l2, Ak3, Ak4, Aldh18a1, Ass1, Atad3a, Atp5b, Atp5h, Atp5o, Bckdhb, Bdh1, COX2, Cfl1, Clpx, Coq5, Cox4i1, Cox5a, Cpt2, Crat, Csde1, Dnm1l, Dnm2, Dtymk, Eci1, Fdxr, Gcdh, Glud1, Gpd2, H2-Ke6, Hadh, Hadha, Hadhb, Idh2, Ivd, Mdh2, Mpst, Ndufa10, Ndufa9, Ndufs1, Ndufs2, Ndufv1, Nipsnap1, Pebp1, Rps3, Sdhb, Sfxn1, Shmt2, Slc25a1, Slc25a20, Slc25a22, Slc25a3, Snca, Srgap2, Timm44, Trap1, Tst

mitochondrial protein- containing complex	38	14.61538506	Afg3l2, Atp5b, Atp5h, Atp5o, Bckdha, Bckdhb, Clpx, Cox4i1, Cox5a, Dap3, Dlat, Etfa, Etfb, Hadha, Hadhb, Mrpl1, Mrpl10, Mrpl16, Mrpl19, Mrpl3, Mrpl37, Mrpl38, Mrpl39, Mrpl45, Mrpl46, Mrpl9, Mrps23, Mrps27, Mrps30, Mrps35, Mrps7, Ndufa10, Ndufa9, Ndufs1, Ndufs2, Ndufv1, Sdhb, Suclg2
cytoskeleton	96	4.125904083	Acot13, Actb, Aldoa, Ank2, Arhgef2, Arl8a, Arl8b, Arpc1a, Bin1, Camk2b, Camsap1, Camsap3, Cap1, Cbx3, Cdc42bpa, Cep170, Cep170b, Cfl1, Ckap5, Clasp2, Cltc, Cnn3, Coro1c, Cotl1, Crmp1, Cttn, Dbnl, Dctn1, Dcx, Ddx3x, Dnm1l, Dnm2, Dpysl2, Dpysl3, Dvl2, Eml4, Epb41l2, Epb41l3, Fermt2, Flna, Flnb, Fscn1, Gapdh, Gsk3a, Gsk3b, Hspa8, Inppl1, Ist1, Kif21b, Kif5b, Lasp1, Lrpprc, Macf1, Map1b, Map2, Map4, Map6, Mapre1, Mtpn, Myh9, Nav1, Nudc, Pclo, Pdlim4, Pdlim5, Pfn2, Ppp1r9b, Prkar2a, Prkar2b, Ptpn23, Rac1, Ran, Rps3, Septin5, Septin7, Septin9, Sh3pxd2b, Shmt2, Sirt2, Snca, Sorbs1, Srcin1, Stmn1, Tbcb, Tnik, Tpt1, Tuba1a, Tuba1b, Tubb2a, Tubb2b, Tubb3, Tubb4b, Tubb5, Vim, Wdr1, Ywhae
neuron projection	84	4.929577351	Aak1, Abat, Acad9, Acadm, Actb, Afdn, Ahcy, Ank2, Arhgef2, Arl8a, Arl8b, Ass1, Atp2b1, Bcr, Bin1, Camk2b, Cfl1, Clasp2, Cnn3, Crip2, Crmp1, Cttn, Dbnl, Dctn1, Dcx, Dnm2, Dpysl2, Dpysl3, Dpysl5, Eif4b, Eif4g2, Eif5a, Epb41l3, Flna, Flnb, Fscn1, Fus, Fxr1, Glrx5, Gnao1, Gprin1, Gsk3a, Gsk3b, Hcfc1, Hnrnpa3, Hsp90aa1, Hsp90ab1, Hspa8, Kif21b, Kif5b, Map1b, Map2, Map4, Map6, Mpst, Mtpn, Nap1l4, Nav1, Nsf, Pabpc1, Pclo, Pdlim4, Pebp1, Ppm1a, Ppp1r9b, Prkar2b, Psmc2, Pygb, Rac1, Rps3, Septin5, Septin7, Sirt2, Snap47, Snca, Sncb, Srcin1, Srgap2, Stmn1, Strn4, Tubb3, Uchl1, Vim, Ywhae

microtubule cytoskeleton	62	4.751299381	Arhgef2, Arl8a, Arl8b, Bin1, Camk2b, Camsap1, Camsap3, Cbx3, Cep170, Cep170b, Ckap5, Clasp2, Cltc, Crmp1, Cttn, Dctn1, Dcx, Ddx3x, Dnm1l, Dnm2, Dpysl2, Eml4, Gapdh, Gsk3a, Gsk3b, Hspa8, Ist1, Kif21b, Kif5b, Lrpprc, Macf1, Map1b, Map2, Map4, Map6, Mapre1, Myh9, Nav1, Nudc, Prkar2a, Prkar2b, Ptpn23, Rac1, Ran, Rps3, Septin5, Septin7, Septin9, Shmt2, Sirt2, Sorbs1, Stmn1, Tbcb, Tpt1, Tuba1a, Tuba1b, Tubb2a, Tubb2b, Tubb3, Tubb4b, Tubb5, Ywhae
microtubule	41	9.213482857	Arhgef2, Bin1, Camsap1, Camsap3, Cep170, Cep170b, Ckap5, Clasp2, Cltc, Dctn1, Dcx, Dnm1l, Dnm2, Dpysl2, Eml4, Gsk3a, Gsk3b, Hspa8, Kif21b, Kif5b, Lrpprc, Macf1, Map1b, Map2, Map4, Map6, Mapre1, Nav1, Nudc, Septin9, Sirt2, Stmn1, Tbcb, Tpt1, Tuba1a, Tuba1b, Tubb2a, Tubb2b, Tubb3, Tubb4b, Tubb5
organelle inner membrane	47	9.845560074	Acaa2, Aldh18a1, Atad3a, Atp5b, Atp5h, Atp5o, Bckdhb, Bdh1, COX2, Clpx, Coq5, Cox4i1, Cox5a, Cpt2, Crat, Csde1, Eci1, Fdxr, Gcdh, Glud1, Gpd2, Hadh, Hadha, Hadhb, Idh2, Lrpprc, Mdh2, Mpst, Ndufa10, Ndufa9, Ndufs1, Ndufs2, Ndufv1, Nipsnap1, Rps3, Sdhb, Sfxn1, Shmt2, Slc25a1, Slc25a20, Slc25a22, Slc25a3, Snca, Srgap2, Timm44, Trap1, Tst
supramolecular fiber	61	5.888031006	Actb, Aldoa, Ank2, Arhgef2, Bin1, Camsap1, Camsap3, Cep170, Cep170b, Ckap5, Clasp2, Cltc, Cotl1, Cttn, Dbnl, Dctn1, Dcx, Dnm1l, Dnm2, Dpysl2, Dpysl3, Eml4, Fermt2, Flna, Flnb, Fxr1, Gsk3a, Gsk3b, Hspa8, Kif21b, Kif5b, Lrpprc, Macf1, Map1b, Map2, Map4, Map6, Mapre1, Myh9, Nav1, Nudc, Pdlim4, Pdlim5, Rac1, Rpl15, Rpl4, Rpl7, Septin9, Sirt2, Snca, Stmn1, Tbcb, Tpt1, Tuba1a, Tuba1b, Tubb2a, Tubb2b, Tubb3, Tubb4b, Tubb5, Vim

axon	52	6.110458374	Aak1, Acadm, Actb, Afdn, Arl8a, Arl8b, Bcr, Bin1, Cfl1, Clasp2, Crip2, Crmp1, Cttn, Dctn1, Dcx, Dnm2, Dpysl2, Dpysl3, Eif4g2, Epb41l3, Flna, Fscn1, Fxr1, Gprin1, Gsk3a, Gsk3b, Hcfc1, Hsp90aa1, Hsp90ab1, Hspa8, Kif21b, Kif5b, Map1b, Map2, Map4, Map6, Mtpn, Nav1, Pclo, Pebp1, Ppp1r9b, Pygb, Septin5, Septin7, Sirt2, Snca, Sncb, Srcin1, Tubb3, Uchl1, Vim, Ywhae
postsynapse	50	6.180469513	Actb, Ank2, Arhgef2, Atp2b1, Bcr, Camk2b, Cfl1, Ckap5, Cnn3, Crkl, Cttn, Dbnl, Dclk1, Dnm2, Eif4b, Eif4g1, Eif4g2, Epb41l3, Flna, Fus, Fxr1, Gapdh, Gsk3b, Hnrnpa3, Hspa8, Macf1, Map1b, Map2, Map4, Nsf, Pak2, Pcbp2, Pclo, Pdlim4, Pdlim5, Pfn2, Ppp1r9b, Prkar2b, Psmc2, Rac1, Rpl14, Rpl4, Rpl7, Rps3, Snap47, Snca, Srcin1, Srgap2, Strn4, Tnik
dendrite	48	5.73476696	Acad9, Arhgef2, Atp2b1, Bcr, Bin1, Camk2b, Cfl1, Cnn3, Crmp1, Cttn, Dbnl, Dcx, Dnm2, Dpysl2, Dpysl5, Eif4b, Eif5a, Flna, Fscn1, Fus, Fxr1, Glrx5, Gnao1, Gsk3b, Hcfc1, Hsp90aa1, Hsp90ab1, Hspa8, Kif21b, Kif5b, Map1b, Map2, Map6, Nap1l4, Nsf, Pabpc1, Pclo, Pdlim4, Ppp1r9b, Prkar2b, Psmc2, Rac1, Rps3, Snap47, Srcin1, Srgap2, Strn4, Tubb3
distal axon	34	7.852193832	Aak1, Actb, Bin1, Cfl1, Clasp2, Crip2, Crmp1, Cttn, Dcx, Dnm2, Dpysl2, Dpysl3, Flna, Fscn1, Fxr1, Gprin1, Gsk3b, Hsp90aa1, Hsp90ab1, Hspa8, Kif21b, Kif5b, Map1b, Map2, Pclo, Pebp1, Ppp1r9b, Septin5, Septin7, Sirt2, Snca, Sncb, Tubb3, Ywhae
postsynaptic density	34	7.744874477	Actb, Ank2, Arhgef2, Bcr, Camk2b, Cnn3, Dbnl, Dclk1, Dnm2, Eif4g2, Epb41l3, Fxr1, Gapdh, Gsk3b, Hnrnpa3, Hspa8, Macf1, Map1b, Map2, Map4, Nsf, Pak2, Pcbp2, Pclo, Pdlim5, Ppp1r9b, Rpl14, Rpl4, Rpl7, Rps3, Snap47, Srcin1, Srgap2, Tnik

polymeric cytoskeletal fiber	51	6.488549709	Actb, Arhgef2, Bin1, Camsap1, Camsap3, Cep170, Cep170b, Ckap5, Clasp2, Cltc, Cotl1, Cttn, Dbnl, Dctn1, Dcx, Dnm1l, Dnm2, Dpysl2, Dpysl3, Eml4, Flna, Gsk3a, Gsk3b, Hspa8, Kif21b, Kif5b, Lrpprc, Macf1, Map1b, Map2, Map4, Map6, Mapre1, Nav1, Nudc, Pdlim4, Pdlim5, Rac1, Septin9, Sirt2, Stmn1, Tbcb, Tpt1, Tuba1a, Tuba1b, Tubb2a, Tubb2b, Tubb3, Tubb4b, Tubb5, Vim
actin cytoskeleton	36	6.923077106	Actb, Aldoa, Arhgef2, Arpc1a, Cap1, Cdc42bpa, Cfl1, Cnn3, Coro1c, Cotl1, Crmp1, Cttn, Dbnl, Dpysl3, Epb41l2, Fermt2, Flna, Flnb, Fscn1, Lasp1, Macf1, Map2, Mtpn, Myh9, Pdlim4, Pdlim5, Ppp1r9b, Rac1, Septin5, Septin7, Septin9, Sh3pxd2b, Snca, Sorbs1, Srcin1, Wdr1
ribosome	36	14.87603283	Dap3, Ddx3x, Dhx29, Eef2, Hba-a1, Mrpl1, Mrpl10, Mrpl16, Mrpl19, Mrpl3, Mrpl37, Mrpl38, Mrpl39, Mrpl45, Mrpl46, Mrpl9, Mrps23, Mrps27, Mrps30, Mrps35, Mrps7, Ptcd3, Rpl11, Rpl13, Rpl14, Rpl15, Rpl22, Rpl3, Rpl4, Rpl7, Rps15a, Rps3, Rps9, Rpsa, Snca, Zcchc17
ribosomal subunit	33	15.86538506	Dap3, Ddx3x, Dhx29, Hba-a1, Mrpl1, Mrpl10, Mrpl16, Mrpl19, Mrpl3, Mrpl37, Mrpl38, Mrpl39, Mrpl45, Mrpl46, Mrpl9, Mrps23, Mrps27, Mrps30, Mrps35, Mrps7, Rpl11, Rpl13, Rpl14, Rpl15, Rpl22, Rpl3, Rpl4, Rpl7, Rps15a, Rps3, Rps9, Rpsa, Zcchc17
large ribosomal subunit	21	15.67164135	Mrpl1, Mrpl10, Mrpl16, Mrpl19, Mrpl3, Mrpl37, Mrpl38, Mrpl39, Mrpl45, Mrpl46, Mrpl9, Mrps30, Rpl11, Rpl13, Rpl14, Rpl15, Rpl22, Rpl3, Rpl4, Rpl7, Zcchc17
cytosolic ribosome	17	13.7096777	Ddx3x, Dhx29, Hba-a1, Mrpl1, Rpl11, Rpl13, Rpl14, Rpl15, Rpl22, Rpl3, Rpl4, Rpl7, Rps15a, Rps3, Rps9, Rpsa, Zcchc17

mitochondrial ribosome	17	18.88888931	Dap3, Mrpl1, Mrpl10, Mrpl16, Mrpl19, Mrpl3, Mrpl37, Mrpl38, Mrpl39, Mrpl45, Mrpl46, Mrpl9, Mrps23, Mrps27, Mrps30, Mrps35, Mrps7
cell cortex	30	8.40336132	Actb, Anxa2, Cap1, Cfl1, Clasp2, Coro1c, Cotl1, Crip2, Ctbp1, Cttn, Dbnl, Dctn1, Dvl2, Epb41l2, Fermt2, Flna, Flnb, Fscn1, Lasp1, Macf1, Mapre1, Myh9, Pclo, Ppp1r9b, Rac1, Septin5, Septin7, Septin9, Snca, Wdr1
growth cone	27	10.93117428	Cfl1, Clasp2, Crip2, Crmp1, Cttn, Dcx, Dnm2, Dpysl2, Dpysl3, Flna, Fscn1, Fxr1, Gprin1, Gsk3b, Hsp90aa1, Hsp90ab1, Kif21b, Kif5b, Map1b, Map2, Pclo, Ppp1r9b, Sirt2, Snca, Sncb, Tubb3, Ywhae
presynapse	27	4.02985096	Aak1, Actb, Atp2b1, Bin1, Btbd8, Cltc, Ctbp1, Dnm1l, Dnm2, Dpysl2, Fxr1, Hspa8, Pclo, Pdlim5, Pebp1, Pfn2, Rab14, Rab2a, Rab7, Rpl22, Septin5, Septin7, Snap47, Snca, Sncb, Srcin1, Tnik
dendritic spine	18	7.594936848	Atp2b1, Bcr, Cfl1, Cnn3, Cttn, Dnm2, Fus, Fxr1, Gsk3b, Hspa8, Map1b, Pdlim4, Ppp1r9b, Prkar2b, Psmc2, Rac1, Srgap2, Strn4
ribonucleoprotein granule	15	5.836575985	Actb, Csde1, Ddx3x, Eif4g1, Fxr1, G3bp1, Hnrnpa3, Pabpc1, Pcbp1, Psmc2, Rac1, Tardbp, Top1, Tuba1a, Tubb5
cortical cytoskeleton	14	11.19999981	Actb, Cap1, Cfl1, Clasp2, Cotl1, Cttn, Dbnl, Flna, Lasp1, Mapre1, Myh9, Pclo, Ppp1r9b, Wdr1
actin filament bundle	13	13.26530647	Actb, Cfl1, Fermt2, Flna, Flnb, Fscn1, Myh9, Pdlim4, Pdlim5, Septin5, Septin7, Septin9, Sorbs1
melanosome	13	12.0370369	Ahcy, Anxa2, Anxa6, Atp6v1b2, Cltc, Hsp90aa1, Hsp90ab1, Hspa8, Rab2a, Rab7, Rac1, Ran, Ywhae
actomyosin	12	12.12121201	Actb, Cdc42bpa, Fermt2, Flnb, Fscn1, Myh9, Pdlim4, Pdlim5, Septin5, Septin7, Septin9, Sorbs1

inner mitochondrial membrane protein complex	12	9.677419662	Afg3l2, Atp5b, Atp5h, Atp5o, Cox4i1, Cox5a, Ndufa10, Ndufa9, Ndufs1, Ndufs2, Ndufv1, Sdhb
mitochondrial large ribosomal subunit	12	20.6896553	Mrpl1, Mrpl10, Mrpl16, Mrpl19, Mrpl3, Mrpl37, Mrpl38, Mrpl39, Mrpl45, Mrpl46, Mrpl9, Mrps30
neuron projection terminus	12	5.381165981	Aak1, Actb, Bin1, Dpysl2, Hspa8, Pclo, Pebp1, Septin5, Septin7, Snca, Sncb, Uchl1
peroxisome	12	7.547169685	Crat, Dhrs4, Dnm1l, Eci2, Idh2, Pex5, Prdx1, Prdx5, Prdx6, Vim, Vwa8, Zadh2
small ribosomal subunit	12	14.28571415	Dap3, Ddx3x, Dhx29, Hba-a1, Mrps23, Mrps27, Mrps35, Mrps7, Rps15a, Rps3, Rps9, Rpsa
cytosolic large ribosomal subunit	10	13.33333302	Mrpl1, Rpl11, Rpl13, Rpl14, Rpl15, Rpl22, Rpl3, Rpl4, Rpl7, Zcchc17
mitochondrial nucleoid	10	20.83333397	Acadvl, Atad3a, Atp5b, Clpx, Hadha, Hadhb, Lonp1, Lrpprc, Poldip2, Shmt2
actin filament	9	6.617647171	Actb, Cotl1, Cttn, Dbnl, Dpysl3, Flna, Pdlim4, Pdlim5, Rac1
cortical actin cytoskeleton	9	10.11236	Cap1, Cfl1, Cotl1, Cttn, Dbnl, Lasp1, Myh9, Ppp1r9b, Wdr1
respiratory chain complex	9	12.16216183	COX2, Cox4i1, Cox5a, Ndufa10, Ndufa9, Ndufs1, Ndufs2, Ndufv1, Sdhb
synaptic vesicle membrane	9	6.766917229	Atp2b1, Bin1, Cltc, Dnm1l, Rab14, Rab2a, Rab7, Snap47, Snca
mitochondrial respirasome	8	11.4285717	Cox4i1, Cox5a, Ndufa10, Ndufa9, Ndufs1, Ndufs2, Ndufv1, Sdhb
cytosolic small ribosomal subunit	7	14	Ddx3x, Dhx29, Hba-a1, Rps15a, Rps3, Rps9, Rpsa
dendritic shaft	7	10.14492798	Arhgef2, Flna, Gsk3b, Hspa8, Map2, Nsf, Prkar2b

microtubule end	6	17.1428566	Camsap1, Camsap3, Ckap5, Clasp2, Dctn1, Mapre1
mitochondrial small ribosomal subunit	5	16.66666603	Dap3, Mrps23, Mrps27, Mrps35, Mrps7
peroxisomal matrix	5	17.8571434	Eci2, Pex5, Prdx1, Prdx5, Prdx6
postsynaptic density, intracellular component	5	15.15151501	Arhgef2, Bcr, Dnm2, Gapdh, Tnik

APPENDIX C

Table 5: List of tau interacting partners identified in ClueGo molecular function pathways

GO term	Number	% Associated	Associated genes found
	of genes	genes	
nucleotide binding	124	5.218446732	Acadm, Acads, Acadsb, Acadvl, Acat1, Acss1, Actb, Afg3l2, Ahcy, Ak3, Ak4, Aldh18a1, Aldh2, Aldh4a1, Aldh9a1, Anxa6, Arhgdia, Arhgef2, Arl8a, Arl8b, Ass1, Atad3a, Atp2b1, Atp5b, Atp6v1a, Atp6v1b2, Bcr, Camk2b, Cdc42bpa, Clpx, Ctbp1, Dclk1, Ddx17, Ddx39b, Ddx3x, Decr1, Dhx29, Dld, Dnm1l, Dnm2, Dtymk, Eci2, Eef1d, Eef2, Eif4a1, Eif4a2, Eif4b, Eif4g1, Etfa, Etfb, Farsb, Fdxr, G3bp1, Gapdh, Gcdh, Gfm1, Glud1, Gnao1, Gsk3a, Gsk3b, H2-Ke6, Hadh, Hadha, Hint1, Hsp90aa1, Hsp90ab1, Hspa4, Hspa8, Iars2, Idh2, Idh3a, Idh3g, Ivd, Kif21b, Kif5b, Lars2, Ldha, Lonp1, Me2, Mrpl39, Myh9, Nadk2, Ndufs2, Ndufv1, Nsf, Pak2, Pck2, Pebp1, Pfkm, Phgdh, Prkar2a, Prkar2b, Psmc2, Rab14, Rab18, Rab2a, Rab3gap2, Rab7, Rac1, Ran, Sars2, Septin5, Septin7, Septin9, Sirt2, Stmn1, Suclg2, Tars2, Timm44, Tnik, Top1, Trap1, Trio, Tuba1a, Tuba1b, Tubb2a, Tubb2b, Tubb3, Tubb4b, Tubb5, Uba1, Ube2m, Ube2o, Vwa8
RNA binding	71	6.027164459	Auh, Cltc, Csde1, Ddx17, Ddx39b, Ddx3x, Dhx29, Eef1d, Eef1g, Eef2, Eif3c, Eif4a1, Eif4a2, Eif4b, Eif4g1, Eif4g2, Eif5a, Farsb, Fus, Fxr1, G3bp1, Gfm1, Hdlbp, Hnrnpa3, Hnrnpm, Hsp90aa1, Hsp90ab1, Hspa8, Iars2, Lonp1, Lrpprc, Luc7l2, Luc7l3, Mrpl1, Mrpl16, Mrps27, Mrps7, Nfs1, Pabpc1, Pcbp1, Pcbp2, Prkra, Ptcd3, Ran, Rpl11, Rpl13, Rpl14, Rpl15, Rpl22, Rpl3, Rpl4, Rpl7, Rps3, Rps9, Sars2, Serbp1, Shmt2, Srrm1, Srsf10, Srsf3, Srsf7, Syncrip, Tardbp, Thoc2, Trap1, Tst, Tuba1b, Tubb4b, Vim, Zcchc17, Zranb2

Table 5 (cont'd)

purine nucleotide binding	104	4.693140984	Aacs, Aak1, Acad9, Acadl, Acadm, Acads, Acadvl, Acat1, Acss1, Actb, Afg3l2, Ahcy, Ak3, Ak4, Aldh18a1, Anxa6, Arhgdia, Arhgef2, Arl8a, Arl8b, Ass1, Atad3a, Atp2b1, Atp5b, Atp6v1a, Atp6v1b2, Bcr, Camk2b, Cdc42bpa, Clpx, Dclk1, Ddx17, Ddx39b, Ddx3x, Dhx29, Dnm1l, Dnm2, Dtymk, Eci2, Eef1d, Eef2, Eif4a1, Eif4a2, Eif4b, Eif4g1, Farsb, G3bp1, Gcdh, Gfm1, Glud1, Gnao1, Gsk3a, Gsk3b, Hadha, Hsp90aa1, Hsp90ab1, Hspa4, Hspa8, lars2, Idh3g, Kif21b, Kif5b, Lars2, Lonp1, Myh9, Nadk2, Nsf, Pak2, Pck2, Pebp1, Pfkm, Prkar2a, Prkar2b, Psmc2, Rab14, Rab18, Rab2a, Rab3gap2, Rab7, Rac1, Ran, Sars2, Septin5, Septin7, Septin9, Stmn1, Suclg2, Tars2, Timm44, Tnik, Top1, Trap1, Trio, Tuba1a, Tuba1b, Tubb2a, Tubb2b, Tubb3, Tubb4b, Tubb5, Uba1, Ube2m, Ube2o, Vwa8
ribonucleotide binding	104	4.684684753	Aacs, Aak1, Acad9, Acadl, Acadm, Acads, Acadvl, Acat1, Acss1, Actb, Afg3l2, Ak3, Ak4, Aldh18a1, Anxa6, Arhgdia, Arhgef2, Arl8a, Arl8b, Ass1, Atad3a, Atp2b1, Atp5b, Atp6v1a, Atp6v1b2, Bcr, Camk2b, Cdc42bpa, Clpx, Dclk1, Ddx17, Ddx39b, Ddx3x, Dhx29, Dnm1l, Dnm2, Dtymk, Eci2, Eef1d, Eef2, Eif4a1, Eif4a2, Eif4b, Eif4g1, Farsb, G3bp1, Gcdh, Gfm1, Glud1, Gnao1, Gsk3a, Gsk3b, Hadha, Hsp90aa1, Hsp90ab1, Hspa4, Hspa8, Iars2, Idh3g, Kif21b, Kif5b, Lars2, Lonp1, Myh9, Nadk2, Ndufv1, Nsf, Pak2, Pck2, Pebp1, Pfkm, Prkar2a, Prkar2b, Psmc2, Rab14, Rab18, Rab2a, Rab3gap2, Rab7, Rac1, Ran, Sars2, Septin5, Septin7, Septin9, Stmn1, Suclg2, Tars2, Timm44, Tnik, Top1, Trap1, Trio, Tuba1a, Tuba1b, Tubb2a, Tubb2b, Tubb3, Tubb4b, Tubb5, Uba1, Ube2m, Ube2o, Vwa8

Table 5 (cont'd)

cytoskeletal protein binding	69	6.66023159	Actb, Afdn, Aldoa, Ank2, Anxa2, Anxa6, Arhgef2, Arl8b, Arpc1a, Bin1, Camsap1, Camsap3, Cap1, Cfl1, Ckap5, Clasp2, Cltc, Cnn3, Coro1c, Cotl1, Crmp1, Cttn, Dbnl, Dctn1, Dcx, Ddx3x, Dnm1l, Dnm2, Dpysl2, Dpysl3, Dpysl4, Dpysl5, Eef2, Eml4, Epb41l2, Epb41l3, Fermt2, Flna, Flnb, Fscn1, Fus, Gapdh, Gsk3b, Hsp90aa1, Hsp90ab1, Inppl1, Kif21b, Kif5b, Lasp1, Lrpprc, Macf1, Map1b, Map2, Map4, Map6, Mapre1, Myh9, Pdlim4, Pdlim5, Pfn2, Ppp1r9b, Ppp2r2a, Prune1, Rab14, Rps3, Snca, Sncb, Stmn1, Wdr1
ATP binding	62	4.060248852	Aacs, Aak1, Acss1, Actb, Afg3l2, Ak3, Ak4, Aldh18a1, Ass1, Atad3a, Atp2b1, Atp5b, Atp6v1a, Atp6v1b2, Bcr, Camk2b, Cdc42bpa, Clpx, Dclk1, Ddx17, Ddx39b, Ddx3x, Dhx29, Dtymk, Eif4a1, Eif4a2, Eif4b, Eif4g1, Farsb, G3bp1, Glud1, Gsk3a, Gsk3b, Hsp90aa1, Hsp90ab1, Hspa4, Hspa8, Iars2, Idh3g, Kif21b, Kif5b, Lars2, Lonp1, Myh9, Nadk2, Nsf, Pak2, Pebp1, Pfkm, Psmc2, Sars2, Suclg2, Tars2, Timm44, Tnik, Top1, Trap1, Trio, Uba1, Ube2m, Ube2o, Vwa8
kinase binding	42	4.833141327	Actb, Ank2, Arhgdia, Atp1b1, Camk2b, Clasp2, Cltc, Dctn1, Dcx, Dnm2, Dpysl2, Dvl2, Eef2, Fermt2, Flna, Gsk3a, Gsk3b, Gstm1, Gstp1, Hsp90aa1, Hsp90ab1, Kif5b, Ldha, Map2, Mapre1, Nsf, Pak2, Pdlim5, Pebp1, Pfkm, Ppp1r9b, Prdx3, Prkar2a, Prkar2b, Prkra, Ptpn23, Rac1, Rps3, Sorbs1, Srcin1, Trap1, Vim
actin binding	34	7.439825058	Afdn, Anxa6, Arpc1a, Bin1, Camsap3, Cap1, Cfl1, Clasp2, Cnn3, Coro1c, Cotl1, Crmp1, Cttn, Dbnl, Eef2, Epb41l2, Epb41l3, Fermt2, Flna, Flnb, Fscn1, Inppl1, Lasp1, Lrpprc, Macf1, Map1b, Map2, Myh9, Pdlim4, Pdlim5, Pfn2, Ppp1r9b, Snca, Wdr1

tubulin binding	30	7.556674957	Arhgef2, Arl8b, Camsap1, Camsap3, Ckap5, Clasp2, Cnn3, Dctn1, Dcx, Ddx3x, Dnm1l, Dnm2, Dpysl2, Dpysl5, Eml4, Gapdh, Kif21b, Kif5b, Lrpprc, Macf1, Map1b, Map2, Map4, Map6, Mapre1, Prune1, Rps3, Snca, Sncb, Stmn1
mRNA binding	26	8.30670929	Auh, Ddx3x, Eif3c, Eif4g1, Eif4g2, Fus, Fxr1, G3bp1, Hdlbp, Hnrnpa3, Hnrnpm, Hsp90aa1, Luc7l2, Luc7l3, Mrps7, Pabpc1, Pcbp1, Pcbp2, Rpl7, Rps3, Serbp1, Shmt2, Srsf3, Syncrip, Tardbp, Thoc2
microtubule binding	24	8.450704575	Arhgef2, Camsap1, Camsap3, Ckap5, Clasp2, Cnn3, Dctn1, Dcx, Dnm1l, Dnm2, Dpysl2, Dpysl5, Eml4, Gapdh, Kif21b, Kif5b, Macf1, Map1b, Map2, Map4, Map6, Mapre1, Rps3, Snca
actin filament binding	22	10	Afdn, Anxa6, Arpc1a, Bin1, Camsap3, Cfl1, Clasp2, Coro1c, Cotl1, Crmp1, Cttn, Dbnl, Eef2, Fermt2, Flna, Fscn1, Lasp1, Lrpprc, Macf1, Myh9, Ppp1r9b, Wdr1
GTPase binding	19	5.9375	Afdn, Anxa2, Arhgap1, Arhgdia, Arhgef2, Bin1, Coro1c, Dnm1l, Dvl2, Flna, Hsp90aa1, Nsf, Pak2, Pex5, Rab3gap2, Rab7, Rac1, Rbsn, Srgap2
ubiquitin protein ligase binding	19	5.9375	Dnm1l, Elob, Gsk3b, Hsp90aa1, Hsp90ab1, Hspa8, Lrpprc, Ndufs2, Pcbp2, Prdx5, Prdx6, Prkar2a, Prkar2b, Rpl11, Sorbs1, Tuba1b, Tubb5, Uchl1, Ywhae
small GTPase binding	17	6.007067204	Afdn, Anxa2, Arhgap1, Arhgdia, Arhgef2, Coro1c, Dnm1l, Dvl2, Flna, Nsf, Pak2, Pex5, Rab3gap2, Rab7, Rac1, Rbsn, Srgap2
translation regulator activity, nucleic acid binding	14	13.5922327	Dhx29, Eef1d, Eef1g, Eef2, Eif3c, Eif4a1, Eif4a2, Eif4b, Eif4g1, Eif4g2, Eif5a, Gfm1, Pcbp1, Shmt2
oxidoreductase activity, acting on the CH-CH group of donors	13	20.3125	Acad8, Acad9, Acadl, Acadm, Acads, Acadsb, Acadvl, Crat, Decr1, Gcdh, Ivd, Sdhb, Zadh2
rRNA binding	12	15	Eef2, Mrpl16, Mrps27, Mrps7, Ptcd3, Rpl11, Rpl3, Rpl4, Rpl7, Rps3, Rps9, Tst

translation factor activity, RNA binding	12	14.28571415	[Dhx29, Eef1d, Eef1g, Eef2, Eif3c, Eif4a1, Eif4a2, Eif4b, Eif4g1, Eif4g2, Eif5a, Gfm1]
ribonucleoprotein complex binding	12	7.272727489	[Ckap5, Ddx3x, Dhx29, Eef2, Eif3c, Eif4b, Eif4g1, Eif5a, Mrps27, Ptcd3, Rpsa, Serbp1]
electron transfer activity	11	12.94117641	[Acadsb, COX2, Cox4i1, Cox5a, Etfa, Etfb, Ndufa10, Ndufs1, Ndufs2, Ndufv1, Sdhb]
flavin adenine dinucleotide binding	11	12.2222233	[Acad8, Acad9, Acadl, Acadm, Acads, Acadsb, Acadvl, Dld, Etfa, Gcdh, Ivd]
double-stranded RNA binding	10	11.49425316	[Cltc, Ddx3x, Eif4a1, Eif4b, Fxr1, Hsp90ab1, Prkra, Tuba1b, Tubb4b, Vim]
acyl-CoA dehydrogenase activity	9	81.8181839	[Acad8, Acad9, Acadl, Acadm, Acads, Acadsb, Acadvl, Gcdh, Ivd]
fatty-acyl-CoA binding	8	29.62962914	[Acad9, Acadl, Acadm, Acads, Acadvl, Eci2, Gcdh, Hadha]
peroxidase activity	8	12.5	[Gstp1, Hba-a1, Prdx1, Prdx2, Prdx3, Prdx5, Prdx6, Snca]
5S rRNA binding	6	46.15384674	[Eef2, Rpl11, Rpl3, Rpl4, Rpl7, Tst]
tau protein binding	6	25	[Bin1, Gsk3b, Hsp90aa1, Hsp90ab1, Ppp2r2a, Snca]
thioredoxin peroxidase activity	5	71.42857361	[Prdx1, Prdx2, Prdx3, Prdx5, Prdx6]
translation elongation factor activity	5	25	[Eef1d, Eef1g, Eef2, Eif5a, Gfm1]
NADH dehydrogenase activity	5	21.73913002	[Ndufa10, Ndufa9, Ndufs1, Ndufs2, Ndufv1]
negative regulation of oxidoreductase activity	5	15.15151501	[Gsk3b, Gstp1, Prdx5, Prdx6, Snca]
NADH dehydrogenase (ubiquinone) activity	4	22.2222137	[Ndufa10, Ndufs1, Ndufs2, Ndufv1]
ribosomal small subunit binding	4	22.2222137	[Ddx3x, Dhx29, Eif4b, Ptcd3]

REFERENCES

REFERENCES

- Ahmed, T., van der Jeugd, A., Blum, D., Galas, M. C., D'Hooge, R., Buee, L., & Balschun, D. (2014). Cognition and hippocampal synaptic plasticity in mice with a homozygous tau deletion. *Neurobiology of Aging*, *35*(11), 2474–2478. https://doi.org/10.1016/j.neurobiolaging.2014.05.005
- Alonso, A. del C., Zaidi, T., Novak, M., Grundke-Iqbal, I., & Iqbal, K. (2001). Hyperphosphorylation induces self-assembly of τ into tangles of paired helical filaments/straight filaments. *Proceedings of the National Academy of Sciences*, *98*(12), 6923–6928.
- Alquezar, C., Arya, S., & Kao, A. W. (2021). Tau Post-translational Modifications: Dynamic Transformers of Tau Function, Degradation, and Aggregation. In *Frontiers in Neurology* (Vol. 11). Frontiers Media S.A. https://doi.org/10.3389/fneur.2020.595532
- ALZFORUM. (2022). *Mutations/MAPT*. ALZFORUM. https://www.alzforum.org/mutations/mapt
- Alzheimer, A. (1911). über eigenartige Krankheitsfälle des späteren Alters. Zeitschrift Für Die Gesamte Neurologie Und Psychiatrie, 4(1), 356–385. https://doi.org/10.1007/BF02866241
- Andreadis, A., Brown, W. M., & Kosik, K. S. (1992). Structure and novel exons of the human .tau. gene. *Biochemistry*, 31(43), 10626–10633. https://doi.org/10.1021/bi00158a027
- Apicco, D. J., Ash, P. E. A., Maziuk, B., Leblang, C., Medalla, M., al Abdullatif, A., Ferragud, A., Botelho, E., Ballance, H. I., Dhawan, U., Boudeau, S., Cruz, A. L., Kashy, D., Wong, A., Goldberg, L. R., Yazdani, N., Zhang, C., Ung, C. Y., Tripodis, Y., ... Wolozin, B. (2018). Reducing the RNA binding protein TIA1 protects against tau-mediated neurodegeneration in vivo. *Nature Neuroscience*, *21*(1), 72–82. https://doi.org/10.1038/s41593-017-0022-z
- Arendt, T., Stieler, J. T., & Holzer, M. (2016). Tau and tauopathies. In *Brain Research Bulletin* (Vol. 126, pp. 238–292). Elsevier Inc. https://doi.org/10.1016/j.brainresbull.2016.08.018
- Baba, Y., Baker, M. C., le Ber, I., Brice, A., Maeck, L., Kohlhase, J., Yasuda, M., Stoppe, G., Bugiani, O., Sperfeld, A. D., Tsuboi, Y., Uitti, R. J., Farrer, M. J., Ghetti, B., Hutton, M. L., & Wszolek, Z. K. (2007). Clinical and genetic features of families with frontotemporal dementia and parkinsonism linked to chromosome 17 with a

- P301S tau mutation. *Journal of Neural Transmission*, *114*(7), 947–950. https://doi.org/10.1007/s00702-007-0632-9
- Berggård, T., Linse, S., & James, P. (2007). Methods for the detection and analysis of protein-protein interactions. In *Proteomics* (Vol. 7, Issue 16, pp. 2833–2842). https://doi.org/10.1002/pmic.200700131
- Bindea, G., Mlecnik, B., Hackl, H., Charoentong, P., Tosolini, M., Kirilovsky, A., Fridman, W. H., Pagès, F., Trajanoski, Z., & Galon, J. (2009). ClueGO: A Cytoscape plug-in to decipher functionally grouped gene ontology and pathway annotation networks. *Bioinformatics*, *25*(8), 1091–1093. https://doi.org/10.1093/bioinformatics/btp101
- Braak, H., Alafuzoff, I., Arzberger, T., Kretzschmar, H., & Tredici, K. (2006). Staging of Alzheimer disease-associated neurofibrillary pathology using paraffin sections and immunocytochemistry. *Acta Neuropathologica*, 112(4), 389–404. https://doi.org/10.1007/s00401-006-0127-z
- Braak, H., & Braak, E. (1991). Acta H' pathologica Neuropathological stageing of Alzheimer-related changes. In *Acta Neuropathol* (Vol. 82).
- Braak, H., Braak, E., & Braak, E. (1995). Staging of Alzheimer's Disease-Related Neurofibrillary Changes. In *Neurobiology of Aging* (Vol. 16, Issue 95).
- Bramblett, G. T., Goedert, M., Jakes, R., Merrick, S. E., Trojanowski, J. Q., & Lee, V. M. Y. (1993). Abnormal tau phosphorylation at Ser396 in Alzheimer's disease recapitulates development and contributes to reduced microtubule binding. *Neuron*, 10(6), 1089–1099.
- Brandt, R., Léger, J., & Lee, G. (1995). Interaction of tau with the neural plasma membrane mediated by tau's amino-terminal projection domain. *The Journal of Cell Biology*, 131(5), 1327–1340.
- Brohée, S., & van Helden, J. (2006). Evaluation of clustering algorithms for protein-protein interaction networks. *BMC Bioinformatics*, 7. https://doi.org/10.1186/1471-2105-7-488
- Caillet-Boudin, M. L., Buée, L., Sergeant, N., & Lefebvre, B. (2015). Regulation of human MAPT gene expression. In *Molecular Neurodegeneration* (Vol. 10, Issue 1). BioMed Central Ltd. https://doi.org/10.1186/s13024-015-0025-8
- Camero, S., Benítez, M. J., Barrantes, A., Ayuso, J. M., Cuadros, R., Ávila, J., & Jiménez, J. S. (2014). Tau Protein Provides DNA with Thermodynamic and Structural Features which are Similar to those Found in Histone-DNA Complex. *Journal of Alzheimer's Disease*, *39*, 649–660. https://doi.org/10.3233/JAD-131415

- Carmel, G., Mager, E. M., Binder, L. I., & Kuret, J. (1996). The structural basis of monoclonal antibody Alz50's selectivity for Alzheimer's disease pathology. *Journal of Biological Chemistry*, 271(51), 32789–32795.
- Carroll, T., Guha, S., Nehrke, K., & Johnson, G. V. W. (2021). Tau post-translational modifications: Potentiators of selective vulnerability in sporadic alzheimer's disease. *Biology*, *10*(10). https://doi.org/10.3390/biology10101047
- Cheah, J. S., & Yamada, S. (2017). A simple elution strategy for biotinylated proteins bound to streptavidin conjugated beads using excess biotin and heat. *Biochemical and Biophysical Research Communications*, *493*(4), 1522–1527. https://doi.org/10.1016/j.bbrc.2017.09.168
- Chin, K. S., Yassi, N., Churilov, L., Masters, C. L., & Watson, R. (2020). Prevalence and clinical associations of tau in Lewy body dementias: A systematic review and meta-analysis. *Parkinsonism & Related Disorders*, *80*, 184–193. https://doi.org/https://doi.org/10.1016/j.parkreldis.2020.09.030
- Chung, D. eun C., Roemer, S., Petrucelli, L., & Dickson, D. W. (2021). Cellular and pathological heterogeneity of primary tauopathies. In *Molecular Neurodegeneration* (Vol. 16, Issue 1). BioMed Central Ltd. https://doi.org/10.1186/s13024-021-00476-x
- Cline, M. S., Smoot, M., Cerami, E., Kuchinsky, A., Landys, N., Workman, C., Christmas, R., Avila-Campilo, I., Creech, M., & Gross, B. (2007). Integration of biological networks and gene expression data using Cytoscape. *Nature Protocols*, 2(10), 2366–2382.
- Combs, B., Christensen, K. R., Richards, C., Kneynsberg, A., Mueller, R. L., Morris, S. L., Morfini, G. A., Brady, S. T., & Kanaan, N. M. (2021). Frontotemporal Lobar Dementia Mutant Tau Impairs Axonal Transport through a Protein Phosphatase 1γ-Dependent Mechanism. *Journal of Neuroscience*, *41*(45), 9431–9451.
- Combs, B., & Gamblin, T. C. (2012). FTDP-17 tau mutations induce distinct effects on aggregation and microtubule interactions. *Biochemistry*, *51*(43), 8597–8607. https://doi.org/10.1021/bi3010818
- Combs, B., Hamel, C., & Kanaan, N. M. (2016). Pathological conformations involving the amino terminus of tau occur early in Alzheimer's disease and are differentially detected by monoclonal antibodies. *Neurobiology of Disease*, *94*, 18–31.
- Combs, B., Mueller, R. L., Morfini, G., Brady, S. T., & Kanaan, N. M. (2019). Tau and axonal transport misregulation in tauopathies. *Tau Biology*, 81–95.
- Cowan, C. M., & Mudher, A. (2013). Are tau aggregates toxic or protective in tauopathies? *Frontiers in Neurology*, *4 AUG*. https://doi.org/10.3389/fneur.2013.00114

- Crary, J. F., Trojanowski, J. Q., Schneider, J. A., Abisambra, J. F., Abner, E. L., Alafuzoff, I., Arnold, S. E., Attems, J., Beach, T. G., Bigio, E. H., Cairns, N. J., Dickson, D. W., Gearing, M., Grinberg, L. T., Hof, P. R., Hyman, B. T., Jellinger, K., Jicha, G. A., Kovacs, G. G., ... Nelson, P. T. (2014). Primary age-related tauopathy (PART): a common pathology associated with human aging. *Acta Neuropathologica*, *128*(6), 755–766. https://doi.org/10.1007/s00401-014-1349-0
- Cummins, N., Tweedie, A., Zuryn, S., Bertran-Gonzalez, J., & Götz, J. (2019). Disease-associated tau impairs mitophagy by inhibiting Parkin translocation to mitochondria. *The EMBO Journal*, *38*(3), e99360.
- Delacourte, A., Robitaille, Y., Sergeant, N., Buée, L., Hof, P. R., Wattez, A., Laroche-Cholette, A., Mathieu, J., Chagnon, P., & Gauvreau, D. (1996). Specific Pathological Tau Protein Variants Characterize Pick's Disease. *Journal of Neuropathology & Experimental Neurology*, *55*(2), 159–168. https://doi.org/10.1097/00005072-199602000-00004
- Dickson, D. W., Rademakers, R., & Hutton, M. L. (2007). Progressive supranuclear palsy: pathology and genetics. *Brain Pathology*, *17*(1), 74–82.
- Dixit, R., Ross, J. L., Goldman, Y. E., & Holzbaur, E. L. F. (2008). Differential regulation of dynein and kinesin motor proteins by tau. *Science*, *319*(5866), 1086–1089. https://doi.org/10.1126/science.1152993
- Doncheva, N. T., Morris, J. H., Gorodkin, J., & Jensen, L. J. (2019). Cytoscape StringApp: Network Analysis and Visualization of Proteomics Data. *Journal of Proteome Research*, 18(2), 623–632. https://doi.org/10.1021/acs.jproteome.8b00702
- Drummond, E., Pires, G., MacMurray, C., Askenazi, M., Nayak, S., Bourdon, M., Safar, J., Ueberheide, B., & Wisniewski, T. (2020). Phosphorylated tau interactome in the human Alzheimer's disease brain. *Brain*, *143*(9), 2803–2817. https://doi.org/10.1093/brain/awaa223
- Du, F., Yu, Q., Kanaan, N. M., & Yan, S. S. (2022). Mitochondrial oxidative stress contributes to the pathological aggregation and accumulation of tau oligomers in Alzheimer's disease. *Human Molecular Genetics*, ddab363. https://doi.org/10.1093/hmg/ddab363
- Ebneth, A., Godemann, R., Stamer, K., Illenberger, S., Trinczek, B., Mandelkow, E.-M., & Mandelkow, E. (1998). Overexpression of tau protein inhibits kinesin-dependent trafficking of vesicles, mitochondria, and endoplasmic reticulum: implications for Alzheimer's disease. *The Journal of Cell Biology*, *143*(3), 777–794.
- Esposito, A., Dohm, C. P., Kermer, P., Bähr, M., & Wouters, F. S. (2007). α-Synuclein and its disease-related mutants interact differentially with the microtubule protein

- tau and associate with the actin cytoskeleton. *Neurobiology of Disease*, 26(3), 521–531.
- Feng, W., Liu, C., Spinozzi, S., Wang, L., Evans, S. M., & Chen, J. (2020). Identifying the cardiac dyad proteome in vivo by a BioID2 knock-in strategy. *Circulation*, 141(11), 940–942.
- Fernández-Nogales, M., Cabrera, J. R., Santos-Galindo, M., Hoozemans, J. J. M., Ferrer, I., Rozemuller, A. J. M., Hernández, F., Avila, J., & Lucas, J. J. (2014). Huntington's disease is a four-repeat tauopathy with tau nuclear rods. *Nature Medicine*, *20*(8), 881–885. https://doi.org/10.1038/nm.3617
- Ferrer-Acosta, Y., Rodríguez-Cruz, E. N., Orange, F., de Jesús-Cortés, H., Madera, B., Vaquer-Alicea, J., Ballester, J., Guinel, M. J., Bloom, G. S., & Vega, I. E. (2013). EF hd2 is a novel amyloid protein associated with pathological tau in Alzheimer's disease. *Journal of Neurochemistry*, *125*(6), 921–931.
- García-Sierra, F., Ghoshal, N., Quinn, B., Berry, R. W., & Binder, L. I. (2003). Conformational changes and truncation of tau protein during tangle evolution in Alzheimer's disease. *Journal of Alzheimer's Disease*, *5*, 65–77. https://doi.org/10.3233/JAD-2003-5201
- Gauthier-Kemper, A., Alonso, M. S., Sündermann, F., Niewidok, B., Fernandez, M. P., Bakota, L., Heinisch, J. J., & Brandt, R. (2018a). Annexins A2 and A6 interact with the extreme N terminus of tau and thereby contribute to tau's axonal localization. *Journal of Biological Chemistry*, 293(21), 8065–8076. https://doi.org/10.1074/jbc.RA117.000490
- Gauthier-Kemper, A., Alonso, M. S., Sündermann, F., Niewidok, B., Fernandez, M.-P., Bakota, L., Heinisch, J. J., & Brandt, R. (2018b). Annexins A2 and A6 interact with the extreme N terminus of tau and thereby contribute to tau's axonal localization. *Journal of Biological Chemistry*, 293(21), 8065–8076.
- Geeth Gunawardana, C., Mehrabian, M., Wang, X., Mueller, I., Lubambo, I. B., Jonkman, J. E. N., Wang, H., & Schmitt-Ulms, G. (2015). The Human Tau Interactome: Binding to the Ribonucleoproteome, and Impaired Binding of the Proline-to-Leucine Mutant at Position 301 (P301L) to Chaperones and the Proteasome*

 S. Molecular & Cellular Proteomics, 14, 3000–3014.
 https://doi.org/10.1074/mcp
- Gingras, A. C., Abe, K. T., & Raught, B. (2019). Getting to know the neighborhood: using proximity-dependent biotinylation to characterize protein complexes and map organelles. In *Current Opinion in Chemical Biology* (Vol. 48, pp. 44–54). Elsevier Ltd. https://doi.org/10.1016/j.cbpa.2018.10.017

- Goedert, M., Anthony Crowther, ‡ R, & Spillantini, M. G. (1998). Tau Mutations Cause Minireview Frontotemporal Dementias other by the presence or absence of 29-or 58-amino-acid inserts located in the amino-terminal half and a 31-amino-acid repeat located in the carboxy-terminal half. In *Neuron* (Vol. 21).
- Goedert, M., & Jakes, R. (1990). Expression of separate isoforms of human tau protein: correlation with the tau pattern in brain and effects on tubulin polymerization. *The EMBO Journal*, *9*(13), 4225–4230.
- Goedert, M., & Jakes, R. (2005). Mutations causing neurodegenerative tauopathies. In *Biochimica et Biophysica Acta Molecular Basis of Disease* (Vol. 1739, Issue 2, pp. 240–250). https://doi.org/10.1016/j.bbadis.2004.08.007
- Goedert, M., Spillantini, M. G., Cairns, N. J., & Crowther, R. A. (1992). Tau Proteins of Alzheimer Paired Helical Filaments: Abnormal Phosphorylation of All Six Brain Isoforms I. In *Neuron* (Vol. 8).
- Goedert, M., Spillantini, M. G., Jakes, R., Rutherford, D., & Crowther, R. A. (1989). Multiple isoforms of human microtubule-associated protein tau: sequences and localization in neurofibrillary tangles of Alzheimer's disease. *Neuron*, *3*(4), 519–526.
- Götz, J., & Ittner, L. M. (2008). Animal models of Alzheimer's disease and frontotemporal dementia. In *Nature Reviews Neuroscience* (Vol. 9, Issue 7, pp. 532–544). Nature Publishing Group. https://doi.org/10.1038/nrn2420
- Grundke-Iqbal, I., Iqbal, K., Tung, Y. C., Quinlan, M., Wisniewski, H. M., & Binder, L. I. (1987). Abnormal phosphorylation of the microtubule-associated protein?(tau) in Alzheimer cytoskeletal pathology. *Alzheimer Disease & Associated Disorders*, *1*(3), 202.
- Guo, T., Noble, W., & Hanger, D. P. (2017). Roles of tau protein in health and disease. In *Acta Neuropathologica* (Vol. 133, Issue 5, pp. 665–704). Springer Verlag. https://doi.org/10.1007/s00401-017-1707-9
- Hagestedt, T., Lichtenberg, B., Wille, H., Mandelkow, E. M., & Mandelkow, E. (1989). Tau protein becomes long and stiff upon phosphorylation: correlation between paracrystalline structure and degree of phosphorylation. *The Journal of Cell Biology*, *109*(4), 1643–1651.
- Harada, A., Oguchi, K., Okabe, S., Kuno, J., Terada, S., Ohshima, T., Sato-Yoshitake, R., Takei, Y., Noda, T., & Hirokawa, N. (1994). Altered microtubule organization in small-calibre axons of mice lacking tau protein. *Nature*, *369*(6480), 488–491.
- Haugland, R. P., & You, W. W. (2008). Coupling of antibodies with biotin. In *Avidin-Biotin Interactions* (pp. 13–23). Springer.

- Hayes, S., Malacrida, B., Kiely, M., & Kiely, P. A. (2016). Studying protein-protein interactions: Progress, pitfalls and solutions. *Biochemical Society Transactions*, 44(4), 994–1004. https://doi.org/10.1042/BST20160092
- Hernández, F., Merchán-Rubira, J., Vallés-Saiz, L., Rodríguez-Matellán, A., & Avila, J. (2020a). Differences between human and murine tau at the N-terminal end. *Frontiers in Aging Neuroscience*, *12*, 11.
- Hernández, F., Merchán-Rubira, J., Vallés-Saiz, L., Rodríguez-Matellán, A., & Avila, J. (2020b). Differences Between Human and Murine Tau at the N-terminal End. In *Frontiers in Aging Neuroscience* (Vol. 12). Frontiers Media S.A. https://doi.org/10.3389/fnagi.2020.00011
- Himmlert, A. (1989). Structure of the Bovine Tau Gene: Alternatively Spliced Transcripts Generate a Protein Family. In *MOLECULAR AND CELLULAR BIOLOGY* (Vol. 9, Issue 4). https://journals.asm.org/journal/mcb
- Hong, X., Peng, C., Wei, W., Tian, Q., Liu, Y., Yao, X., Zhang, Y., Cao, F., Wang, Q., & Wang, J. (2010). Essential role of tau phosphorylation in adult hippocampal neurogenesis. *Hippocampus*, 20(12), 1339–1349.
- IHARA, Y., NUKINA, N., MIURA, R., & OGAWARA, M. (1986). Phosphorylated tau protein is integrated into paired helical filaments in Alzheimer's disease. *The Journal of Biochemistry*, *99*(6), 1807–1810.
- Irwin, D. J., Lee, V. M. Y., & Trojanowski, J. Q. (2013). Parkinson's disease dementia: Convergence of α-synuclein, tau and amyloid-β pathologies. In *Nature Reviews Neuroscience* (Vol. 14, Issue 9, pp. 626–636). https://doi.org/10.1038/nrn3549
- Ittner, L. M., Ke, Y. D., Delerue, F., Bi, M., Gladbach, A., van Eersel, J., Wölfing, H., Chieng, B. C., Christie, M. J., & Napier, I. A. (2010). Dendritic function of tau mediates amyloid-β toxicity in Alzheimer's disease mouse models. *Cell*, *142*(3), 387–397.
- Jack, C. R., Bennett, D. A., Blennow, K., Carrillo, M. C., Dunn, B., Haeberlein, S. B., Holtzman, D. M., Jagust, W., Jessen, F., Karlawish, J., Liu, E., Molinuevo, J. L., Montine, T., Phelps, C., Rankin, K. P., Rowe, C. C., Scheltens, P., Siemers, E., Snyder, H. M., ... Silverberg, N. (2018). NIA-AA Research Framework: Toward a biological definition of Alzheimer's disease. *Alzheimer's and Dementia*, 14(4), 535– 562. https://doi.org/10.1016/j.jalz.2018.02.018
- Jeganathan, S., von Bergen, M., Brutlach, H., Steinhoff, H. J., & Mandelkow, E. (2006). Global hairpin folding of tau in solution. *Biochemistry*, *45*(7), 2283–2293. https://doi.org/10.1021/bi0521543

- Jiang, L., Lin, W., Zhang, C., Ash, P. E. A., Verma, M., Kwan, J., van Vliet, E., Yang, Z., Cruz, A. L., Boudeau, S., Maziuk, B. F., Lei, S., Song, J., Alvarez, V. E., Hovde, S., Abisambra, J. F., Kuo, M. H., Kanaan, N., Murray, M. E., ... Wolozin, B. (2021). Interaction of tau with HNRNPA2B1 and N6-methyladenosine RNA mediates the progression of tauopathy. *Molecular Cell*, 81(20), 4209-4227.e12. https://doi.org/10.1016/j.molcel.2021.07.038
- Joachim, C. L., Morris, J. H., Kosik, K. S., & Selkoe, D. J. (1987). Tau antisera recognize neurofibrillary tangles in a range of neurodegenerative disorders. *Annals of Neurology*, 22(4), 514–520.
- Josephs, K. A. (2017). Current understanding of neurodegenerative diseases associated with the protein tau. *Mayo Clinic Proceedings*, *92*(8), 1291–1303.
- Kadavath, H., Hofele, R. v., Biernat, J., Kumar, S., Tepper, K., Urlaub, H., Mandelkow, E., & Zweckstetter, M. (2015). Tau stabilizes microtubules by binding at the interface between tubulin heterodimers. *Proceedings of the National Academy of Sciences of the United States of America*, 112(24), 7501–7506. https://doi.org/10.1073/pnas.1504081112
- Kanaan, N. M., & Grabinski, T. (2021). Neuronal and glial distribution of tau protein in the adult rat and monkey. *Frontiers in Molecular Neuroscience*, 61.
- Kanaan, N. M., Hamel, C., Grabinski, T., & Combs, B. (2020). Liquid-liquid phase separation induces pathogenic tau conformations in vitro. *Nature Communications*, 11(1), 1–16.
- Kanaan, N. M., Morfini, G. A., LaPointe, N. E., Pigino, G. F., Patterson, K. R., Song, Y., Andreadis, A., Fu, Y., Brady, S. T., & Binder, L. I. (2011a). Pathogenic forms of tau inhibit kinesin-dependent axonal transport through a mechanism involving activation of axonal phosphotransferases. *Journal of Neuroscience*, 31(27), 9858–9868. https://doi.org/10.1523/JNEUROSCI.0560-11.2011
- Kanaan, N. M., Morfini, G. A., LaPointe, N. E., Pigino, G. F., Patterson, K. R., Song, Y., Andreadis, A., Fu, Y., Brady, S. T., & Binder, L. I. (2011b). Pathogenic forms of tau inhibit kinesin-dependent axonal transport through a mechanism involving activation of axonal phosphotransferases. *Journal of Neuroscience*, 31(27), 9858–9868. https://doi.org/10.1523/JNEUROSCI.0560-11.2011
- Katsumoto, A., Takeuchi, H., & Tanaka, F. (2019). Tau Pathology in Chronic Traumatic Encephalopathy and Alzheimer's Disease: Similarities and Differences. In *Frontiers in Neurology* (Vol. 10). Frontiers Media S.A. https://doi.org/10.3389/fneur.2019.00980
- Kim, D. I., Birendra, K. C., Zhu, W., Motamedchaboki, K., Doye, V., & Roux, K. J. (2014). Probing nuclear pore complex architecture with proximity-dependent

- biotinylation. *Proceedings of the National Academy of Sciences of the United States of America*, 111(24). https://doi.org/10.1073/pnas.1406459111
- Kim, D. I., Jensen, S. C., Noble, K. A., Kc, B., Roux, K. H., Motamedchaboki, K., & Roux, K. J. (2016). An improved smaller biotin ligase for BioID proximity labeling. *Molecular Biology of the Cell*, *27*(8), 1188–1196. https://doi.org/10.1091/mbc.E15-12-0844
- Kimura, T., Whitcomb, D. J., Jo, J., Regan, P., Piers, T., Heo, S., Brown, C., Hashikawa, T., Murayama, M., Seok, H., Sotiropoulos, I., Kim, E., Collingridge, G. L., Takashima, A., & Cho, K. (2014). Microtubule-associated protein tau is essential for long-term depression in the hippocampus. *Philosophical Transactions of the Royal Society B: Biological Sciences*, 369(1633). https://doi.org/10.1098/rstb.2013.0144
- Komori, T. (1999). Tau-positive dial Inclusions in Progressive Supranuclear Palsy, Corticobasal Degeneration and Pick's Disease. *Brain Pathology*, *9*(4), 663–679.
- Komori, T., Arai, N., Oda, M., Nakayama, H., Mori, H., Yagishita, S., Takahashi, T., Amano, N., Murayama, S., & Murakami, S. (1998). Astrocytic plaques and tufts of abnormal fibers do not coexist in corticobasal degeneration and progressive supranuclear palsy. *Acta Neuropathologica*, *96*(4), 401–408.
- Labbadia, J., & Morimoto, R. I. (2013). Huntington's disease: Underlying molecular mechanisms and emerging concepts. In *Trends in Biochemical Sciences* (Vol. 38, Issue 8, pp. 378–385). https://doi.org/10.1016/j.tibs.2013.05.003
- Lam, S. S., Martell, J. D., Kamer, K. J., Deerinck, T. J., Ellisman, M. H., Mootha, V. K., & Ting, A. Y. (2014). Directed evolution of APEX2 for electron microscopy and proximity labeling. *Nature Methods*, *12*(1), 51–54. https://doi.org/10.1038/nmeth.3179
- Lee, V. M.-Y., Goedert, M., & Trojanowski, J. Q. (2001a). Neurodegenarative tauopathies. *Annual Review of Neuroscience*, *24*, 1121–1159. http://ezproxy.msu.edu/login?url=https://www.proquest.com/scholarly-journals/neurodegenarative-tauopathies/docview/198862232/se-2?accountid=12598
- Lee, V. M.-Y., Goedert, M., & Trojanowski, J. Q. (2001b). Neurodegenerative Tauopathies. *Annual Review of Neuroscience*, *24*(1), 1121–1159. https://doi.org/10.1146/annurev.neuro.24.1.1121
- Lewis, J., Mcgowan, E., Rockwood, J., Melrose, H., Nacharaju, P., van Slegtenhorst, M., Gwinn-Hardy, K., Murphy, M. P., Baker, M., Yu, X., Duff, K., Hardy, J., Corral, A., Lin, W.-L., Yen, S.-H., Dickson, D. W., Davies, P., & Hutton, M. (2000). Neurofibrillary tangles, amyotrophy and progressive motor disturbance in mice expressing mutant (P301L) tau protein. http://genetics.nature.com

- Li, X.-C., Hu, Y., Wang, Z., Luo, Y., Zhang, Y., Liu, X.-P., Feng, Q., Wang, Q., Ye, K., Liu, G.-P., & Wang, J.-Z. (2016). Human wild-type full-length tau accumulation disrupts mitochondrial dynamics and the functions via increasing mitofusins. *Scientific Reports*, *6*(1), 24756. https://doi.org/10.1038/srep24756
- Limorenko, G., & Lashuel, H. A. (2022). Revisiting the grammar of Tau aggregation and pathology formation: How new insights from brain pathology are shaping how we study and target Tauopathies. In *Chemical Society Reviews* (Vol. 51, Issue 2, pp. 513–565). Royal Society of Chemistry. https://doi.org/10.1039/d1cs00127b
- Lindwall, G., & Cole, R. D. (1984). Phosphorylation affects the ability of tau protein to promote microtubule assembly. *Journal of Biological Chemistry*, *259*(8), 5301–5305.
- Liu, C., Song, X., Nisbet, R., & Götz, J. (2016). Co-immunoprecipitation with Tau isoform-specific antibodies reveals distinct protein interactions and highlights a putative role for 2N Tau in disease. *Journal of Biological Chemistry*, 291(15), 8173–8188. https://doi.org/10.1074/jbc.M115.641902
- Liu, G., Thangavel, R., Rysted, J., Kim, Y., Francis, M. B., Adams, E., Lin, Z., Taugher, R. J., Wemmie, J. A., & Usachev, Y. M. (2019). Loss of tau and Fyn reduces compensatory effects of MAP2 for tau and reveals a Fyn-independent effect of tau on calcium. *Journal of Neuroscience Research*, *97*(11), 1393–1413.
- Llorens-Martin, M., Lopez-Domenech, G., Soriano, E., & Avila, J. (2011). GSK3β is involved in the relief of mitochondria pausing in a Tau-dependent manner. *PLoS One*, *6*(11), e27686.
- Loomis, P. A., Howardt, T. H., Castleberryt, R. P., & Binder, L. 1. (1990). Identification of nuclear X isoforms in human neuroblastoma cells (nucleolus/microtubule-associated proteins/Alzheimer disease/Down syndrome). In *Cell Biology* (Vol. 87). https://www.pnas.org
- LoPresti, P., Szuchet, S., Papasozomenos, S. C., Zinkowski, R. P., & Binder, L. I. (1995). Functional implications for the microtubule-associated protein tau: localization in oligodendrocytes. *Proceedings of the National Academy of Sciences of the United States of America*, *92*(22), 10369–10373. https://doi.org/10.1073/pnas.92.22.10369
- Ma, Q.-L., Zuo, X., Yang, F., Ubeda, O. J., Gant, D. J., Alaverdyan, M., Kiosea, N. C., Nazari, S., Chen, P. P., & Nothias, F. (2014). Loss of MAP function leads to hippocampal synapse loss and deficits in the Morris Water Maze with aging. *Journal of Neuroscience*, *34*(21), 7124–7136.

- Mamun, A. al, Uddin, M. S., Mathew, B., & Ashraf, G. M. (2020). Toxic tau: Structural origins of tau aggregation in Alzheimer's disease. In *Neural Regeneration Research* (Vol. 15, Issue 8, pp. 1417–1420). Wolters Kluwer Medknow Publications. https://doi.org/10.4103/1673-5374.274329
- Mandelkow, E., Biernat, J., Drewes, G., Gustke, N., Trinczek, B., & Mandelkow, E. (1995). Tau Domains, Phosphorylation, and Interactions With Microtubules. In *Neurobiology of Aging* (Vol. 16, Issue 95).
- Martell, J. D., Deerinck, T. J., Sancak, Y., Poulos, T. L., Mootha, V. K., Sosinsky, G. E., Ellisman, M. H., & Ting, A. Y. (2012). Engineered ascorbate peroxidase as a genetically encoded reporter for electron microscopy. *Nature Biotechnology*, 30(11), 1143–1148. https://doi.org/10.1038/nbt.2375
- Maziuk, B. F., Apicco, D. J., Cruz, A. L., Jiang, L., Ash, P. E. A., da Rocha, E. L., Zhang, C., Yu, W. H., Leszyk, J., Abisambra, J. F., Li, H., & Wolozin, B. (2018a). RNA binding proteins co-localize with small tau inclusions in tauopathy. *Acta Neuropathologica Communications*, 6(1), 71. https://doi.org/10.1186/s40478-018-0574-5
- Maziuk, B. F., Apicco, D. J., Cruz, A. L., Jiang, L., Ash, P. E. A., da Rocha, E. L., Zhang, C., Yu, W. H., Leszyk, J., Abisambra, J. F., Li, H., & Wolozin, B. (2018b). RNA binding proteins co-localize with small tau inclusions in tauopathy. *Acta Neuropathologica Communications*, 6(1), 71. https://doi.org/10.1186/s40478-018-0574-5
- McInnes, J., Wierda, K., Snellinx, A., Bounti, L., Wang, Y.-C., Stancu, I.-C., Apóstolo, N., Gevaert, K., Dewachter, I., & Spires-Jones, T. L. (2018). Synaptogyrin-3 mediates presynaptic dysfunction induced by tau. *Neuron*, *97*(4), 823–835.
- Mietelska-Porowska, A., Wasik, U., Goras, M., Filipek, A., & Niewiadomska, G. (2014). Tau protein modifications and interactions: Their role in function and dysfunction. In *International Journal of Molecular Sciences* (Vol. 15, Issue 3, pp. 4671–4713). MDPI AG. https://doi.org/10.3390/ijms15034671
- Mohan, R., & John, A. (2015). Microtubule-associated proteins as direct crosslinkers of actin filaments and microtubules. In *IUBMB Life* (Vol. 67, Issue 6, pp. 395–403). Blackwell Publishing Ltd. https://doi.org/10.1002/iub.1384
- Morfini, G., Pigino, G., Mizuno, N., Kikkawa, M., & Brady, S. T. (2007). Tau binding to microtubules does not directly affect microtubule-based vesicle motility. *Journal of Neuroscience Research*, *85*(12), 2620–2630.
- Morris, J. H., Apeltsin, L., Newman, A. M., Baumbach, J., Wittkop, T., Su, G., Bader, G. D., & Ferrin, T. E. (2011). clusterMaker: a multi-algorithm clustering plugin for

- Cytoscape. *BMC Bioinformatics*, 12(1), 436. https://doi.org/10.1186/1471-2105-12-436
- Morris, M., Maeda, S., Vossel, K., & Mucke, L. (2011). The Many Faces of Tau. In *Neuron* (Vol. 70, Issue 3, pp. 410–426). https://doi.org/10.1016/j.neuron.2011.04.009
- Mueller, R. L., Combs, B., Alhadidy, M. M., Brady, S. T., Morfini, G. A., & Kanaan, N. M. (2021). Tau: a signaling hub protein. *Frontiers in Molecular Neuroscience*, 34.
- Neve, R. L., Harris, P., Kosik, K. S., Kurnit, D. M., & Donlon, T. A. (1986). Identification of cDNA clones for the human microtubule-associated protein tau and chromosomal localization of the genes for tau and microtubule-associated protein 2. *Molecular Brain Research*, 1(3), 271–280. https://doi.org/https://doi.org/10.1016/0169-328X(86)90033-1
- Pallas-Bazarra, N., Jurado-Arjona, J., Navarrete, M., Esteban, J. A., Hernández, F., Ávila, J., & Llorens-Martín, M. (2016). Novel function of Tau in regulating the effects of external stimuli on adult hippocampal neurogenesis. *The EMBO Journal*, *35*(13), 1417–1436. https://doi.org/10.15252/embj.201593518
- Papasozomenos, S. C., & Binder, L. I. (1987). Phosphorylation Determines Two Distinct Species of Tau in the Central Nervous System. In *Cell Motility and the Cytoskeleton* (Vol. 8).
- Paul Shannon, 1, Andrew Markiel, 1, Owen Ozier, 2 Nitin S. Baliga, 1 Jonathan T. Wang, 2 Daniel Ramage, 2, Nada Amin, 2, Benno Schwikowski, 1, 5 and Trey Ideker2, 3, 4, 5, 山本隆久, 豊田直平, 深瀬吉邦, & 大森敏行. (1971). Cytoscape: A Software Environment for Integrated Models. *Genome Research*, *13*(22), 426. https://doi.org/10.1101/gr.1239303.metabolite
- Pickering-Brown, S. M., Baker, M., Nonaka, T., Ikeda, K., Sharma, S., Mackenzie, J., Simpson, S. A., Moore, J. W., Snowden, J. S., de Silva, R., Revesz, T., Hasegawa, M., Hutton, M., & Mann, D. M. A. (2004). Frontotemporal dementia with Pick-type histology associated with Q336R mutation in the tau gene. *Brain*, *127*(6), 1415–1426. https://doi.org/10.1093/brain/awh147
- Pîrşcoveanu, D. F. V., Pirici, I., Tudorică, V., Bălşeanu, T.-A., Albu, V.-C., Bondari, S., Bumbea, A. M., & Pîrşcoveanu, M. (2017). Tau protein in neurodegenerative diseases-a review. *Rom. J. Morphol. Embryol*, *58*(4), 1141–1150.
- Porzig, R., Singer, D., & Hoffmann, R. (2007). Epitope mapping of mAbs AT8 and Tau5 directed against hyperphosphorylated regions of the human tau protein. Biochemical and Biophysical Research Communications, 358(2), 644–649.

- Pronobis, M. I., Zheng, S., Singh, S. P., Goldman, J. A., & Poss, K. D. (2021). In vivo proximity labeling identifies cardiomyocyte protein networks during zebrafish heart regeneration. *Elife*, *10*, e66079.
- Qiang, L., Sun, X., Austin, T. O., Muralidharan, H., Jean, D. C., Liu, M., Yu, W., & Baas, P. W. (2018). Tau Does Not Stabilize Axonal Microtubules but Rather Enables Them to Have Long Labile Domains. *Current Biology*, 28(13), 2181-2189.e4. https://doi.org/10.1016/j.cub.2018.05.045
- Qin, W., Cho, K. F., Cavanagh, P. E., & Ting, A. Y. (2021). Deciphering molecular interactions by proximity labeling. In *Nature Methods* (Vol. 18, Issue 2, pp. 133–143). Nature Research. https://doi.org/10.1038/s41592-020-01010-5
- Rhee, H. W., Zou, P., Udeshi, N. D., Martell, J. D., Mootha, V. K., Carr, S. A., & Ting, A. Y. (2013). Proteomic mapping of mitochondria in living cells via spatially restricted enzymatic tagging. *Science*, 339(6125), 1328–1331. https://doi.org/10.1126/science.1230593
- Richter-Landsberg, C. (2016). Protein aggregate formation in oligodendrocytes: tau and the cytoskeleton at the intersection of neuroprotection and neurodegeneration. *Biological Chemistry*, 397(3), 185–194.
- Rodríguez-Martín, T., Pooler, A. M., Lau, D. H. W., Mórotz, G. M., de Vos, K. J., Gilley, J., Coleman, M. P., & Hanger, D. P. (2016). Reduced number of axonal mitochondria and tau hypophosphorylation in mouse P301L tau knockin neurons. *Neurobiology of Disease*, *85*, 1–10. https://doi.org/https://doi.org/10.1016/j.nbd.2015.10.007
- Roux, K. J., Kim, D. I., & Burke, B. (2013a). BioID: a screen for protein-protein interactions. *Current Protocols in Protein Science*, 74, 19.23.1-19.23.14. https://doi.org/10.1002/0471140864.ps1923s74
- Roux, K. J., Kim, D. I., & Burke, B. (2013b). BioID: A screen for protein-protein interactions. *Current Protocols in Protein Science*, 2013, 19.23.1-19.23.14. https://doi.org/10.1002/0471140864.ps1923s74
- Roux, K. J., Kim, D. I., Raida, M., & Burke, B. (2012). A promiscuous biotin ligase fusion protein identifies proximal and interacting proteins in mammalian cells. *Journal of Cell Biology*, 196(6), 801–810. https://doi.org/10.1083/jcb.201112098
- RStudio Team. (2021). RStudio: integrated development for R. RStudio, Inc., Boston, MA URL Http://Www. Rstudio. Com, 42(14), 84. http://www.rstudio.com/
- Ruben, G. C., Iqbal, K., Grundke-Iqbal, I., Wisniewski, H. M., Ciardelli, T. L., & Johnson, J. E. (1991). The microtubule-associated protein tau forms a triple-stranded left-hand helical polymer. *Journal of Biological Chemistry*, *266*(32), 22019–22027. https://doi.org/10.1016/s0021-9258(18)54739-6

- Samavarchi-Tehrani, P., Samson, R., & Gingras, A. C. (2020). Proximity dependent biotinylation: Key enzymes and adaptation to proteomics approaches. In *Molecular and Cellular Proteomics* (Vol. 19, Issue 5, pp. 757–773). American Society for Biochemistry and Molecular Biology Inc. https://doi.org/10.1074/mcp.R120.001941
- Schindelin, J., Arganda-Carreras, I., Frise, E., Kaynig, V., Longair, M., Pietzsch, T., Preibisch, S., Rueden, C., Saalfeld, S., & Schmid, B. (2012). Fiji: an open-source platform for biological-image analysis. *Nature Methods*, *9*(7), 676–682.
- Sergeant, N., Delacourte, A., & Buée, L. (2005). Tau protein as a differential biomarker of tauopathies. In *Biochimica et Biophysica Acta Molecular Basis of Disease* (Vol. 1739, Issue 2, pp. 179–197). https://doi.org/10.1016/j.bbadis.2004.06.020
- Sinsky, J., Majerova, P., Kovac, A., Kotlyar, M., Jurisica, I., & Hanes, J. (2020). Physiological Tau Interactome in Brain and Its Link to Tauopathies. *Journal of Proteome Research*, 19(6), 2429–2442. https://doi.org/10.1021/acs.jproteome.0c00137
- Sperfeld, A. D., Collatz, M. B., Baier, H., Palmbach, M., Storch, A., Schwarz, J., Tatsch, K., Reske, S., Joosse, M., & Heutink, P. (1999). FTDP-17: an early-onset phenotype with parkinsonism and epileptic seizures caused by a novel mutation. *Annals of Neurology: Official Journal of the American Neurological Association and the Child Neurology Society, 46*(5), 708–715.
- Stancu, I. C., Ferraiolo, M., Terwel, D., & Dewachter, I. (2019). Tau Interacting Proteins: Gaining Insight into the Roles of Tau in Health and Disease. In *Advances in Experimental Medicine and Biology* (Vol. 1184, pp. 145–166). Springer. https://doi.org/10.1007/978-981-32-9358-8_13
- Strang, K. H., Golde, T. E., & Giasson, B. I. (2019a). MAPT mutations, tauopathy, and mechanisms of neurodegeneration. In *Laboratory Investigation* (Vol. 99, Issue 7, pp. 912–928). Nature Publishing Group. https://doi.org/10.1038/s41374-019-0197-x
- Strang, K. H., Golde, T. E., & Giasson, B. I. (2019b). MAPT mutations, tauopathy, and mechanisms of neurodegeneration. In *Laboratory Investigation* (Vol. 99, Issue 7, pp. 912–928). Nature Publishing Group. https://doi.org/10.1038/s41374-019-0197-x
- Sultan, A., Nesslany, F., Violet, M., Bégard, S., Loyens, A., Talahari, S., Mansuroglu, Z., Marzin, D., Sergeant, N., Humez, S., Colin, M., Bonnefoy, E., Buée, L., & Galas, M. C. (2011). Nuclear Tau, a key player in neuronal DNA protection. *Journal of Biological Chemistry*, 286(6), 4566–4575. https://doi.org/10.1074/jbc.M110.199976
- Szklarczyk, D., Franceschini, A., Wyder, S., Forslund, K., Heller, D., Huerta-Cepas, J., Simonovic, M., Roth, A., Santos, A., Tsafou, K. P., Kuhn, M., Bork, P., Jensen, L. J., & von Mering, C. (2015). STRING v10: Protein-protein interaction networks,

- integrated over the tree of life. *Nucleic Acids Research*, *43*(D1), D447–D452. https://doi.org/10.1093/nar/gku1003
- Tatebayashi, Y., Haque, N., Tung, Y.-C., Iqbal, K., & Grundke-Iqbal, I. (2004). Role of tau phosphorylation by glycogen synthase kinase-3β in the regulation of organelle transport. *Journal of Cell Science*, *117*(9), 1653–1663.
- Terada, T., Therriault, J., Kang, M. S. P., Savard, M., Pascoal, T. A., Lussier, F., Tissot, C., Wang, Y.-T., Benedet, A., Matsudaira, T., Bunai, T., Obi, T., Tsukada, H., Ouchi, Y., & Rosa-Neto, P. (2021). Mitochondrial complex I abnormalities is associated with tau and clinical symptoms in mild Alzheimer's disease. *Molecular Neurodegeneration*, 16(1), 28. https://doi.org/10.1186/s13024-021-00448-1
- Tracy, T. E., Madero-Pérez, J., Swaney, D. L., Chang, T. S., Moritz, M., Konrad, C., Ward, M. E., Stevenson, E., Hüttenhain, R., Kauwe, G., Mercedes, M., Sweetland-Martin, L., Chen, X., Mok, S. A., Wong, M. Y., Telpoukhovskaia, M., Min, S. W., Wang, C., Sohn, P. D., ... Gan, L. (2022). Tau interactome maps synaptic and mitochondrial processes associated with neurodegeneration. *Cell*, *185*(4), 712-728.e14. https://doi.org/10.1016/j.cell.2021.12.041
- Vanderweyde, T., Apicco, D. J., Youmans-Kidder, K., Ash, P. E. A., Cook, C., Lummertz da Rocha, E., Jansen-West, K., Frame, A. A., Citro, A., Leszyk, J. D., Ivanov, P., Abisambra, J. F., Steffen, M., Li, H., Petrucelli, L., & Wolozin, B. (2016). Interaction of tau with the RNA-Binding Protein TIA1 Regulates tau Pathophysiology and Toxicity. *Cell Reports*, *15*(7), 1455–1466. https://doi.org/10.1016/j.celrep.2016.04.045
- Violet, M., Delattre, L., Tardivel, M., Sultan, A., Chauderlier, A., Caillierez, R., Talahari, S., Nesslany, F., Lefebvre, B., Bonnefoy, E., Buée, L., & Galas, M. C. (2014). A major role for Tau in neuronal DNA and RNA protection in vivo under physiological and hyperthermic conditions. *Frontiers in Cellular Neuroscience*, 8(MAR). https://doi.org/10.3389/fncel.2014.00084
- Vuono, R., Winder-Rhodes, S., de Silva, R., Cisbani, G., Drouin-Ouellet, J., Spillantini, M. G., Cicchetti, F., & Barker, R. A. (2015). The role of tau in the pathological process and clinical expression of Huntington's disease. *Brain*, *138*(7), 1907–1918. https://doi.org/10.1093/brain/awv107
- Wang, P., Joberty, G., Buist, A., Vanoosthuyse, A., Stancu, I. C., Vasconcelos, B., Pierrot, N., Faelth-Savitski, M., Kienlen-Campard, P., Octave, J. N., Bantscheff, M., Drewes, G., Moechars, D., & Dewachter, I. (2017). Tau interactome mapping based identification of Otub1 as Tau deubiquitinase involved in accumulation of pathological Tau forms in vitro and in vivo. *Acta Neuropathologica*, 133(5), 731–749. https://doi.org/10.1007/s00401-016-1663-9
- Wang, Y., & Mandelkow, E. (2016). Tau in physiology and pathology. *Nature Reviews Neuroscience*, *17*(1), 22–35.

- Weingarten, M. D., Lockwood, A. H., Hwo, S.-Y., & Kirschner, M. W. (1975). A protein factor essential for microtubule assembly. *Proceedings of the National Academy of Sciences*, 72(5), 1858–1862.
- Wszolek, Z. K., Tsuboi, Y., Ghetti, B., Pickering-Brown, S., Baba, Y., & Cheshire, W. P. (2006). Frontotemporal dementia and parkinsonism linked to chromosome 17 (FTDP-17). In *Orphanet Journal of Rare Diseases* (Vol. 1, Issue 1). https://doi.org/10.1186/1750-1172-1-30
- Wu, M., Zhang, M., Yin, X., Chen, K., Hu, Z., Zhou, Q., Cao, X., Chen, Z., & Liu, D. (2021). The role of pathological tau in synaptic dysfunction in Alzheimer's diseases. *Translational Neurodegeneration*, 10(1), 1–11.
- Yoshiyama, Y., Higuchi, M., Zhang, B., Huang, S.-M., Iwata, N., Saido, T. C., Maeda, J., Suhara, T., Trojanowski, J. Q., & Lee, V. M.-Y. (2007). Synapse loss and microglial activation precede tangles in a P301S tauopathy mouse model. *Neuron*, *53*(3), 337–351.
- Zhou, Y., & Zou, P. (2021). The evolving capabilities of enzyme-mediated proximity labeling. In *Current Opinion in Chemical Biology* (Vol. 60, pp. 30–38). Elsevier Ltd. https://doi.org/10.1016/j.cbpa.2020.06.013